Final Technical Report (FTR)

Cover Page

a. Federal Agency	Department of Energy	
b. Award Number	DE-EE0008774	
c. Project Title	Optimal Reconfiguaration and Resilient Control Framework for Real-Time Photopholtaic Dispatch to Manage Critical Infrastructure (ReDis-PV)	
d. Recipient Organization	University of North Carolina at Charlotte	
e. Project Period	*Start: Nov. 2019*	*End: April 2023*
f. Principal Investigator (PI)	Sukumar Kamalasadan Professor skamalas@uncc.edu 704-687-7099	
g. Business Contact (BC)	Darlene "Darl" Booker Executive Director, Grants & Contracts Administration grants-contracts@uncc.edu 704-687-1862	
h. Certifying Official (if different from the PI or BC)	Not Applicable	

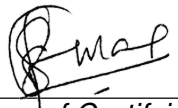

Signature of Certifying Official

07/30/2023

Date

By signing this report, I certify to the best of my knowledge and belief that the report is true, complete, and accurate. I am aware that any false, fictitious, or fraudulent information, misrepresentations, half-truths, or the omission of any material fact, may subject me to criminal, civil or administrative penalties for fraud, false statements, false claims or otherwise. (U.S. Code Title 18, Section 1001, Section 287 and Title 31, Sections 3729-3730). I further understand and agree that the information contained in this report are material to Federal agency's funding decisions and I have any ongoing responsibility to promptly update the report within the time frames stated in the terms and conditions of the above referenced Award, to ensure that my responses remain accurate and complete.

Acknowledgment: "This material is based upon work supported by the U.S. Department of Energy's Office of Energy Efficiency and Renewable Energy (EERE) Solar Energy Technologies Office (SETO) under the DE-FOA-0001987, Award Number DE-EE0008774."

Executive Summary

The consortium is conducting cutting-edge collaborative research that will allow advancing solar energy's role in strengthening the resilience of the U.S. electricity grid. The U.S Department of Energy Solar Technologies Office (SETO) has awarded 4.6 million to Professor Sukumar Kamalasadan (The University of North Carolina at Charlotte) for the project "Optimal Reconfiguration and Resilient Control Framework for Real-Time Photovoltaic Dispatch to Manage Critical Infrastructure (ReDis-PV)". The project developed a grid management tool that detects cyber and physical threats and forms dynamic clusters to manage photovoltaic and energy optimally. The project collaborating team includes the University of North Carolina at Charlotte, Clemson University, New Mexico State University, Florida International University, Argonne National Laboratory, Idaho National Laboratory, OPAL-RT Corporation, and Duke Energy.

The objective of this project is to design a grid management tool (ReDis-PV) that is threat-aware, resilient, grid reconfigurable, and can form dynamic clusters to optimally manage PV and energy storage for improving grid resiliency and supporting critical infrastructure. ReDis-PV consists of the following:

- A situational awareness module.
- Proactive resiliency diagnosis and predictive adaptation module.
- A hierarchical control with dynamic clustering and organization module.
- Optimal power flow module.
- A network reconfiguration and cyber security threat detection module.

The proposed approach is to develop a vendor-agnostic tool comprising of the above-mentioned modules requiring minimal communication between active PV stations, storage nodes, and distribution control center (DCC).

In this project, the tool has been successfully developed and verified with IEEE test system and Duke Energy Feeder. The tool has been delivered to Duke Energy, verified by the Duke for full functionality and a completion certificate has been obtained. The capabilities of the tool is a) It can group the DERs allowing the DERs to support the electric grid b) It can provide optimal management of DERs based on grid objectives to improve grid reliability, c) It can be used during outages to improve the load generation balance and support to critical loads, d) It can be used to improve grid resilience, and e) the tool is scalable and field implementable.
Going forward our objective is to have this tool implemented on a utility feeder as a pilot study which will help us (the project team and the utility) assess the tool's impact to improve grid reliability and resilience on a real-feeder. Further, the tool's adoptability will be evaluated and work in this direction will be initiated.

Table of Contents

1 Backgound

Increased penetration of photovoltaic (PV) systems on distribution grid bring operational challenges and opportunities both [5]. With recent developments in dispatchable inverters, PV systems including behind-the-meter (BTM) PV can be aggregated for a variety of grid functionalities. With the 4-quadrant control of the inverters, it is possible to modulate the active and reactive power of PVs for grid services that would have been traditionally provided by the large conventional generators. Distributed Generators (DGs) whether renewable or not can fulfill the demand locally and can be extremely useful [16]. However, a growing number of active devices and their control in the power distribution system can make grid management extremely complex [14]. Furthermore, the variations in the load on an unbalanced distribution system are not uniform thus a central control architecture can be inefficient and non-optimal in managing each local part of the power grid. Assigning local control by developing groups of DERs as clusters can efficiently manage respective zones in the distribution system.

Power grid partitioning has a wide spectrum of applications. In planning and analysis of the power grids, partitioning is used in network reduction and parallel processing of the grid partitions. Ref. [31, 29, 30] discusses the network partitioning based on the generator coherency to improve the reliability of the network and [11] and [27] proposes the use of network clustering to restart the power grid zones in from a blackout scenario. Several methods of grouping have been discussed in the literature based on clustering. Kernel-based clustering is performed through non-linear mapping of data in the feature space [26, 13, 33]. This has been applied to Intentional Islanding[25], Multi-Machine Equivalence [37], Bad data detection[34, 20]. In density-based clustering, the clusters are formed based on the density of the data points[6, 8, 36]. The area with a relatively higher density of the data points forms a cluster. In power system, electricity theft detection[40], fault detection [19], site selection decision for wind farms[3], generator coherency detection[42] are some of the areas in which these clustering methods are used.

In the distribution grids, the clustering methods have been primarily applied to identify the micro-grids during grid contingencies for an islanded operation [15, 7]. Since a power network can be modeled as a graph, various graph-based methods can be applied for the partitioning[21, 17]. Hierarchical and spectral-based clustering approaches are the commonly used approaches of power grid clustering [28]. Even though the approach is very effective, the results of the spectral clustering are an approximate solution and may not ensure the minimum k-way partition of a graph. In addition to that, the spectral clustering clusters' results are often found to be discontinuous. The issues of discontinuity and non-optimum cut are not addressed in the literature. Ref. [31] proposes the pre-processing and post-processing approaches to improve the cluster quality and remove the discontinuities. However, considering the iterative nature of these approaches, the application in real-time applications of a larger distribution network may not be feasible.

One of the traditional approaches for control and management of DG units is the centralized approach. The centralized schemes may not be able to operate under the significantly increased number of DG units [38, 4, 23, 1, 22]. The main factors that make the centralized control not feasible are (a) the absence of a committed management unit; (b) computational stress due to the presence of a large number of the controllable assets, e.g., DGs and loads;

(c) frequent restructuring requirements since a change in even one entity influences the main controller; (d) safety and reliability sensitivity of the main controller as a common point of failure; (e) trouble in sharing data, due lack of the way or unwillingness; (f) Also, the load distribution, as well as the variation, is not uniform in the distribution grids. Therefore, the centralized control module for all the controllable elements will be complicated and inefficient.

The non-centralized techniques may be decentralized or distributed which can overcome the limitations associated with the centralized approach. In the decentralized approach, the communication and information exchange between subsystems is assumed to be unimportant or negligible. This supposition, however, is not always rational and may result in poor system-wide performance. The blackout or complete power failure during 2003 in North America is a pertinent example of such decentralized control system failure [38]. In that particular unfortunate event, each subsystem was putting their effort into maintaining their stability by tripping and transferring the additional loads or demands to another subsystem, thus resulting in severe overloading and tripping of the entire system because of cascaded events.

Distributed management and adaptive control algorithms [18, 39, 12] consider the interaction between units. They allocate the control work to pertinent units or subsystems based on their functioning in different periods which constitutes the idea of control hierarchy (primary, secondary, and tertiary controls). To have the control approach distributed, a distributed model is required either through optimization or based on clustering that gives set-points and in tandem develop dynamics included in the control objective, or we use the distributed control approaches such as model predictive control (MPC) framework where dynamic optimization and control objectives are included in one objective. Several works related to distributed control have been proposed in the recent past [35, 41, 2, 10, 9]. Several limitations are associated with these distributed optimization-based control approaches, such as missing communication features [41, 10, 9]. Alongside scalability issues, most of these approaches were also not tested [35, 41, 2, 10]. Importantly the distributed control fulfilling such pertinent requirements has not yet been introduced or solved in the literature.

In our earlier works, we have developed distributed control architectures with spectral clustering [24]. In that work, we focused on developing active power clustering and distributed control of DERs. Preliminary results were presented and verified. In this work, a method for grouping DERs in the grid based on spectral clustering is proposed that can not only group but also check the quality of the clusters and regroup if necessary. Based on creating such virtual clusters of DERs (based on the net power balance in each cluster), further, a distributed control of controlled assets (in this paper, control of BESS) is presented. The approach not only provides an optimal set-point for BESS but also takes into account the state of charge and provides inter-cluster balance. The main advantage of such a framework is that it can manage the local part of the grid effectively, considering any state of BESS and any number of DERs. Compared to other architectures and [24], the main advantage of this tool is its ability to perform multiple objectives, including a) grid support functions of DERs, b) optimal management of grid objectives, c) improve grid resilience and support critical infrastructure, d) assess grid vulnerability in the presence of DERs, e) provide visualization and operator interface, f) assess the grid risk during physical and cyber-related threats and perform improved load generation balance without affecting the grid and g) protect critical infrastructure and asset from any cyber related threats.

2 Project Objectives

The main goal of this project is to develop a tool that can identify potential PV farm energy storage clusters and manage the cluster for improving grid resiliency during natural and man-made attacks and at the same time improve grid reliability during normal operation. To achieve this goal, the following major technical objectives are set, **Objective# 1:** Dynamic integrated transmission and distribution (T& D) model with situational awareness module: We plan to develop a dynamic T& D model that updates the operation of the grid in the presence of DER cluster that participates in improving reliability and resiliency during normal or abnormal operational phases of the distribution grid. **Objective# 2:** Cluster organization and hierarchical area control module: A module that organizes the DER cluster and develops an area controller. **Objective# 3:** Grid level optimization module: A module that helps optimally manage active and reactive power in DER clusters considering grid conditions. **Objective# 4:** Dynamic cluster control architecture and risk/threat resiliency module: A module that organizes all the cluster level controllers dynamically based on the risk and measures the level of risk. **Objective# 5:** Protection and network reconfiguration module: A module that reconfigures the network and provides protection schemes to harden the cluster. **Objective# 6:** Grid-aware communication and cybersecurity threat detection module: A module that provides a communication infrastructure for implementing the control and protection schemes and detects and analyzes cybersecurity-related threats. **Objective# 7:** Overall integration, real-time lab-scale, and field validation. The final objective is to develop a software platform that is tested in the lab and partly in the field and can be integrated with hardware. The results are validated and verified in the hardware in the field. The tasks have been classified for three budget periods. For the budget period 1, the tasks are categorized as follows: **Task 1:** Model integrated T& D system with control (device level) and communication layer and incorporating DER **Task 2:** Design and develop algorithms for forming DER clusters **Task 3:** Build a centralized version of distribution optimal power flow-DOPF **Task 4:** Develop dynamic control architecture, controller design adaptation, and lead controller selection **Task 5:**Evaluate conventional protection schemes in the presence of renewables and propose/evaluate a suitable method **Task 6:** Creating a communication network model that provides robust communication structures for enabling the communications in the distributed PV systems enabled the smart grid and integrating the model with Task 1 **Task 7:** Transmission and Distribution network model development/conversion and validation using the OPAL-RT simulator.
For the budget period 2, the tasks are categorized as follows: **Task 8:** Identify and model physical vulnerabilities based on the power grid model. **Task 9:** Develop area controller for dynamically selected clusters and evaluating the architecture. **Task 10:** Large-scale distribution optimal power flow (DOPF) and integration with other modules. **Task 11:** Development of risk/health-based resiliency modeling/monitoring framework. **Task 12:** Integrate (with Task 9, Task 13 and Task 14) the protection methodology with the controller. **Task 13:** Design threat detection model and latency sensitive communication considering vulnerability assessments from Task 8 and risk threats from Task 11. **Task 14:** T & D network large-scale model development/conversion, validation and interfacing of communication and other modules with OPAL-RT simulator.For the budget period 3, the tasks are categorized as follows: **Task 8:** Identify and model physical vulnerabilities based on the power grid model. **Task 15:** Develop a situational awareness module (Integrate with Tasks 2, 3, 5). **Task 16:** Integration and scalability testing of clustering/area control including network reconfiguration/protection. **Task 17:** Inclusion of integer and distributed version of Distributed Optimal Power Flow (DOPF))

for large network and integration with other modules. **Task 18:** Application of hybrid anomaly detection mechanisms and their integration with risk-informed adaptation. **Task 19:** Validation of protection design using scenarios (Assist Task 16, 21) and harmonizing the scheme with transmission system protection. **Task 20:** Integrate the grid-aware communication network topology to the protection and reconfiguration framework. **Task 21:** Incorporate all the final modules and integrate/validate the network reconfiguration/control/optimization with real-time/HIL testing. **Task 22:** Validation and verification of final tool with respect to field and test case data.

3 Project Results and Discussion:

3.1 Acronyms

Nomenclature

λ The optimal dimension of cluster embedding

$BESS$ Battery Energy Storage Systems

L^n Normalized Laplacian

M_i The set of indices of the areas that contain bus i

P_{ij} The real power flowing from the bus i and j

Q_{ij} The real power flowing from the bus i and j

SOC The state of charge of BESS

V Vertex set of the graph

V_i The voltage magnitude of bus i

W_{ij} The weight of the edge or line

ADMM Alternating Direction Method of Multipliers

DER Distributed Energy Resources

DRCA Dynamic Re-configurable Control Architecture

EMT Electro-Magnetic Transient

iCAAP Information-centric Network Architecture for Application-Specific Prioritization

MISOCP Mixed Integer Second Order Conic Programming

NDN Named data Networking

OPF-R Distribution Grid Optimal Power Flow with Network Reconfiguration

RICE Risk-Informed Condition Evaluation

SOCP Second Order Conic Programming

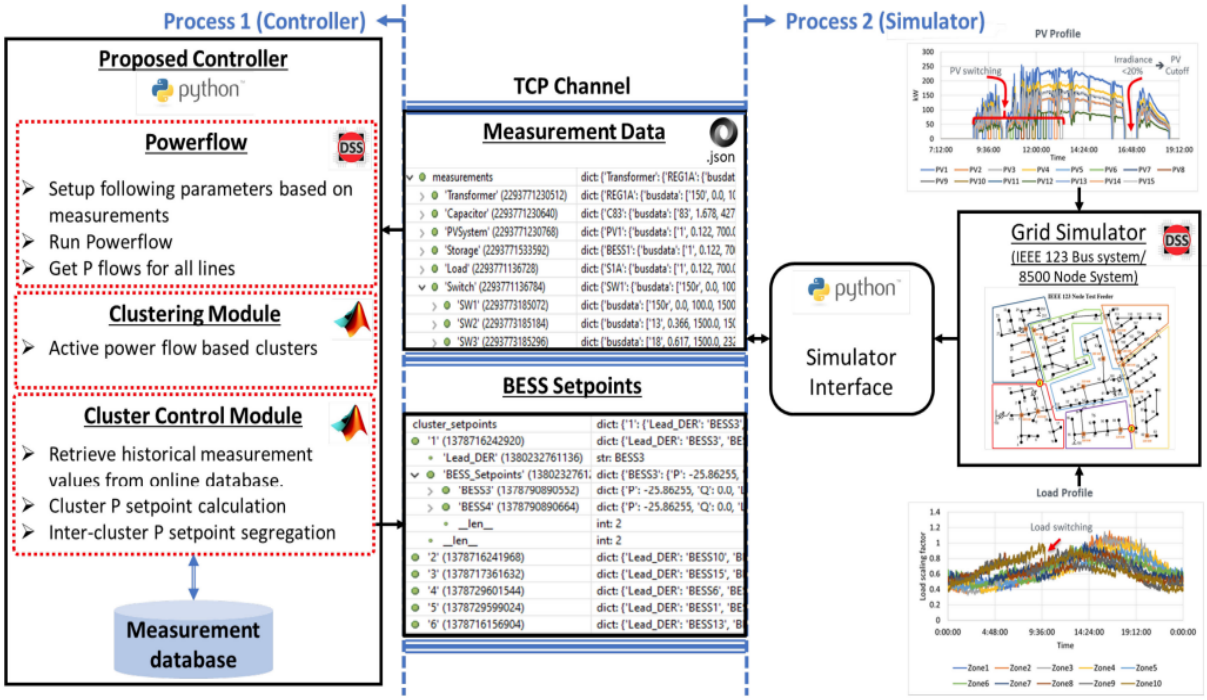

Figure 1: Formulation of cluster formulation module and grid simulator.

3.2 Cluster Formation and Clustering

3.3 Module 1: Clustering of IBRs and Types

3.4 Spectral clustering Based Distributed Control Approach

Spectral clustering is a graph-based partitioning algorithm treating the data points as graph nodes and partitions the graph based on the weight of the connections among the graph nodes.

3.4.1 Proposed Active Power Clustering Methodology

Consider the multi phase power distribution network shown in Fig. 2 represented as a undirected graph $G = (V, E)$, where $V = \{1, 2, 3, 4, 5\}$ and $E = \{\{1, 2\}, \{2, 3\}, \{2, 4\}, \{4, 5\}\}$. The vertex set ($V$) of the graph represents the set of network buses and the edge set (E) represents the connections among the vertices. Let ϕ be the number of phases and B is the total number of buses. For ϕ phase lines connecting two vertices i and j the weight of the edge or line can be represented in terms of the power flowing between two buses as

$$W_{ij} = |\sum_{x=1}^{\phi}(P_{ij})_x| \tag{1}$$

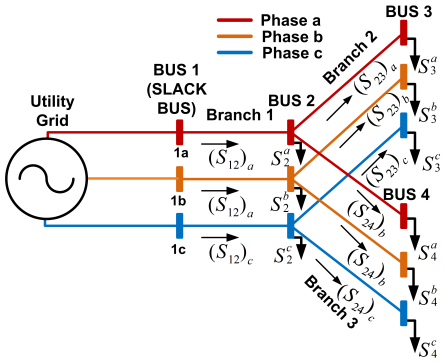

Figure 2: Graphical representation of a 4 bus distribution system.

where P_{ij} represents the power flowing between bus i and j. In terms of a graph depicting the electrical network, the weight of an edge is related to the strength of the electrical connection between two buses. As the updates in active power change with load and DER changes, the weights (representing the 'strength' of the connection) change based on the network conditions.

The significance is that weight of a line connected between two vertices measures the importance of the line in a given operating condition. Line weights can be interpreted as a penalty for cutting the corresponding line when clustering but also as a measure of the connection strength, as strongly connected vertices are more likely to be clustered together.

Using (1), the weighted adjacency matrix of a generalised N bus power grid can be represented as

$$A_{ij} = \begin{cases} 0, & \text{if vertices } i \text{ and } j \text{ are not connected} \\ W_{ij} & \text{if vertices } i \text{ and } j \text{ are connected} \\ 0, & \text{if } i = j \end{cases} \tag{2}$$

where $i = 1, 2, 3, ...B$, $j = 1, 2, 3, ...B$, and A is the measure of power flow between bus i and j.

The significance is that for the power distribution grid, where a graph represents a distribution network the weighted adjacency matrix depicts the strength of the electrical connection (power flow) between buses. Thus it measures the importance of all the edges or lines affiliated with the distribution network in a given operating condition.

According to the graph theory, degree matrix (D) is a diagonal matrix in which each diagonal element $(D_{ii}, D_{22}.....D_{BB})$ represents the degree. The degree of a vertex or a bus can be computed by summing the strength of weights of all edges attached to that particular vertex. The overall strength or degree of each of the B buses can then be

$$D_{ii} = \sum_{j=1}^{B} W_{ij} \tag{3}$$

The degree matrix of graph G representing a distribution network defines the electrical strength of buses. This matrix depicts the amount of power incident at each bus in the distribution

network.

$$L_{ij} = \begin{cases} D_{ii}, & \text{if } i = j \\ -A_{ij}, & \text{if } i \neq j \\ 0, & (i,j) \notin E \end{cases} \tag{4}$$

The degree is one of the most significant parameters to justify the quality of the cluster. With the above consideration, the Laplacian matrix (L) of the distribution system can be represented using L. The L is the BXB matrix and can be computed as

$$L_{ij} = \begin{cases} D_{ii}, & \text{if } i = j \\ -A_{ij}, & \text{if } i \neq j \\ 0, & (i,j) \notin E \end{cases} \tag{5}$$

The normalized Laplacian (L^n) can be derived using pertinent mathematical operations on the degree and Laplacian matrices.

$$L_{ij}^n = \begin{cases} 1, & \text{if } i = j \text{ and } D_{ii} \neq 0 \\ -\frac{1}{\sqrt{D_{ii} \times D_{jj}}} & \text{if } i \neq j \text{ bus } i \text{ is adjacent to } j \\ 0, & (i,j) \notin E \end{cases} \tag{6}$$

In simplest form, the normalized Laplacian (L^n) matrix can be derived using equation below:

$$L^n = D^{-\frac{1}{2}} L D^{-\frac{1}{2}} \tag{7}$$

By looking at the Eigenvalue of the Laplacian matrix having zero values, the number of connected components can be identified. For clustering purposes, the normalized Laplacian matrix is used for the randomly weighted network in terms of cluster solution quality. The higher relative Eigen gap and lower Eigenvalue define the quality of good clusters. The higher the relative Eigen gap or smaller the Eigenvalue, the lower will be the size of the boundary thus clustering quality will be excellent. The grouping of the DERs (clustering) is based on the power flowing in the distribution network such that the net power (load-generation) between clusters is minimum. We name the lines connecting clusters as tie-line. Thus the clustering approach provides active clusters that have the lowest power flow in the tie-lines. In the field, of ADMS-based power flow, the branch power calculated from ADMS can be used as the weight for the spectral clustering.

A distribution circuit with high PV penetration at the downstream level provides a power drop or dip in the distribution lines. This represents that there are PVs that is supporting downstream loads at various location. Considering this dip, each of the clusters around the power dip area can be presented as local microgrids. If there are sudden PV changes or fluctuations in power, the clustering algorithm identifies the changes and performs re clustering. For our approach, a time-based clustering (clustering performed periodically) is designed. The quality of the cluster is checked every time the cluster is formed based on the optimal dimension of cluster embedding using the Eigen gap calculated as follows.

$$\lambda_k^g = \frac{\lambda_{k+1} - \lambda_k}{\lambda_k} \tag{8}$$

$$u_k = \frac{v_k}{||v_k||} \tag{9}$$

where k represents the optimum number of clusters and it is computed based on indices or position of the highest Eigen gap $\{k^{optimal} = index(max(\lambda_k^g))\}$. The higher the relative Eigen gap, the lower will be tie-line weight or power flow (power between clusters), making the partition optimal. Represent the distribution network as a undirected Graph G such that $G = (V, E)$.
Identify the vertices V and edges E.
Intitalize the timestep $k = \Delta t, P_{ij}$, A of dimension $B \times B$, D of dimension $B \times B$.
$k = 1 : n \;\; x = 1 : \phi$ Compute the power flow through the lines that correspond to edges, P_{ij}
Compute the weight of each edge in the distribution system using (1)
$i = 1 : B \;\; j = 1 : B \;\; A_{ij}$ = 0; if *vertices i and j are not connected*
A_{ij} = W_{ij}; if *vertices i and j are connected*
A_{ij} = 0; if *i=j*
Compute the Laplacian, and normalized Laplacian matrix using (5) and (6).
Compute the Eigenvalue and the Eigenvectors of the normalized Laplacian matrix.
Compute the Eigen gap using (8).
Determine optimum number of cluster k using $\{k^{optimal} = index(max(\lambda_k^g))\}$.
calculate $\phi(C_t)$.
$\phi(C_t) \leq \epsilon$ Continue Go to Step 19 and compute the subsequent optimum cluster
return

3.4.2 Cluster Quality Assessment

Let us say a cluster $C_t = (V_t, E_t)$, which is also a sub graph of original distribution network $G = (V, E)$ (i.e $C_t \in G$, $V_t \in V$ and $E_t \in E$). The quality of a partition is measured based on the volume of the cluster and its boundary size. The volume of a cluster C_t ($vol(C_t)$) can be computed as

$$vol(C_t) = \sum_{i \in V_t} D_{ii} \tag{10}$$

The boundary of cluster C_t is computed using:

$$\beta(C_t) = \sum_{i \in C_t, j \notin C_t} W_{ij} \tag{11}$$

The overall quality of cluster will be measured as a ratio of boundary and volume of the cluster and is called as expansion.

$$\phi(C_t) = \frac{\beta(C_t)}{vol(C_t)} \tag{12}$$

If the expansion value C_t is small, the clusters are considered of good quality. This means the tie-line power flow is minimal indicating that the clusters are weakly connected to the remaining power network. It is important to note that providing both the good cluster volume and lower power between clusters is extremely critical for a high-quality cluster. The detailed clustering approach is provided in Algorithm 3.4.1.

3.4.3 Quality of overall cluster formations

The quality of overall partitioning of a graph representing a distribution network can be quantified by computing the following metrics: Ncut Normalized cut or Ncut of a graph $\mathbb{G}$ is the average of sum of the expansions of all the islands or clusters existing in the graph represented as

$$\zeta_{\mathbb{G}} = \frac{1}{K}\sum_{t=1}^{K}\frac{\beta(C_t)}{vol(C_t)} \tag{13}$$

where K represents the total number of clusters of a graph or network. Maximum expansion For cluster $C_t = (V_t, E_t)$, which is also a sub graph of original distribution network $G = (V, E)$ (i.e $C_t \in G$, $V_t \in V$ and $E_t \in E$), the overall quality of K numbers of clusters ($G = \{G_1 \cup G_2 \cup G_3 \cup ..... \cup G_K\}$) can be computed by taking maximum of all the expansion among the islands as

$$\xi(max) = max(\frac{\beta(C_1)}{vol(C_1)}, \frac{\beta(C_2)}{vol(C_2)}, ...\frac{\beta(C_K)}{vol(C_K)}) \tag{14}$$

Discontinuity The K-means and K-Melodies clustering approach for partitioning the distribution network into K number of clusters may sometimes result in the discontinuity of the partitions or clusters [32]. This becomes more evident while partitioning the distribution network with low inter-cluster connections. For this, a discontinuity flag (1 or 0) has been utilized to identify clustering discontinuity every time clusters are formed and corrected. Cluster size ratio ($\mathbb{R}$) The cluster size ratio can be computed by dividing the number of nodes $\mathbb{N}^s$ in the smallest cluster of graph G by the total number of nodes $\mathbb{N}^L$ in the largest cluster of graph G. This metric has been used to signify the balance between the smallest and largest partition and can be computed as:

$$\mathbb{R} = \frac{\mathbb{N}^s}{\mathbb{N}^L} \tag{15}$$

3.4.4 Factors affecting the cluster quality

Laplacian normalization For the purpose of minimisation of $NCut$, the normalized Laplacian works way better than un-normalized Laplacian. On normalization, the non-diagonal elements of normalized matrix can be written as:

$$L_{ij}^n = \frac{L_{ij}}{\sqrt{D_{ii} \times D_{jj}}} \tag{16}$$

An example related to displaying the benefits of normalized Laplacian is illustrated in Fig. 3. It can be seen from the power flow results that, the real power flow (P) is reduced while transitioning from bus 105 to nodes 11, 107, and 114. This is obvious since there is only one PV farm. However, the normalized power Pn flow does not follow the same trend as the un-normalized one (16). The Normalization assists in preventing the scenario of the formation of an unwanted cut close to the feeder end where the amount of real power flow is small and thereby improving the size ratio. Fig. 4 shows the improvement with normalization in the size ratio for 1000 active power-flow-based clustering instances.
Number of clusters (k) On running the spectral clustering over the normalized Laplacian for k_{opt} clusters, considerable improvement in the clustering quality has been observed. To illustrate this, clustering based on 120 snapshots of power flow scenarios is performed with

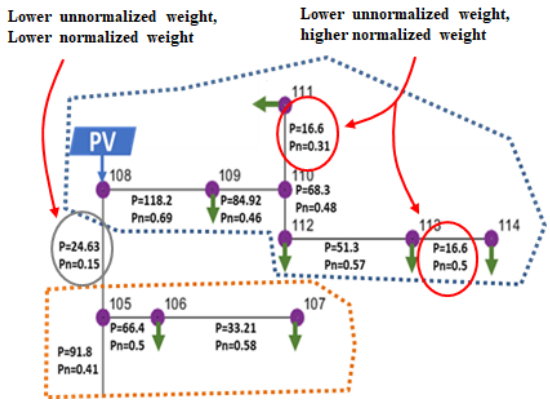

Figure 3: Edge weights with and without Laplacian normalization.

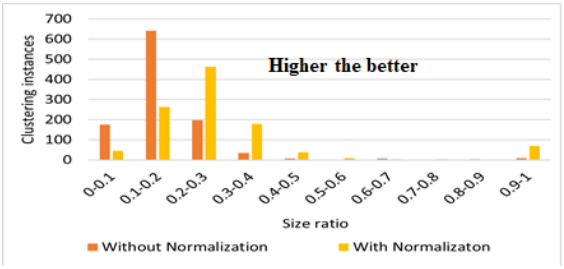

Figure 4: Effect of normalization on the size ratio of the clusters.

optimum k clusters obtained using the relative eigengap, with k ranging from 2 to 10. The summary of the analysis is presented in Table 1.

3.4.5 Power Grid Model with Normalized Laplacian Matrix:

The power flow model of the distribution network in Fig.2 can be represented as

$$V_j(t) = V_i^{\phi_{ij}}(t) - Z_{ij}[(P_{ij}(t) - Q_{ij}(t)) * V_i^{\phi_{ij}}(t)] \tag{17}$$

Similarly, the power flowing through the lines can be represented as

$$P_{ij}(t) = \sum_{k \in N_j} P_{jk}(t) + P_j(t) \tag{18}$$

$$Q_{ij}(t) = \sum_{k \in N_j} Q_{jk}(t) + Q_j(t) \tag{19}$$

The above power flow model can be written in the compact form

$$V_j(t) = V_i^{\phi_{ij}}(t) - 2(R_{ij}P_{ij}(t) + X_{ij}Q_{ij}(t)) + (R_{ij}^2 + X_{ij}^2) * \ell_{ij} \tag{20}$$

where ℓ represents the square of the currents in the branch.
Considering the distribution system properties $(R >> X)$ for all the non boundary nodes in

Table 1: Effect of optimal k on the clustering quality

Quality Parameter	Random $k \in \{2, 10\}$	$k_{opt} \in \{2, 10\}$
Ncut	0.14	0.06
Maximum expansion	0.32	0.12
Discontinuities for every 10 clustering instances	2.27	0.25
Size Ratio	0.295	0.31

the cluster

$$V_j(t) = V_i^{\phi_{ij}}(t) - 2(R_{ij}P_{ij}(t)) + R_{ij}^2 * \ell_{ij} \tag{21}$$

The above equation can be represented in terms of Laplacian:

$$V_j(t) = V_i^{\phi_{ij}}(t) - 2(R_{ijij}(t)) + R_{ij}^2 * \ell_{ij} \tag{22}$$

where $j \in v_{x(nb)}$, $i \in v_{x(nb)}$, $v_{x(nb)}$ is set of all the non-boundary nodes in cluster K.
For all the boundary nodes connecting between clusters K and M, the voltage equation is given as:

$$V_{bM}(t) = V_{bK}^{\phi_{ib}}(t) - 2(R_{ib}P_{ib}(t) + R_{ib}^2 * \ell_{ib} \tag{23}$$

The above equation can be represented in terms of cluster boundary as follows:

$$V_{bM}(t) = V_{bK}^{\phi_{ib}}(t) - 2(R_{ib}\beta_{ib}(t) + R_{ib}^2 * \ell_{ib} \tag{24}$$

where $b \in v_{x(B)}$, $i \notin v_{x(B)}, i \notin v_{x(nb)}\ v_{x(B)}$ is set of all the boundary nodes in cluster K and M. Taking the difference between subsequent time steps, $t+1$, and with high cluster quality (where the power between clusters are minimum), (23) and (24) can be written as

$$\Delta V_j(t) = \Delta V_i^{\phi_{ij}}(t) - 2R_{ij}L_{ij}^n(t) \tag{25}$$

$$\Delta V_{bM}(t) = \Delta V_{bK}^{\phi_{ib}}(t) - 2R_{ib}\phi_{ib}^n(t) \tag{26}$$

In (25), knowing that the voltage dynamics are based on the net load, $\Delta V_i^{\phi_{ij}}(t) = \Upsilon(k) * P_{nl}$ where $\Upsilon(k)$ represents the net-load coefficients. Also, considering the formation of stable cluster, the expansion coefficient is small. Thus in (26), $\Delta V_{bM}(t) = \Delta V_{bK}^{\phi_{ib}}(t)$ can be represented as $\alpha * P_{set}(t)$ to make the interclusteral deviations minimum. With this (25) and (26) can be represented as

$$\Delta V_j(t) = \underbrace{\Upsilon(k) * P_{nl}(k,n)}_{\Delta V_i^{\phi_{ij}}(t)} - \hat{L}_{ij}^n \tag{27}$$

where $\hat{L}_{ij}^n = 2R_{ij}L_{ij}^n(t)$

$$\Delta V_{bM}(t) = \underbrace{\alpha * P_{set}(t) - \epsilon}_{\Delta V_{bK}^{\phi_{ib}}(t) - \hat{\phi}_{ij}^n} \tag{28}$$

where $\hat{\phi}_{ij}^{n} = 2R_{ib}\phi_{ib}^{n}(t)$.
Thus the cluster formation can be synthesized to develop the dynamic distributed model of the power distribution system attributed to the changes in DER outputs. This distributed model can then be used for developing a distributed control framework without the need for any optimization model.

3.5 Spectral Clustering Based Distributed Control Approach

The goal of the spectral clustering-based distributed control approach is to utilize the DERs for both grid support and maximum solar penetration (PVs). Thus with the proposed distributed control approach, DERs operation and output are supervised and controlled utilizing the control capability feature of smart inverter-based DERs, The objective of the cluster control module is to support a locally connected load and reduce the chance of disturbance arising due to PV interruption and load fluctuations in a cluster and across the cluster. [!t] Identify DER clusters from Algorithm 1.
Initialize k with time step Δt.
$n = t : N$ For cluster k, compute the net load without BESS for each cluster using (29)
For k, compute the reference net load using (30)
Compute the error between computed and reference net load of cluster k.
Optimize the error using (31).
Determine the active power dispatched by overall BESS of the k^{th} cluster ($P_{BESS}(k,n)$) using (33).
Provide the $(e_{soc}(j,n))$ and $(BESS_{kWh})$.
Compute the active power set points (P_{set}^{i})) for the individual BESS say i.
For every BESS of cluster, based on the $e_{soc}(j,n)$ value, calculate the ramp-rate coefficient (ζ_{soc}^{j}) using (36)
$e_{soc} < e_{soc}^{th}$ ζ_{soc}^{j}=k_p ζ_{soc}^{j}=$k_i \sum_{i=n-N}^{n} e_{soc}(j,i)$ Calculate active power dispatch for every BESS within each cluster using (37).
Adjust the setpoint if the SoC is not within the tolerance limit.
$n = t + \Delta t$

Let the DER dynamics due to PVs in a cluster can be represented as a net-load for cluster k at any time n given by (29). Here $P_{nl}(k,i)$ is the net-load without BESS for cluster k at time-step i. If the criticality level is known for the feeder-loads, the net-load (P_{nl}) can be made same as the critical net-load $(P_{nl}^{c}(k,i))$.

$$P_{nl}(k,n) = Pload(k,n) - P_{pv}(k,n) \tag{29}$$

In the proposed approach, the reference net-load $P_{nl}^{ref}(k,n)$ for a k cluster is calculated by taking the moving average of the net-load (P_{nl}) or the critical net-load$(P_{nl}^{c}(k,i))$. For the past N measurements, this can be obtained from the Laplacian as shown in (30).

$$P_{nl}^{ref}(k,n) = \frac{1}{N} \sum_{i=n-N}^{n} \hat{L}_{ij}^{n} \tag{30}$$

N is the number of historical measurement samples, i is the computational window start time,

n is the current time.
As shown in (31), the linear least square optimization approach is applied to minimize the error between the reference net-load P_{ref}^{nl} and the measured net-load (P_{nl}) for the k^{th} cluster over past N measurements. Here $\Upsilon(k)$ is the optimization co-efficient. The proposed approach calculates the cluster dispatch set-points for the next time-step by minimizing the square error through-out the sample window (N).

$$min\ U = \sum_{i=n-N}^{n} \frac{1}{2} * (\eta * P_{nl}(k,i) - \Upsilon(k) * P_{nl}^{ref}(k,i))^2 \tag{31}$$

The net-load support provided by the BESS within the cluster is limited by the active power rating (kW) rating of the BESS within the cluster. For m BESS within the cluster, the total active power support available for the cluster k is represented by $P_{kW}(k) = P_1^{BESS} + P_2^{BESS} + ...P_m^{BESS}$. Based on the $P_{kW}(k)$, the upper and the lower bounds of the optimization coefficient $\Upsilon(k)$ can be formulated as shown in (32). The upper and lower bounds limit the support capabilities for each cluster based on the total kW ratings of all BESS within the cluster. With $\Upsilon(k)$, the optimal active support from the m number of BESS for cluster k can be calculated as

$$\frac{-P_{kW} + P_{nl}(n)}{P_{ref}} < \Upsilon(k) < \frac{P_{kW} + P_{nl}(n)}{P_{ref}} \tag{32}$$

$$P_{BESS}(k,n) = P_{nl}(k,n) - \Upsilon(k) * P_{nl}^{ref}(k,n) \tag{33}$$

The $P_{BESS}(k,n)$ determines the total active power to be dispatched by the BESS of the k^{th} cluster. The dispatch from an individual BESS is distributed among the cluster BESS based on the decreasing order of the state of charge error $(e_{soc}(j,n))$ and the storage capacity of the BESS $(BESS_{kWh})$ as

$$e_{soc}(j,n) = SOC_t(j,n) - SOC(j,n) \tag{34}$$

$$ekWh_{soc}(j,n) = e_{soc}(j,n) * BESS_{kWh} \tag{35}$$

A PI-based approach is used to calculate the active power setpoints (P_{set}^i)) for the individual BESS. This approach aims to improve the SOC recovery for the targeted state of charge ($SOC_t(j,n)$) and was found to be efficient in keeping the BESS state of charge within the upper and lower limits. For every BESS within the cluster, based on the $e_{soc}(j,n)$ value, the ramp-rate coefficient (ζ_{soc}^j) is calculated as shown in (36). When the SOC error (e_{soc}) is smaller compared to the error threshold e_{soc}^{th}, the proportional component ramp-rate coefficient is based on the proportional component (k_p) which controls the sudden changes in the BESS dispatch. When the SOC error (e_{soc}) is larger compared to the error threshold e_{soc}^{th}, the integral component based on errors for the last N measurements is used to control the BESS dispatch. The values of K_i can be further varied dynamically based on charging and discharging opportunities to improve the SOC recovery.

$$\zeta_{soc}^j = \left\{ \begin{array}{l} k_p, \text{ for } e_{soc}(j,n) \leq e_{soc}^{th} \\ k_i \sum_{i=n-N}^{n} e_{soc}(j,i), \text{ for } {}_{soc}(j,n) \geq e_{soc}^{th} \end{array} \right\} \tag{36}$$

Based on the ζ_{soc}^j, the value of active power dispatch for every BESS within the cluster is

calculated sequentially as shown in (37) limited by BESS kW limits P_{kW}^{j} as shown in (38).

$$P_{set}^{j} = \zeta_{soc}^{j} * \frac{P_{BESS}(k,n) - \sum_{\forall j>1, m=1}^{j-1} P_{set}^{m}}{N_k - j + 1} \tag{37}$$

$$-P_{kW}^{j} \geq P_{set}^{j} \leq P_{kW}^{j} \tag{38}$$

3.6 Inter-cluster Set-point Segregation

Eq. 37 segregates the cluster set-point for every BESS on the system based on the ζ_{soc}^{j} coefficient. The sequential segregation of the set-point may not be optimal. Also, the approach may not support inter-cluster power exchanges between the BESS. ie. A BESS with higher SOC may not be able to support BESS with lower SOC. Hence, an inter-cluster optimization was developed to keep the BESS SOC within the tolerance limit.
For every cluster(k), the objective function for BESS set-point segregation can be formulated as follows:

$$min\frac{1}{2}||SOC_i^{target} - SOC_i(t)||^2 \tag{39}$$

subjected to the kW support limit of the BESS

$$-P_i^{kw} \leq P_i(t) \leq P_i^{kw} \tag{40}$$

From (40) the storage capacity of BESS can be represented as

$$P_i(t) = Ebess_i(t-1) - Ebess_i(t) \tag{41}$$

Since $Ebess_i(t)$ can also be represented in the form of SoC, (41) can be modified to

$$P_i(t) = Ebess_i(t-1) - SOC_i(t) * Ebess_i \tag{42}$$

Substituting $P_i(t)$ in (40)

$$-P_i^{kw} \leq Ebess_i(t-1) - SOC_i(t) * Ebess_i \leq P_i^{kW} \tag{43}$$

Rearranging (43) to obtain the lower and upper bounds of the optimization variable $SOC_i(t)$

$$P_i^{kW} - Ebess_i(t-1) \leq x_i * Ebess_i \leq -P_i^{kw} - Ebess_i(t-1) \tag{44}$$

$$\frac{P_i^{kW} - Ebess_i(t-1)}{Ebess_i} \leq x_i \leq \frac{-P_i^{kw} - Ebess_i(t-1)}{Ebess_i} \tag{45}$$

For multiple BESS within the cluster, the equality constraint to meet cluster set-point can be given by

$$\sum_{i=1}^{N} P_i(t) = P_{set}(t) \tag{46}$$

Substituting $P_i(t)$ in (46)

$$\sum_{i=1}^{N} Ebess_i(t-1) - \sum_{i=1}^{N} SOC_i(t) * Ebess_i = P_{set}(t) \tag{47}$$

Re-arranging (47), the equality constraint in terms of optimization variable $SOC_i(t)$ can be formulated as:

$$\sum_{i=1}^{N} Ebess_i(t-1) - P_{set}(t) = \sum_{i=1}^{N} SOC_i(t) * Ebess_i \tag{48}$$

$$\frac{\sum_{i=1}^{N} Ebess_i(t-1) - P_{set}(t)}{\sum_{i=1}^{N} Ebess_i} = \sum_{i=1}^{N} SOC_i(t) \tag{49}$$

Meeting the cluster set-point may not always be possible because of the limited support capability of BESS. Hence, the equality constraint is added to the objective function as a soft constraint with a penalty coefficient ρ. The final optimization formulation for the inter-cluster set-point segregation can be represented as $\min_{SOC_i(t)} \quad \frac{1}{2}||SOC_i^{target} - SOC_i(t)||^2 + \frac{\rho}{2}||\frac{\sum_{i=1}^{N} Ebess_i(t-1) - P_{set}(t)}{\sum_{i=1}^{N} Ebess_i} - \sum_{i=1}^{N} SOC_i(t)||^2$
s.t. $\frac{P_i^k W - Ebess_i(t-1)}{Ebess_i} \leq x_i \leq \frac{-P_i^{kw} - Ebess_i(t-1)}{Ebess_i}$
The detailed cluster control algorithm has been described in Algorithm 3.5. Fig. 5 provides the schematic of the proposed architecture.

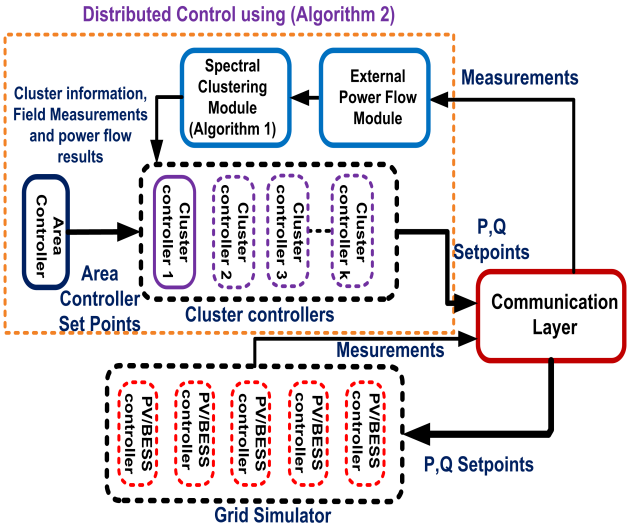

Figure 5: Distributed control architecture (DCA).

4 Implementation of the proposed approach

Fig. 5 and Fig. 6 shows the flow of the implementation processes in the co-simulated environment. The measurements are collected every 5 seconds and sent to the simulator in a

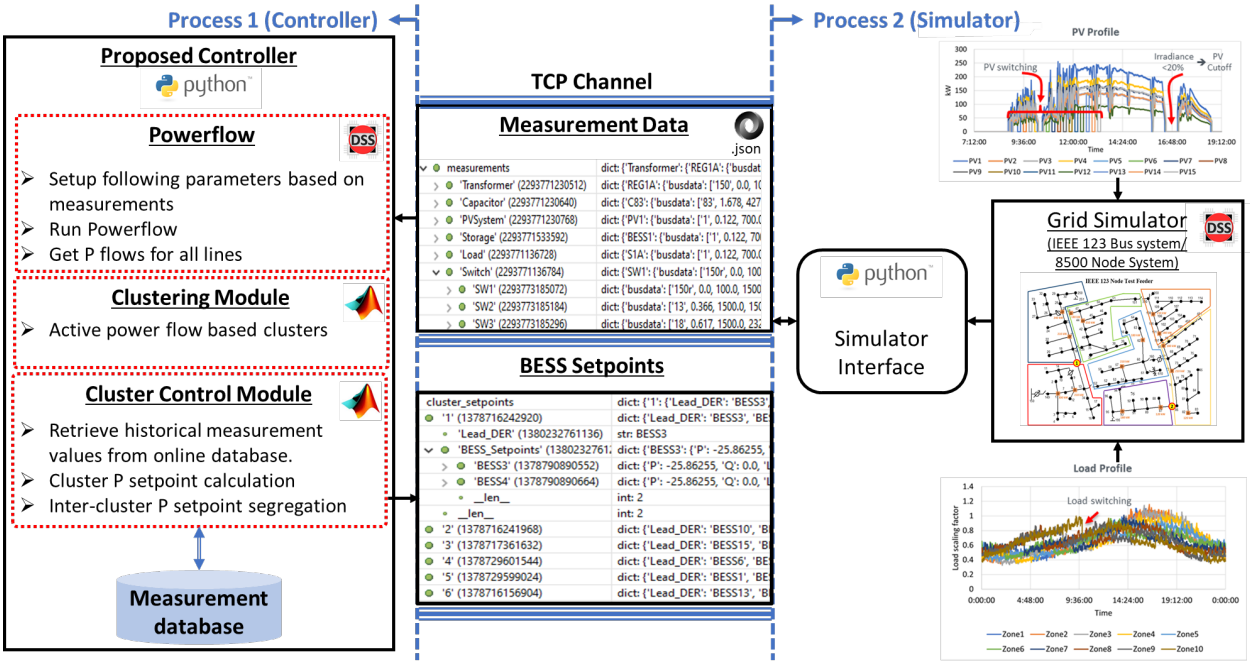

Figure 6: Co-simulation of cluster formation module and grid simulator.

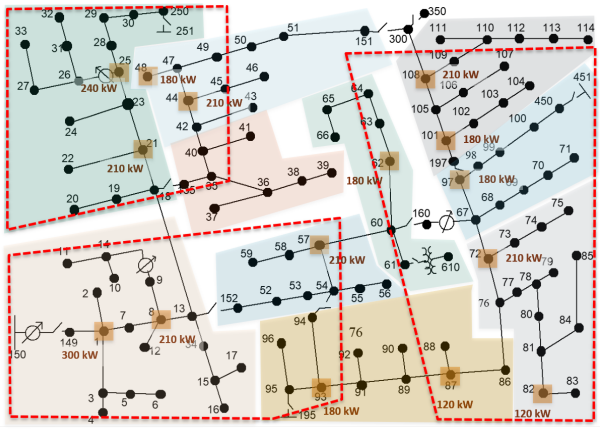

Figure 7: PV and load areas in 123 bus system.

standardized $JSON$ format. For implementation, an ethernet based communication is proposed much like as it is implemented in the SCADA/DMS enabled substation. The proposed controller primarily consist of an external power-flow module, spectral clustering module and a cluster control module. An external power-flow module re-creates the grid scenario by mapping the loads/meter readings, DERs measurements and switch positions to the grid power-flow model. The sectional active power-flow values are then adopted as the line weights for the spectral clustering. To address the changing grid conditions, the proposed clustering approach is repeated at every 3 minutes time interval. The 3 minute time-period between the clustering instances allows sufficient time for the cluster controller to achieve the cluster set-point. For the required cluster configurations, the active power set-points for the clusters and BESS within the clusters are calculated at every 5 seconds and applied to the field through the ethernet

Table 2: Locations and ratings of DERs on IEEE 123 bus system

PV Rating	BESS Rating	NodeIDs
120 kW	30kW/120kWh	82, 87
180 kW	45kW/135kWh	48, 62, 93, 97, 101
210 kW	50kW/150kWh	8, 21,44, 57, 72, 108
240 kW	60kW/180kWh	25
300 kW	75kW/225kWh	1

based channel for the controllable device. Since the proposed approach uses historical data to calculate the set-points, an online database of the past measurement is maintained. For every new cluster configuration, the historical measurements are extracted to re-establish the history of the new cluster based on the past time-step measurements. The setpoints of BESS are sent back to the simulator in the standardized $JSON$ format. The proposed approach of

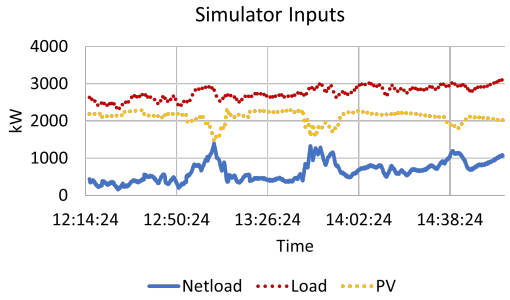

Figure 8: Load and PV generation profiles.

distributed control is implemented on the IEEE 123 bus system with 15 PV and Battery Energy Storage Systems (BESS) (see Fig. 7). The IEEE 123 bus system is modeled in an OpenDSS simulator operating in a time-series model with a 1 second time resolution. A python-based interface library is developed to interact with the online simulation for the collection of measurements and application of the BESS set-points. The ratings and locations of the PV and BESS are summarized in Table. 2. The locations and ratings of PVs were assumed based on the local loads connected in the respective areas of the feeder. Considering the futuristic scenario of distribution feeders with high PV interconnections, the total PV penetration was assumed to be 80% of the total load on the feeder. The BESS kW ratings are assumed to be 25% of the connected PVs at the same node. The simulator is configured to run at a $1s$ time interval in time-series mode. Fig. 8 shows the PV, load, and net-load profile throughout the simulation time window. The distributed control is performed for the net-load management applications.

The scalability of the proposed approach is also demonstrated on the IEEE 8500 node system with 80% of PV penetration. The PV systems rated at 30kW, 60kW, 180kW, 500kW, and 1MW are distributed throughout the 8500 node system. Fig. 8 shows the overall profile of the load, PV, and resulting net load on the system. To increase the efficiency of the cluster formation, the

low voltage and single-phase laterals of the 8500 node systems are assumed to be aggregated for clustering purposes.

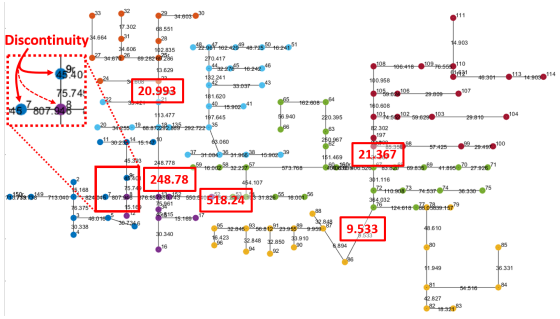

Figure 9: Clustering of IEEE 123 bus system with conventional K-means approach.

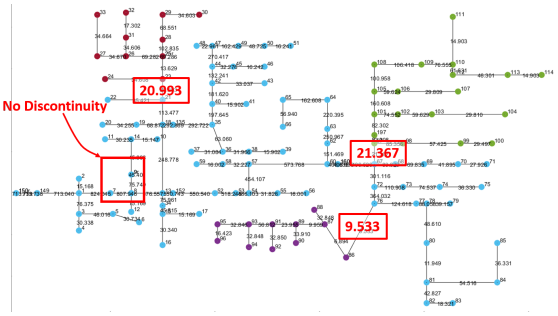

Figure 10: Clustering of IEEE 123 bus system with the proposed approach.

5 Results and Discussion

The load and PV variation for 6 hours was captured in a total of 120 power flow scenarios at an interval of 3 minutes. The performance of clustering algorithms was evaluated based on the quality parameters explained in section II.B. The results from inter-cluster set-point segregation are demonstrated through selected design snapshot scenarios on a cluster with three BESS. Then, the results from the implementation of cluster control are discussed. Finally, the section also discusses the results from the scalability of the proposed approach on the IEEE 8500 node system.

5.1 Evaluation of Active Power-flow based clustering

First, the spectral clustering approach presented in this paper is compared with conventional K-means eigenvector-based spectral clustering. Fig. 9 shows the conventional K-means eigenvector-based spectral clustering scenario over a snapshot of the distribution power flow. The spectral clustering for the "8" clusters (the value of k_{opt} for the normalized Laplacian is 8) shows the discontinuity within the $blue$ cluster. The power flowing through the lines connecting each cluster is also indicated. Similarly, Fig. 10 shows the proposed approach. It can be seen

that there is no discontinuity for the proposed approach as the Eigengaps are amplified based on the proposed similarity index. Also, it can be seen that the power flowing through the lines connecting each cluster is the same or less when compared to the conventional approach.

Table 3: Improvement of the cluster quality

Quality Parameter	Without Normalization	With Normalization	Improvement
Ncut	0.058	0.064	-11%
Maximum expansion	0.121	0.125	-3.5%
Average Cluster count	2.98	3.28	10%
Smallest Cluster Size	11.96	20.04	40.33%
Size Ratio	0.14	0.31	54.21%
Discontinuities	5	3	66.67%

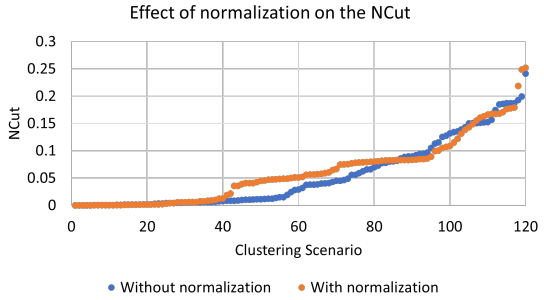

Figure 11: Ncut for 120 instances of IEEE 123 bus system.

The performance of the proposed approach against the conventional spectral clustering ap-

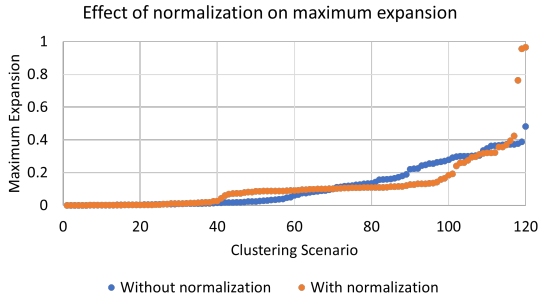

Figure 12: Maximum expansion for 120 instances of IEEE 123 bus system.

proach is summarized in Table 3. It can be seen that the proposed architecture improves the

quality of the cluster. Fig. 11 and 12 compares the Ncut and maximum expansion values for 120 power flow instances. These values are sorted in ascending order to improve the plot visibility. The improvement in the $Ncut$ and Maximum expansion values comes against the reduction in the size ratio. It was also found that the size ratio is reduced. This is expected as the total number of the cluster was changing to reduce the edge power flow. It is also observed that the major advantage of the proposed approach lies in the improvement brought on the aspect of the cluster discontinuities and reduction in the edge power flow.

5.2 Evaluation of Inter-cluster set-point segregation

Table 4 presents 7 cases of inter-cluster set-point segregation for a cluster with 3 BESS. The rated kW capacities for three BESS is assumed to be 50, 75 and 25 kW. The rate storage capacity for the BESS is assumed to be 120, 150 and 50 kWh. The SOC_i^{target} for all cases is assumed to be 0.5 or 50%.

- Case 1: The SOC for all BESS is 0.5. The set-point for the cluster is equal to the combined rated kW of the cluster. Hence all BESS are discharges at the rated capacity.
- Case 2: The SOC for all BESS is 0.5. The set-point for the cluster is higher then the combined rated kW of the cluster. Hence all BESS discharges at the rated capacity to minimize the tracking error.
- Case 3: The SOC for all BESS is 0.5. The set-point for the cluster is lower then the combined rated kW of the cluster. Hence all BESS are discharges are proportionate to the rated storage capacity.
- Case 4: The SOC of BESS2 is low (0.2). The set-point for the cluster is same as in case 3. But, the set-point for the BESS2 is reduced from 59 kW to 25 kW and the reduction in the discharge of BESS2 is compensated by BESS1 and BESS3.
- Case 5: The SOC of BESS2 is low (0.2). The cluster set-point for this case is 75 (lower then previous cases). The set-point is achievable through the discharge from the BESS1 and BESS3. Hence, the BESS2 temporarily set to "idle" mode to avoid any further depletion of the SOC.
- Case 6: The SOC of BESS2 is low (0.2). The cluster set-point for this case is 50 (lower than in previous cases). Hence an additional headroom is available for the power exchange between the BESS after meeting the cluster set-point. Hence, the BESS2 is assigned the set-point to restore the state of charge from the additional dispatch of BESS1 and BESS2.
- Case 7: The SOC of BESS1 is 0.8, BESS2 is 0.3, and BESS3 is 0.4. The cluster set-point for this case is 70. Since BESS1 is having the higher SOC, it is assigned the set-point to discharge at the rated capacity. Although the SOC of BESS2 is lower compared to BESS3, the rated storage capacity of BESS3 is significantly lower (by 33%) than BESS2. Hence, the SOC restoration of BESS3 is prioritized compared to BESS2 and BESS2 discharges at a reduced rate.

Table 4: Inter-cluster set-point segregation

	BESS1	BESS2	BESS3
P_{kW}	50	75	25
Ebess	120	150	50
Case 1	Cluster Set-point = 150 kW		
SOC(t-1)	0.5	0.5	0.5
P(t)	50	75	25
Case 2	Cluster Set-point = 200 kW		
SOC(t-1)	0.5	0.5	0.5
P(t)	50	75	25
Case 3	Cluster Set-point = 100 kW		
SOC(t-1)	0.5	0.5	0.5
P(t)	34.2	59.05	6.65
Case 4	Cluster Set-point = 100 kW		
SOC(t-1)	0.5	0.2	0.5
P(t)	50	25	25
Case 5	Cluster Set-point = 75 kW		
SOC(t-1)	0.5	0.2	0.5
P(t)	50	0	25
Case 6	Cluster Set-point = 50 kW		
SOC(t-1)	0.5	0.2	0.5
P(t)	50	-25	25
Case 7	Cluster Set-point = 70 kW		
SOC(t-1)	0.8	0.3	0.4
P(t)	50	45	-25

5.3 Evaluation of Distributed cluster control for net-load management

The section demonstrates and analyzes the performance of the cluster-based net-load smoothing. To understand the benefits of cluster control and dynamically varying clusters, the following three cases are compared:

- Centralized Control: Here complete grid acts as a single cluster and the set-points are calculated based on the overall grid requirements.

- Control with constant clusters: Here the cluster configuration is kept constant throughout the simulation. Fig. 13 shows the cluster configuration followed throughout the simulation.
- Control with dynamic clusters: Here the cluster configuration is dynamically varying based on power-flows at every 3-minute time interval. Fig. 14 shows the variation of clusters throughout the simulation.

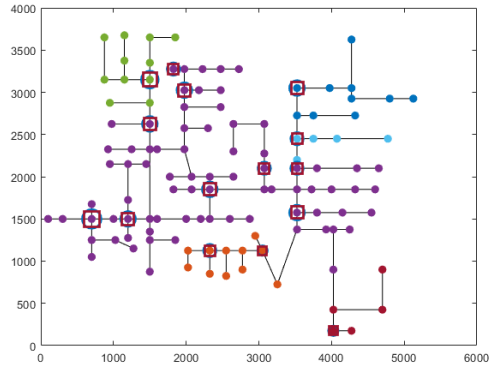

Figure 13: Constant cluster configuration used for control.

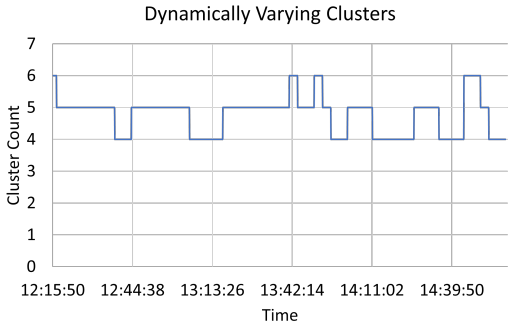

Figure 14: Dynamically varying active power flow-based clusters.

Fig. 15 shows the feeder-head power flow without control and with controls. The net-load smoothing strategy is based on the moving average as a reference. Hence, the measurements from the past time steps help in determining the set-points for the next time steps. Due to the moving average window, the resulting feeder-head power flow with controls shows the time shifts. The approach addresses the intermittencies by reducing the magnitude of the variations and the ramp rate of the variations in the netload. The feeder-head power flow for cluster-based control is compared against the centralized control. The overlapping of the net-load profile validates the consistency of the distributed control approaches. A 1-minute regression-based smoothing index is calculated to compare the improvement in the net-load smoothing. The cluster-based smoothing approaches reduce the net-load intermittencies by 43%. The clustered net-load control is efficient by 4% when compared against the centralized control in reducing the intermittencies. Fig. 16 compares the average active power-loss. The

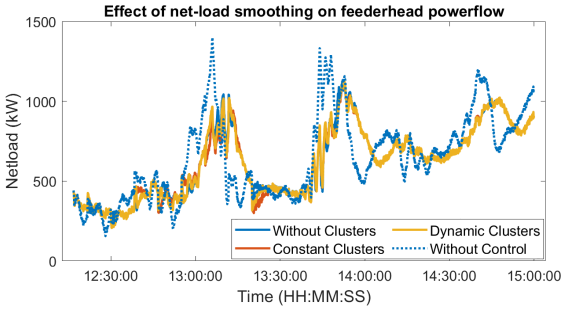

Figure 15: Feeder-head power-flow for net-load smoothing application

losses, as expected, are higher for distributed optimization-based control approach followed by centralized controls. It is to be noted here, that smoothing applications do not have significant power requirements. The reduction in the losses would be higher for applications like net-load minimization. Fig. 17 compares the feeder power flow obtained using cluster dynamic control with distributed optimization-based approach. The overlapping of the feeder-head profile validates the consistency of the distributed control approaches. Fig. 18 compares the voltage

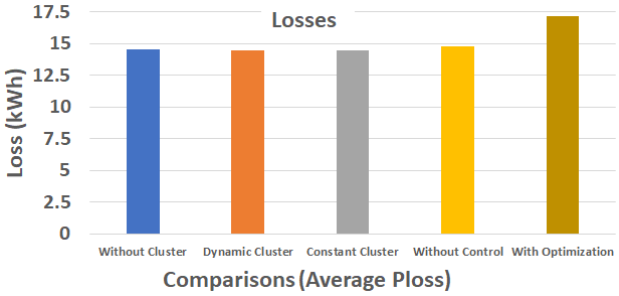

Figure 16: System active power losses

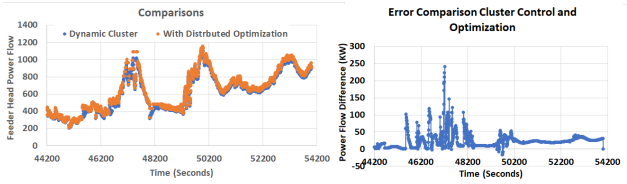

Figure 17: Comparion between Distributed Optimization and Clustering-based Distributed Optimal Control

variations at all nodes on the distribution feeders. The nodes after 75 are near the end of the feeder. Here, the x/r ratio is higher, and hence the voltage variations are also high. The centralized control does not address the variations in the load locally. Hence, a higher voltage variation is observed for the centralized control approach. Constant and dynamic cluster configurations show almost similar variations in the voltage magnitude.
Fig. 19 and fig. 20 shows the cluster net-load for static and dynamic clustering approaches. Since the dynamic clustering, re-configures the clusters with an improved balance of the net-load, the magnitude of cluster net-load is low. The current approach does not minimize the

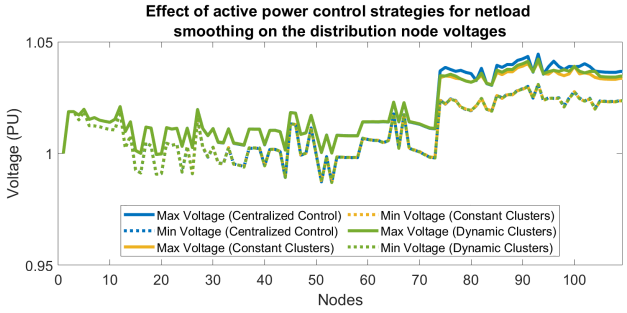

Figure 18: Effect of active power control strategies for net-load smoothing on the distribution node voltages

netload. The balance of load and generation is achieved through re-clustering by the improved spectral clustering-based approach. The improvement in the magnitude of the cluster net-load is summarized in Table 5. The values represent the kW netload. The lower magnitude of the net load denotes a better load-generation balance within the cluster. Here, the imbalance in cluster 4 is marginally higher compared to the constant cluster scenario. However, the net load on the remaining clusters reduces significantly, thereby representing an optimal cluster configuration.

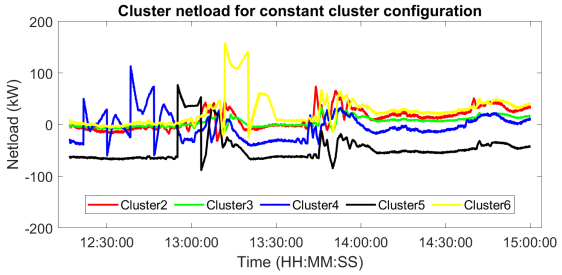

Figure 19: Cluster net-load for constant cluster configuration.

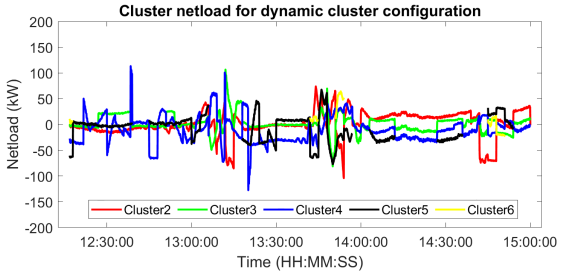

Figure 20: Cluster net-load for dynamic cluster configuration.

Table 5: Improvement in the cluster net-load support through dynamic clustering

	Constant Clusters	Dynamic Clusters
Cluster 2	11.2 kW	0.894 kW
Cluster 3	5.47 kW	1.2 kW
Cluster 4	4.04 kW	9.9 kW
Cluster 5	46.53 kW	7.9 kW
Cluster 6	26.27 kW	11.26 kW

5.4 Evaluation of Distributed cluster real and reactive power control for net-load management

Figure 21 and Figure 22 shows the voltage variation at BESS (measurement node) node and load (non measurement node) node respectively with and without voltage control. It can be observed that the voltage variations are substantially reduced with the PQ control. The voltage profile is flatter when compared with other types of scenarios. The plot also compares the voltage variation of dynamically varying clusters against the constant clusters and without clusters (centralized control). A decrease in the losses was observed in the case of dynamic cluster-based voltage management. The losses can further be reduced by introducing the voltage set-points from the power flow.

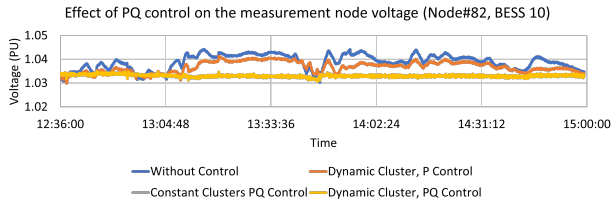

Figure 21: Effect of PQ control on the measurement node voltage (Node-82, BESS 10)

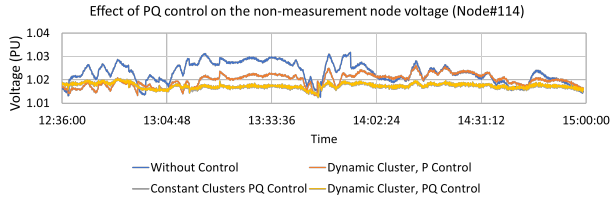

Figure 22: Effect of PQ control on the non-measurement node voltage (Node114)

5.5 Evaluation of scalability of the approach on IEEE 8500 node system

The section demonstrates the scalability of the approach. Here, the proposed approach is implemented on the IEEE 8500 node system for constant and dynamically varying cluster configurations with a simulation window increased to 6 hours. Fig. 23 shows the snapshot of

cluster formation on an IEEE 8500 node system with DERs. Fig. 24 shows the resulting feeder head net-load with cluster control. Based on the "1-minute" smoothing index, the proposed approach of cluster control reduces the intermittencies by 36%. Fig. 25 shows the netload smoothing at cluster level for 4 clusters of 8500 node system. Fig. 26 shows the envelope of BESS SOC for constant and dynamic cluster configuration. The inter-cluster segregating algorithm keeps the variation of the SOC for all BESS between 35% and 70%, a healthy operating range for BESS.

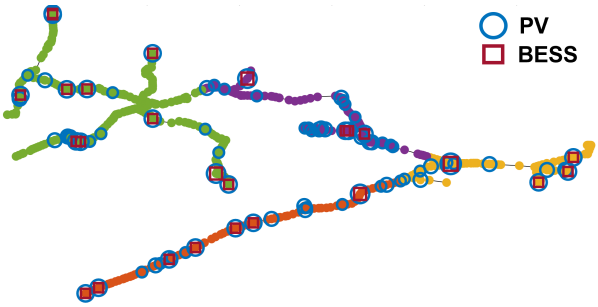

Figure 23: Cluster configuration.

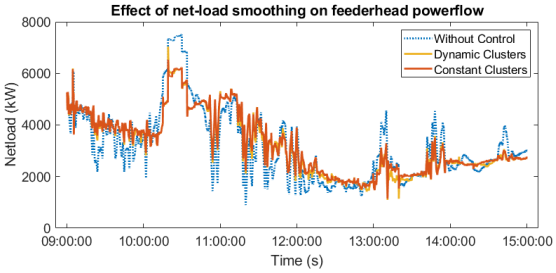

Figure 24: Cluster feeder head net-load.

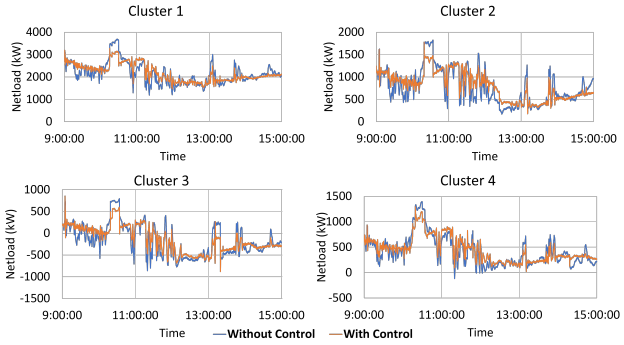

Figure 25: Cluster net-load smoothing.

6 Conclusions

This paper proposes a new distributed control approach for DERs on the distribution grid. Here, the distribution grid is divided into small clusters with DERs using an improved active

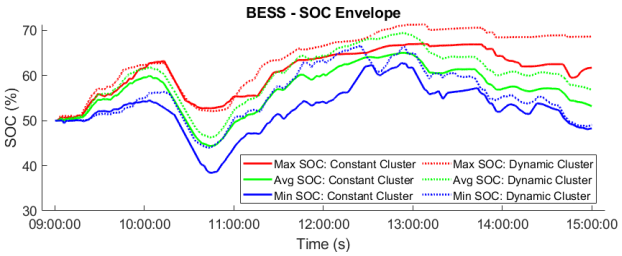

Figure 26: BESS SoC envolope.

power flow-based spectral clustering approach. The proposed spectral clustering approach accurately identifies the clusters with a balance of load and generation. Each cluster is then assigned a virtual controller which manages the DERs within the clusters to reduce the intermittencies in the netload. The state of charge (SOC) of BESS within each cluster is also managed efficiently and optimally through the proposed inter-cluster set-point segregation method. To address the varying grid conditions, the clusters dynamically vary to identify a new optimal cluster configuration. The net-load balance is further improved through the dynamically varying clusters. The proposed approach of cluster-based distributed control is implemented on IEEE 123 bus system in an OpenDSS-based co-simulation environment. The proposed approach is also implemented on the IEEE 8500 node system to demonstrate scalability.
Imports Cluster Formation from Cluster Management package in RedisPV main framework. Cluster Formation is initialized as cm variable by passing the model as an argument.
Class $dsspowerflow$ is initialized in the RedisPV master script with cm variable in $test_pf$ in the external power flow package. This class initializes the OpenDSS and the Matlab engine. The initialization functions include reading the list of sensors, determining the load criticality level, populating the ratings for BESS and setting the protection zones from external files.

6.1 Distribution Grid Optimal Power Flow Model with Integer Control of Legacy Grid Devices (OPF1)

Voltage and reactive power (volt/var) regulation are critical for the operation of distribution feeders. Conventionally, volt/var regulation is achieved through control of legacy grid devices such as load tap changers (LTCs) and switched capacitors. The deployment of distributed energy resources (DERs), such as energy storage and inverter-based renewable generations, make the volt/var control problem more challenging. Optimal control of legacy volt/var control devices is significantly important to maintain the feeder voltage and reactive power feasibility and to reduce the equipment wear and tear. The computational complexity of volt/var optimization problems is reduced in several ways including the adoption of mixed-integer convex programming (MICP). Integer variables are relaxed generally and rounding heuristics are used in to obtain discrete settings of the LTCs and switched capacitors. However, rounding heuristics are combinatorial in nature that prohibit scalability. A linear grid model is also used in literature utilizing McCormick relaxation to reduce the computational complexity, which renders the volt/var optimization as a mixed-integer linear programming (MILP) problem.
The main objective of this work is to present the computational performance of a DOPF model which combines the well known SOCP based model and exact integer-linear models of legacy

devices for active distribution networks with DERs. The adopted model eliminates the need for McCormick relaxation and iterative bound tightening method, which generally adds to the computational burden. In addition, comprehensive analyses of the MISOCP DOPF model are carried out for single-period and multi-period cases with inter-temporal representation, and considering the control of LTCs and switched capacitors together.

MISOCP DOPF Model: Different MISOCP DOPF models are developed based on the choice of the objective function.

$$\text{Min}: \quad J$$
$$\text{Subject to}:$$
$$\text{LTC Constraints } (3)-(10) \qquad \forall (i,j) \in \mathcal{H}, \forall t \in \mathcal{T} \tag{50}$$
$$\text{Capacitor Constraints } (11) \qquad \forall j \in \mathcal{N}, \forall t \in \mathcal{T} \tag{51}$$
$$p_j^{g,t} - p_j^{d,t} = \sum_{k:(j,k)\in\mathcal{E}} P_{jk}^t - \sum_{i:(i,j)\in\mathcal{E}} \left(P_{ij}^t - r_{ij}\ell_{ij}^t\right), \quad \forall j \in \mathcal{N}, \forall t \in \mathcal{T} \tag{52}$$
$$q_j^{g,t} + q_j^{c,t} - q_j^{d,t} = \sum_{k:(j,k)\in\mathcal{E}} Q_{jk}^t - \sum_{i:(i,j)\in\mathcal{E}} \left(Q_{ij}^t - x_{ij}\ell_{ij}^t\right), \quad \forall j \in \mathcal{N}, \forall t \in \mathcal{T} \tag{53}$$
$$v_j^t = v_i^t - 2\left(r_{ij}P_{ij}^t + x_{ij}Q_{ij}^t\right) + \left((r_{ij})^2 + (x_{ij})^2\right)\ell_{ij}^t, \quad \forall (i,j) \in \mathcal{E} \setminus \mathcal{H}, \forall t \in \mathcal{T} \tag{54}$$
$$v_j^t = v_f^t - 2\left(r_{ij}P_{ij}^t + x_{ij}Q_{ij}^t\right) + \left((r_{ij})^2 + (x_{ij})^2\right)\ell_{ij}^t, \quad \forall (i,j) \in \mathcal{H}, \forall t \in \mathcal{T} \tag{55}$$
$$\left\| \begin{array}{c} 2P_{ij}^t \\ 2Q_{ij}^t \\ \ell_{ij}^t - v_i^t \end{array} \right\|_2 \leq \ell_{ij}^t + v_i^t \qquad \forall (i,j) \in \mathcal{E}, \forall t \in \mathcal{T} \tag{56}$$
$$p_j^{g,t} \in [\underline{p_j}^{g,t}, \overline{p_j}^{g,t}], \; v_j^t \in [\underline{v_j}^t, \overline{v_j}^t], \quad \forall j \in \mathcal{N}', \, t \in \mathcal{T} \tag{57}$$
$$u_i^t \in \{0,1\}, b_{ij,n}^t \in \{0,1\}, z_{ij,nm}^t \in \{0,1\} \qquad \forall i \in \mathcal{N}, \, t \in \mathcal{T} \tag{58}$$

where $p_j^{g,t}$ ($q_j^{g,t}$) and $p_j^{d,t}$ ($q_j^{d,t}$) are the real (reactive) power generation and demand respectively at bus j. P_{ij}^t and Q_{ij}^t represent the sending-end real and reactive power flowing on the line (i,j) at time t. $\mathcal{N}'$ is the set of nodes excluding the substation node. In the formulation, (19) represents LTC model, (20) represents switched capacitor constraint, real and reactive power balance equations are given by (21) and (22), voltage drop equations for line segments and LTC branches are given by (23) and (24), respectively. Second-order cone constraint are given by (25), which relates the node voltage and branch current with branch power flow variables. Variable bounds and integrality constraints are provided by (26) - (27).
OPF model with objective function J_2 is obtained by introducing the quadratic deviation term as second order cone constraint in (28) as follows,

$$\text{Min}: \quad J_2$$
$$\text{Subject to}:$$
$$\text{Constraints } (19)-(27)$$
$$\left\| \begin{array}{c} 2(v_i^t - v_i^{\text{nom}}) \\ \Delta\mathcal{V}_i^t - 1 \end{array} \right\|_2 \leq \Delta\mathcal{V}_i^t + 1, \quad \forall i \in \mathcal{N}', \forall t \in \mathcal{T} \tag{59}$$

6.2 Distribution Grid Optimal Power Flow Model with Continuous Variables (OPF2)

SOCP version of centralized three-phase DOPF is built using the dispatch of distributed PV for voltage regulation in distribution network. The mathematical model of PF1 is provided next.

Sets:

$\mathcal{T}$: Time Index Set, $\mathcal{T} = \{1, \ldots, \mathsf{T}\}$
$\mathcal{N}$: Bus set, $\mathcal{N} = \{1, \ldots, \mathsf{N}\}$
$\mathcal{E}$: Branch set, $\mathcal{E} = \{(i,j) : (i,j) \in \ \mathcal{N}\}$
$\mathcal{H}$: LTC branch set, $\mathcal{H} = \{(i,j) : (i,j) \in \ \mathcal{E}\}$
$\mathcal{N}_{\mathsf{PV}}$: PV gen. set, $\mathcal{N}_{\mathsf{PV}} = \{i : i \in \ \mathcal{N}\}$
Φ_i : Bus phase set, $\Phi_i = \{\phi : \phi \in \{a,b,c\}\}$
Φ_{ij} : Branch phase set, $\Phi_{ij} = \{\phi : \phi \in \{a,b,c\}\}$

Parameters:

r_{ij}^{ϕ} : Resistance of line segment (i,j) at phase ϕ
x_{ij}^{ϕ} : Reactance of line segment (i,j) at phase ϕ
$p_{d,i}^{\phi,t}$: Active power demand at bus i phase ϕ
$q_{d,i}^{\phi,t}$: Reactive power demand at bus i phase ϕ
$q_{c,i}^{\phi,t}$: Capacitive power support at bus i phase ϕ
$tap_{ij}^{\phi,t}$: Tap setting of LTC at (i,j) phase ϕ
$S_{g,j}^{rated,\phi}$: Rating of PV inverter at bus i phase ϕ

Variables:

$v_i^{\phi,t}$: Magnitude-squared of voltage at bus i phase ϕ
$\ell_{ij}^{\phi,t}$: Magnitude-squared of current flowing through line segment (i,j) at phase ϕ
$P_{ij}^{\phi,t}$: Sending-end active power flow of line (i,j) at phase ϕ
$Q_{ij}^{\phi,t}$: Sending-end reactive power flow of line (i,j) at phase ϕ
$p_{g,i}^{\phi,t}$: Active power gen. at bus i phase ϕ
$q_{g,i}^{\phi,t}$: Reactive power gen. at bus i phase ϕ

DOPF-2 Formulation:

$$\text{Min}: \quad J$$
$$\text{Subject to}:$$
$$p_{g,j}^{\phi,t} - p_{d,j}^{\phi,t} = \sum_{k:(j,k)\in\mathcal{E}} P_{jk}^{\phi,t} - \sum_{i:(i,j)\in\mathcal{E}} \left(P_{ij}^{\phi,t} - r_{ij}^{\phi} \ell_{ij}^{\phi,t} \right), \quad \forall j \in \mathcal{N}, \forall \phi \in \Phi_j, \forall t \in \mathcal{T} \tag{60}$$
$$q_{g,j}^{\phi,t} + q_{c,j}^{\phi,t} - q_{d,j}^{\phi,t} = \sum_{k:(j,k)\in\mathcal{E}} Q_{jk}^{\phi,t} - \sum_{i:(i,j)\in\mathcal{E}} \left(Q_{ij}^{\phi,t} - x_{ij}^{\phi} \ell_{ij}^{t} \right), \quad \forall j \in \mathcal{N}, \forall \phi \in \Phi_j, \forall t \in \mathcal{T} \tag{61}$$
$$v_j^{\phi,t} = v_i^{\phi,t} - 2\left(r_{ij}^{\phi} P_{ij}^{\phi,t} + x_{ij}^{\phi} Q_{ij}^{\phi,t} \right) + \left((r_{ij}^{\phi})^2 + (x_{ij}^{\phi})^2 \right) \ell_{ij}^{\phi,t}, \forall (i,j) \in \mathcal{E} \setminus \mathcal{H}, \forall \phi \in \Phi_{ij}, \forall t \in \mathcal{T} \tag{62}$$
$$v_{f_{ij}}^{\phi,t} = v_i^{\phi,t} - 2\left(r_{ij}^{\phi} P_{ij}^{\phi,t} + x_{ij}^{\phi} Q_{ij}^{t} \right) + \left((r_{ij}^{\phi})^2 + (x_{ij}^{\phi})^2 \right) \ell_{ij}^{\phi,t}, \forall (i,j) \in \mathcal{H}, \forall \phi \in \Phi_{ij}, \forall t \in \mathcal{T} \tag{63}$$
$$v_j^{\phi,t} = v_{f_{ij}}^{\phi,t} (1 + tap_{ij}^{\phi,t} \cdot \Delta S)^2 \quad \forall (i,j) \in \mathcal{H}, \forall \phi \in \Phi_{ij}, \forall t \in \mathcal{T} \tag{64}$$
$$\left\| \begin{array}{l} 2P_{ij}^{\phi,t} \\ 2Q_{ij}^{\phi,t} \\ \ell_{ij}^{\phi,t} - v_i^{\phi,t} \end{array} \right\|_2 \leq \ell_{ij}^{\phi,t} + v_i^{\phi,t} \qquad \forall (i,j) \in \mathcal{E}, \forall \phi \in \Phi_{ij}, \forall t \in \mathcal{T} \tag{65}$$
$$0 \leq p_{g,j}^{\phi,t} \leq \overline{p_{g_j}}^{\phi,t}, \quad \forall j \in \mathcal{N}_{\mathsf{PV}}, \forall \phi \in \Phi_j, \forall t \in \mathcal{T} \tag{66}$$
$$\underline{q_{g_j}}^{\phi,t} \leq p_{g,j}^{\phi,t} \leq \overline{q_{g_j}}^{\phi,t}, \quad \forall j \in \mathcal{N}_{\mathsf{PV}}, \forall \phi \in \Phi_j, \forall t \in \mathcal{T} \tag{67}$$
$$(p_{g,j}^{\phi,t})^2 + (q_{g,j}^{\phi,t})^2 \leq S_{g,j}^{rated,\phi}, \quad \forall j \in \mathcal{N}_{\mathsf{PV}}, \forall \phi \in \Phi_j, \forall t \in \mathcal{T} \tag{68}$$
$$p_{g,j}^{\phi,t} \in [\underline{p_{g_j}}^{\phi,t}, \overline{p_{g_j}}^{\phi,t}],\ q_{g_j}^{\phi,t} \in [\underline{q_{g_j}}^{\phi,t}, \overline{q_{g_j}}^{\phi,t}],\ v_j^{\phi,t} \in [\underline{v}_j^{t}, \overline{v}_j^{\phi,t}], \quad \forall j \in \mathcal{N}', \forall \phi \in \Phi_j, t \in \mathcal{T} \tag{69}$$

Three-phase DOPF formulation is given by (60)-(69) where the loss minimization objective is considered as,

$$J = \sum_{t\in\mathcal{T}} \sum_{(i,j)\in\mathcal{E}} r_{i,j}^{\phi} \ell_{i,j}^{\phi,t} \tag{70}$$

6.3 Distributed Version of Distribution Grid Optimal Power Flow Model with Continuous Variables (OPF2-Distributed)

In a three-phase network, the power flow can be modelled by the following *LinDist3Flow* formulation in (71)-(73), and is sufficient for approximating bus voltages in unbalanced distribution systems.

$$p_j^{\psi} = \sum_{k:j\to k} P_{jk}^{\psi} - \sum_{i:i\to j} P_{ij}^{\psi}, \quad \forall j \in \mathcal{B}, \forall \psi \in \mathbf{\Psi}_j \tag{71a}$$
$$q_j^{\psi} = \sum_{k:j\to k} Q_{jk}^{\psi} - \sum_{i:i\to j} Q_{ij}^{\psi}, \quad \forall j \in \mathcal{B}, \forall \psi \in \mathbf{\Psi}_j. \tag{71b}$$

$$v_i^{\psi} = v_j^{\psi} - \mathbb{H}_{ij}^{P} P_{ij}^{\phi} - \mathbb{H}_{ij}^{Q} Q_{ij}^{\phi}, \forall (i,j) \in \mathcal{L},\ \forall \psi \in \mathbf{\Psi}_{ij},\ \forall \phi \in \mathbf{\Phi}_{ij} \tag{72}$$

where,

$$\mathbb{H}_{ij}^{P} = \begin{bmatrix} -2r_{ij}^{aa} & r_{ij}^{ab} - \sqrt{3}x_{ij}^{ab} & r_{ij}^{ac} + \sqrt{3}x_{ij}^{ac} \\ r_{ij}^{ba} + \sqrt{3}x_{ij}^{ba} & -2r_{ij}^{bb} & r_{ij}^{bc} - \sqrt{3}x_{ij}^{bc} \\ r_{ij}^{ca} - \sqrt{3}x_{ij}^{ca} & r_{ij}^{cb} + \sqrt{3}x_{ij}^{cb} & -2r_{ij}^{cc} \end{bmatrix} \tag{73a}$$

$$\mathbb{H}_{ij}^{Q} = \begin{bmatrix} -2x_{ij}^{aa} & x_{ij}^{ab} + \sqrt{3}r_{ij}^{ab} & x_{ij}^{ac} - \sqrt{3}r_{ij}^{ac} \\ x_{ij}^{ba} - \sqrt{3}r_{ij}^{ba} & -2x_{ij}^{bb} & x_{bc} + \sqrt{3}r_{ij}^{bc} \\ x_{ij}^{ca} + \sqrt{3}r_{ij}^{ca} & x_{ij}^{cb} - \sqrt{3}r_{ij}^{cb} & -2x_{ij}^{cc} \end{bmatrix}. \tag{73b}$$

The PV inverter model is linearized using a polyhedral norm as in (74).

$$\begin{aligned} -\overline{s}_{i,G}^{\psi} \le \cos(l\gamma)\ p_{i,G}^{\psi} + \sin(l\gamma)\ q_{i,G}^{\psi} \le \overline{s}_{i,G}^{\psi} \\ \gamma = \frac{\pi}{k}, \quad l = 1, \cdots, k, \quad \forall i \in \mathcal{B}^{\mathcal{G}},\ \forall \psi \in \mathbf{\Psi}_i. \end{aligned} \tag{74}$$

The following box constraints ensure the active and reactive power capabilities.

$$0 \le p_{i,G}^{\psi} \le \overline{p}_{i,G}, \quad \forall i \in \mathcal{B}^{\mathcal{G}},\ \forall \psi \in \mathbf{\Psi}_i \tag{75}$$

$$-\overline{q}_{i,G} \le q_{i,G}^{\psi} \le \overline{q}_{i,G}, \quad \forall i \in \mathcal{B}^{\mathcal{G}},\ \forall \psi \in \mathbf{\Psi}_i. \tag{76}$$

The objective for the OPF is to minimize the voltage deviation of the bus voltages from the nominal system voltage.

$$\text{Min} \quad \Delta v_i \tag{77}$$

$$\text{Subject to :}$$

$$v_i - v_0 \le \Delta v_i, \quad \forall i \in \mathcal{B} \tag{78}$$

$$v_0 - v_i \le \Delta v_i. \quad \forall i \in \mathcal{B} \tag{79}$$

Suppose that the distribution network is divided into R areas where each area is indexed by $A = \{1, 2, ..., R\}$ and $A \in \mathcal{A}$. Let $\mathcal{B}^A$ represent the set of buses in area A. Considering the linkage of area A with other areas, the bus set $\mathcal{B}^A$ is then elongated to bus set $\hat{\mathcal{B}}^A$ which comprises $\mathcal{B}^A$ and the interlinking bus of its neighboring area.
Let M_i denote the set of the indices of the areas that contain bus i, i.e. $M_i := \{A | i \in \hat{\mathcal{B}}^A\}$, and let $|M_i|$ be the cardinality of M_i. Evidently, for any bus i that is intersected by multiple neighboring areas, $|M_i| > 1$. Hence the intersecting bus set is $\mathbb{I} := \{i | M_i > 1\}$.
In the consensus version of the ADMM algorithm, each subsystem or area A solves its local optimization problem by minimizing its local objective function subject to its own local set of constraints which show the relationship between a set of global variables that are shared between area A and its neighboring area via the boundary buses at the intersecting region. Since the distributed optimization algorithm must compute the overall objective of the distribution system, the local optimization problem is subject to the condition that the local variables at the boundary bus must be driven to the same value as the global variables. The problem is

solved iteratively until all local copies eventually converge to the global optimal value.
Let σ_A encompass the state variable vector of all buses enclosed in area A,
ie $\sigma_A := \{p_i^\psi, q_i^\psi, v_i^\psi, P_{ij}^\psi, Q_{ij}^\psi\}$, $\forall A \in \mathcal{A}, \forall i \in \hat{\mathcal{B}}^A$, $\forall \psi \in \mathbf{\Psi}_i$.
For every border bus i which is shared by area A and its neighboring area, area A will observe the state variables of bus i as well as state variables of the boundary bus j of its intersected neighboring area, i.e. $(i,j) \in \hat{\mathcal{B}}^A \cap \mathbb{I}$. Let $\sigma_{A,i}$ denote this local state variable vector. Mathematically, this is written as $\sigma_{A,i} := \{p_i^\psi, q_i^\psi, v_i^\psi, v_j^\psi, P_{ij}^\psi, Q_{ij}^\psi, p_j^\psi, q_j^\psi\}$,
$\forall A \in \mathcal{A}, \forall (i,j) \in \hat{\mathcal{B}}^A \cap \mathbb{I}$, $\forall \psi \in \mathbf{\Psi}_i$.
Let τ_i be the set of global state variables at bus i. Then at optimality, the local copies of variables associated with any bus i (provided that bus i is intersected by two neighboring areas), must be equal to the global state variable of bus i, i.e., $\sigma_{A,i} = \tau_i$, $\forall A \in \mathcal{A}$, $\forall i \in \hat{\mathcal{B}}^A \cap \mathbb{I}$.
ADMM is a distributed algorithm that solves a constrained optimization problem using an augmented Lagrangian function. This section provides an overview of the algorithm. ADMM is written in the following compact form,

$$\text{Min} \sum_{A=1}^{R} f_A(\sigma_A) \tag{80a}$$

$$\text{Subject to :}$$

$$\boldsymbol{g}_A(\sigma_A) \geq 0, \quad \forall A \in \mathcal{A} \tag{80b}$$

$$\boldsymbol{h}_A(\sigma_A) = 0, \quad \forall A \in \mathcal{A} \tag{80c}$$

$$\underline{\sigma}_A \leq \sigma_A \leq \overline{\sigma}_A, \quad \forall A \in \mathcal{A} \tag{80d}$$

$$\sigma_{A,i} = \tau_i, \quad \forall A, \forall i \in \hat{\mathcal{B}}^A \cap \mathbb{I}. \tag{80e}$$

80a refers to the local objective function of each area A; local equality and inequality constraints in area A are given by (80b) and (80c) respectively; box constraints of all state variables in area A are given by (80d); (80e) represents the consensus between local copies of variable vectors and global variables. The augmented Lagrangian function is then formulated as 81.

$$\mathcal{L}_A^{\text{ADMM}} = \sum_{A=1}^{R} f_A(\sigma_A) + \sum_{\forall i \in \hat{\mathcal{B}}^A \cap \mathbb{I}} \left(\lambda_{A,i}^T (\sigma_{A,i} - \tau_i) + \frac{\rho}{2} \|\sigma_{A,i} - \tau_i\|_2^2 \right). \tag{81}$$

$\lambda_{A,i}$ represents the dual variable associated with (80e). The quadratic terms in (81) denote the penalty for local variables deviating from global variables. The ADMM algorithm is solved iteratively until convergence is achieved. Each iteration k consists of the following three steps:

- Minimization step:

$$\text{Min} \quad \mathcal{L}_A^{\text{ADMM}}$$
$$\text{Subject to :}$$
$$\text{Constraints 71-76, 78-79}, \quad \forall i \in \hat{\mathcal{B}}^A.$$

- Averaging step : $\tau_i(k+1) = \frac{1}{2} \sum_{\forall i \in \hat{\mathcal{B}}^A \cap \mathbb{I}} (\sigma_{A,i}(k+1) + (1/\rho)\lambda_{A,i}(k))$
- Dual variables update step: $\lambda_{A,i}(k+1) = \lambda_{A,i}(k) + \rho(\sigma_{A,i}(k+1) - \tau_i(k+1)), \forall i \in \hat{\mathcal{B}}^A \cap \mathbb{I}$.

The convergence criteria are determined by checking that the primal residual, $e(k)$, and dual residual, $d(k)$, are less than a predefined tolerance ϵ, given that
$e(k) := \left\{ \left| \sigma_{A,i}(k) - \tau_i(k) \right|, \forall A, \forall \hat{\mathcal{B}}^A \cap \mathbb{I} \right\}$, and $d(k) := \left\{ \left| \tau_i(k) - \tau_i(k-1) \right|, \forall A, \forall \hat{\mathcal{B}}^A \cap \mathbb{I} \right\}$.

6.4 Distribution Grid OPF with Network Reconfiguration (OPF-R)

Distribution Network Reconfiguration for Unbalanced Distribution Networks: The model is established on a linearized representation of 3-phase power flow model, known as *LinDist3Flow*, which includes multi-phase coupling. The discrete operation of load tap-changers of voltage regulators are also included in the devised optimal reconfiguration formulation so that effective voltage regulation can be implemented. The overall formulation is provided next.

$$\text{Min}: \sum_{t\in\mathcal{T}} \sum_{\phi\in\Phi_{iinN\setminus\mathcal{N}'}} P_{g,i}^{\phi,t} \tag{83}$$

$$\text{Subject to}:$$

$$p_{g,j}^{\phi,t} - p_{d,j}^{\phi,t} = \sum_{k:(j,k)\in\mathcal{E}} P_{jk}^{\phi,t} - \sum_{i:(i,j)\in\mathcal{E}} P_{ij}^{\phi,t}, \quad \forall j \in \mathcal{N}, \forall \phi \in \Phi_j, \forall t \in \mathcal{T} \tag{84}$$

$$q_{g,j}^{\phi,t} - q_{d,j}^{\phi,t} = \sum_{k:(j,k)\in\mathcal{E}} Q_{jk}^{\phi,t} - \sum_{i:(i,j)\in\mathcal{E}} Q_{ij}^{\phi,t}, \quad \forall j \in \mathcal{N}, \forall \phi \in \Phi_j, \forall t \in \mathcal{T} \tag{85}$$

$$v_j^{\phi,t} \le M(1-\alpha_{ij}^t) + v_i^{\phi,t} + \sum_{\gamma\in\Phi_{ij}} \mathbb{H}_{ij}^P(\phi,\gamma)\, P_{ij}^{\gamma,t} + \sum_{\gamma\in\Phi_{ij}} \mathbb{H}_{ij}^Q(\phi,\gamma)\, Q_{ij}^{\gamma,t}, \ \forall (i,j) \in \mathcal{E} \setminus \mathcal{E}_R, \phi \in \Phi_{ij}, \forall t \in \mathcal{T} \tag{86}$$

$$v_j^{\phi,t} \ge -M(1-\alpha_{ij}^t) + v_i^{\phi,t} + \sum_{\gamma\in\Phi_{ij}} \mathbb{H}_{ij}^P(\phi,\gamma)\, P_{ij}^{\gamma,t} + \sum_{\gamma\in\Phi_{ij}} \mathbb{H}_{ij}^Q(\phi,\gamma)\, Q_{ij}^{\gamma,t}, \ \forall (i,j) \in \mathcal{E} \setminus \mathcal{E}_R, \phi \in \Phi_{ij}, \forall t \in \mathcal{T} \tag{87}$$

$$-\alpha_{ij}^t \overline{P_{ij}} \le P_{ij}^{\phi,t} \le \alpha_{ij}^t \overline{P_{ij}}, \quad \forall (i,j) \in \mathcal{E}, \phi \in \Phi_{ij}, \forall t \in \mathcal{T} \tag{88}$$

$$-\alpha_{ij}^t \overline{Q_{ij}} \le Q_{ij}^{\phi,t} \le \alpha_{ij}^t \overline{Q_{ij}}, \quad \forall (i,j) \in \mathcal{E}, \phi \in \Phi_{ij}, \forall t \in \mathcal{T} \tag{89}$$

$$\sum_{(i,j)\in\mathcal{E}} \alpha_{ij}^t = |\mathcal{N}| - 1, \quad \forall t \in \mathcal{T} \tag{90}$$

$$\beta_{ij}^t + \beta_{ji}^t = \alpha_{ij}^t, \quad \forall (i,j) \in \mathcal{E}, \forall t \in \mathcal{T} \tag{91}$$

$$\sum_{j\in\mathcal{N}(i)} \beta_{ij}^t = 1, \quad \forall i \in \mathcal{N}', \forall t \in \mathcal{T} \tag{92}$$

$$\beta_{ij}^t = 0, \quad \forall i \in \mathcal{N} \setminus \mathcal{N}' \tag{93}$$

$$\alpha_{ij}^t = 1, \quad \forall (i,j) \in \mathcal{E} \setminus \mathcal{E}_S, \forall t \in \mathcal{T} \tag{94}$$

$$\text{LTC Model}(i,j,\phi,t), \quad \forall (i,j) \in \mathcal{E}_R, \forall \phi \in \Phi_{ij}, \forall t \in \mathcal{T} \tag{95}$$

$$\text{PV Generation Model}(j,\phi,t), \quad \forall j \in \mathcal{N}_{\text{PV}}, \forall \phi \in \Phi_j^{\text{PV}}, \forall t \in \mathcal{T} \tag{96}$$

$$\text{Battery Storage Model}(j,\phi,t), \quad \forall j \in \mathcal{N}_{\text{BSS}}, \forall \phi \in \Phi_j^{\text{BSS}}, \forall t \in \mathcal{T} \tag{97}$$

$$p_{g,j}^{\phi,t} = p_{\text{PV},j}^{\phi,t} + p_{\text{BSS},j}^{\phi,t}, \quad j \in \mathcal{N}, \forall \phi \in \Phi_j, \forall t \in \mathcal{T} \tag{98}$$

$$q_{g,j}^{\phi,t} = q_{\text{PV},j}^{\phi,t} + q_{\text{BSS},j}^{\phi,t}, \quad j \in \mathcal{N}, \forall \phi \in \Phi_j, \forall t \in \mathcal{T} \tag{99}$$

$$p_{g,j}^{\phi,t} \in [p_{g,j}^{\phi,l}, p_{g,j}^{\phi,u}], \ \ q_{g,j}^{\phi,t} \in [q_{g,j}^{\phi,l}, \ q_{g,j}^{\phi,u}], \ \ v_j^{\phi,t} \in [v_j^l, v_j^u], \ \ \forall j \in \mathcal{N}', \forall t \in \mathcal{T} \tag{100}$$

Although the formulation (83)-(100) works well for the networks with single substation, the operation with multiple substations complicates the spanning tree constraints given by (90) - (93). To overcome this limitation the sub-graph connectivity constraint can be formulated via mathematical programming using the single commodity flow method as follows,

$$\sum_{k:(j,k)\in\mathcal{E}} F_{jk}^t - \sum_{i:(i,j)\in\mathcal{E}} F_{ij}^t = -1, \quad \forall j \in \mathcal{N}', \forall t \in \mathcal{T} \tag{101}$$

$$\sum_{k:(j,k)\in\mathcal{E}} F_{jk}^t - \sum_{i:(i,j)\in\mathcal{E}} F_{ij}^t = W_j, \quad \forall i \in \mathcal{N} \setminus \mathcal{N}', \forall t \in \mathcal{T} \tag{102}$$

$$-Mc_{ij}^t \leq F_{ij}^t \leq Mc_{ij}^t, \quad \forall i,j \in \mathcal{E}, \forall t \in \mathcal{T} \tag{103}$$

$$-M(2-c_{ij}^t) \leq F_{ij}^t \leq M(2-c_{ij}^t), \quad \forall i,j \in \mathcal{E}, \forall t \in \mathcal{T} \tag{104}$$

$$W_j^t \geq 1, \quad \forall i \in \mathcal{N} \setminus \mathcal{N}', \forall t \in \mathcal{T}. \tag{105}$$

$$\sum_{(ij)\in\mathcal{E}} c_{ij}^t = |\mathcal{N}| - |\mathcal{N} \setminus \mathcal{N}'|, \quad \forall i \in \mathcal{N} \setminus \mathcal{N}', \forall t \in \mathcal{T}. \tag{106}$$

The spanning constraints (90) - (93) can be replaced by (101) - (106).
In the above formulation, $\mathcal{N}$ indicates the set of buses, $\mathcal{E}$ is the set of branches $\mathcal{E} = \{(i,j) : (i,j) \in \mathcal{N}\}$ where i, j indicate nodes on the feeder. $\mathcal{N}'$ is the set of nodes excluding the substation nodes. $\mathcal{E}_R$ and $\mathcal{E}_S$ are the set of branches of regulators and switches, respectively. $\mathcal{N}_{\text{PV}}$ and $\mathcal{N}_{\text{BSS}}$ are the set of nodes with PV and BSS units, respectively. In addition, Φ_j^{PV} and Φ_j^{BSS} are the phase set for a PV and a BSS units connected to bus j. $v_i^{\phi,t}$ is the magnitude squared node voltage, i.e., $v_i^{\phi,t} = |V_i^{\phi,t}|^2$ and $p_{g,j}^{\phi,t}$ ($q_{g,j}^{\phi,t}$) and $p_{d,j}^{\phi,t}$ ($q_{d,j}^{\phi,t}$) are the real (reactive) power generation and demand respectively at node j phase ϕ time interval t. $P_{ij}^{\phi,t}$ and $Q_{ij}^{\phi,t}$ represent the sending-end real and reactive power respectively flowing on the line (i,j). M refers to a big enough numeric value used for voltage equation relaxation. α_{ij}^t is the line switch status variable indicating 1 if nodes i and j are connected. β_{ij}^t (β_{ji}^t) is a binary variable indicating 1 if node $j(i)$ is parent of node $i(j)$.

6.5 Performance of OPF1 Run in 500 Node Feeder

The metric to evaluate the milestone is in terms of solving time, which should be less than 15 minutes for a test system with 500 nodes, 5 inline voltage regulators, 50 PV inverters. Solve time of 15 minutes is chosen as the LTCs are slower changing devices, which are controlled at sub-hourly intervals; thus, 15 minutes solve for a practical-sized system will suffice for the real-time control purpose. Figure. 27 shows the load and optimized PV profile obtained from the MISOCP model. Figure. 28 shows active power loss on each phase of the feeder with two objective functions J_1 and J_2. Figure. 29 shows voltage histograms, which depict that the nodal voltage is well maintained within the bounds. With $J2$ as an objective, which as the voltage deviation term on the objective function, the voltage was maintained within a narrower band compared to the case with the objective function $J1$. Figure. 30 shows the LTC operations. Solve time taken by a model with J_2 is higher on average compared to J_1. Figure. 31 shows the solve time with the objective function J_2, and the worst case solves time is 100 seconds for one phase and approx. 200 seconds (3.33 minutes) for all three phases, which is substantially less than the desired maximum solution time of 15 minutes.

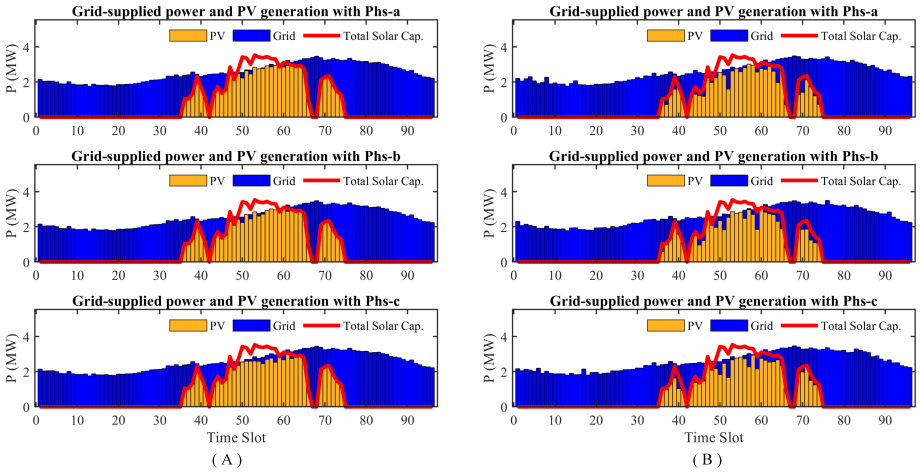

Figure 27: Grid and PV generation profile for each phases A) with J_1 as an objective, and B) with J_2 as an objective.

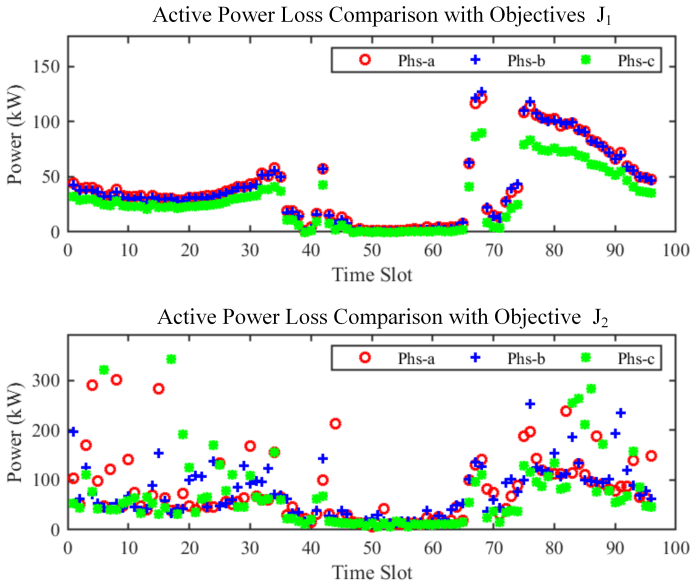

Figure 28: Active power losses for each phases A) with J_1 as an objective, and B) with J_2 as an objective.

6.6 Performance of OPF2 Run in 2500 Node Feeder

We have modeled a SOCP version of distribution OPF and successfully solved the model for a 2522-node system with 114 PV inverters. During the simulation, the optimality gap was set to 0.01%, and the solution time did not exceed 10 seconds. The resulting voltage profile under a zero-tap operation scenario is shown in Figure 33. The simulation codes are files are placed in the shared folder[1].

[1] https://app.box.com/s/cssye0p1wxr5j37xyqtz44y7x46b8ej6

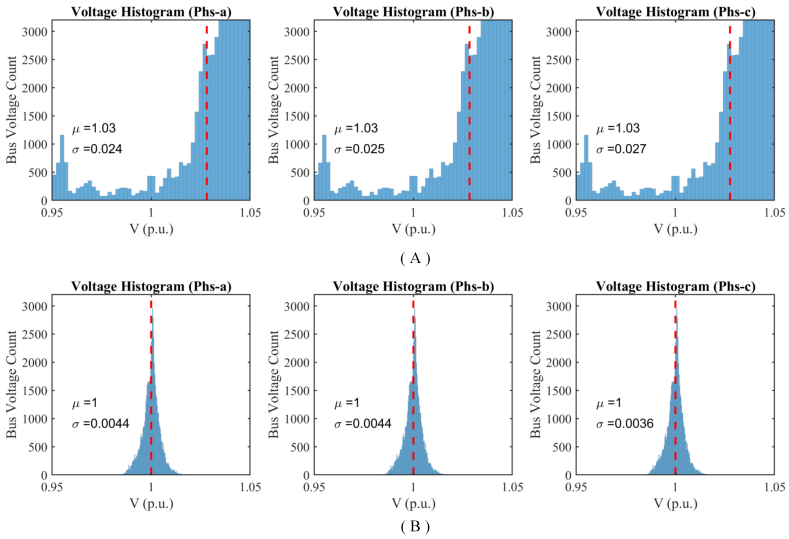

Figure 29: Voltage histograms for each phases A) with J_1 as an objective, and B) with J_2 as an objective.

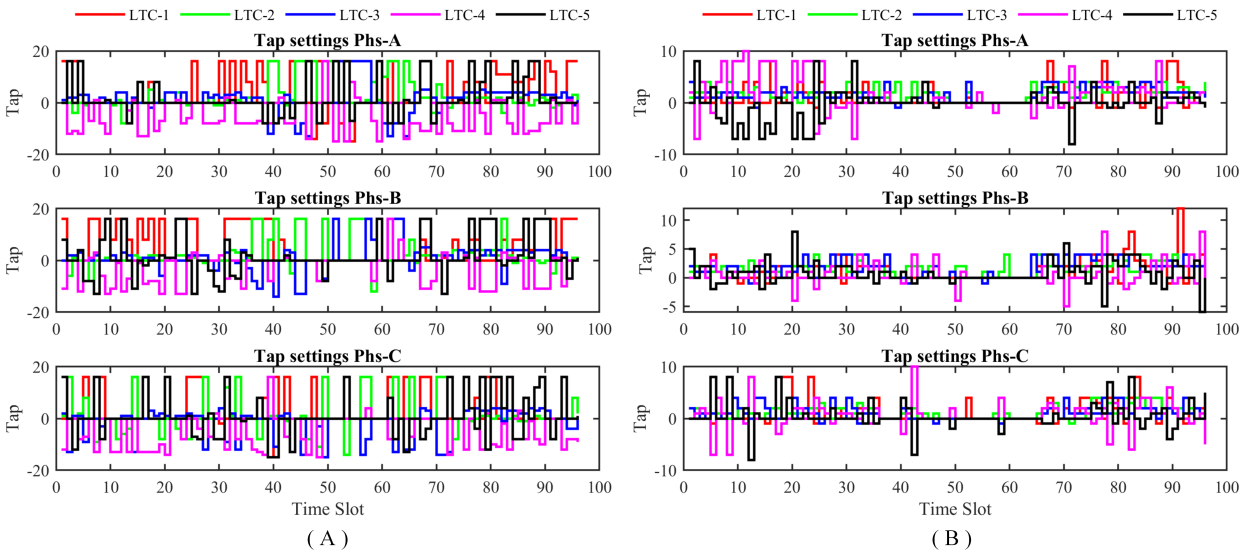

Figure 30: Change of five LTC taps A) with J_1 as an objective, and B) with J_2 as an objective.

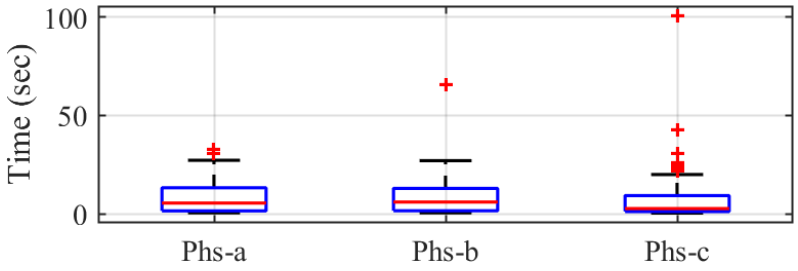

Figure 31: Solve time with J_2 as an objective.

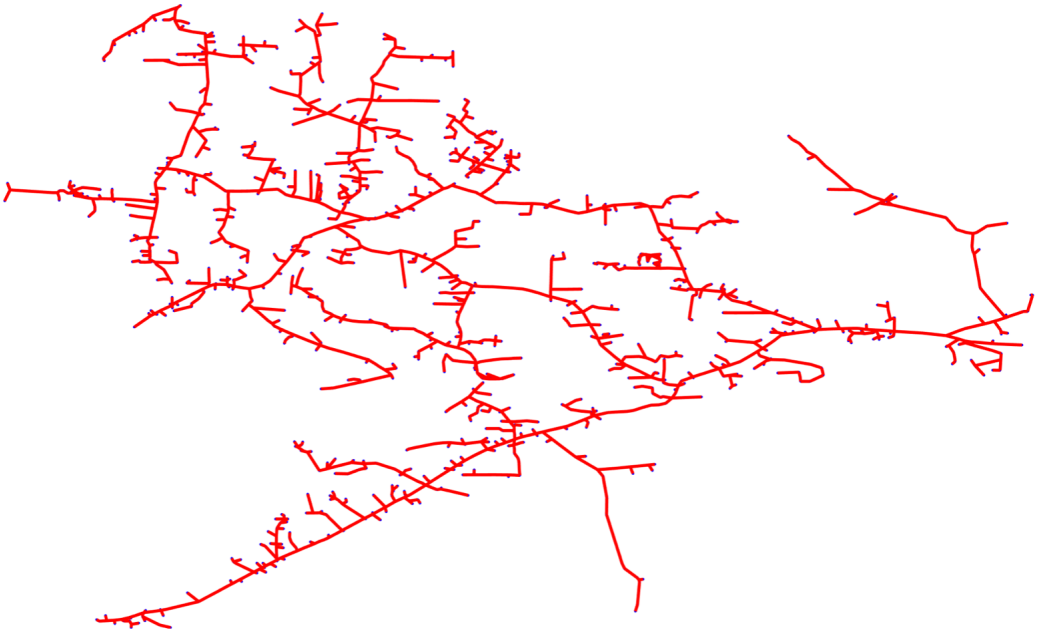

Figure 32: A 2522-node test system obtained by modifying the IEEE 8500-node test system.

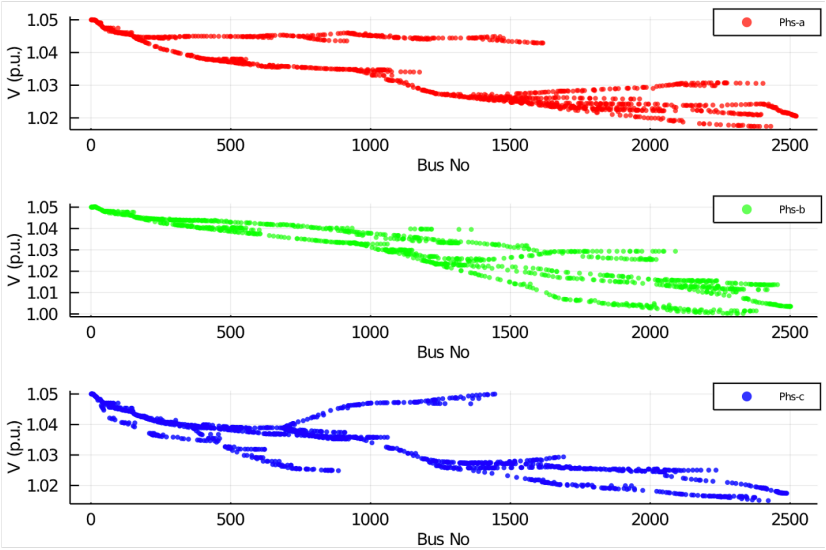

Figure 33: Feeder voltage profile with obtained from SOCP model.

The dispatch of DGs are shown in Figure 34 and total generation, demand and losses are summarized in Table-6.

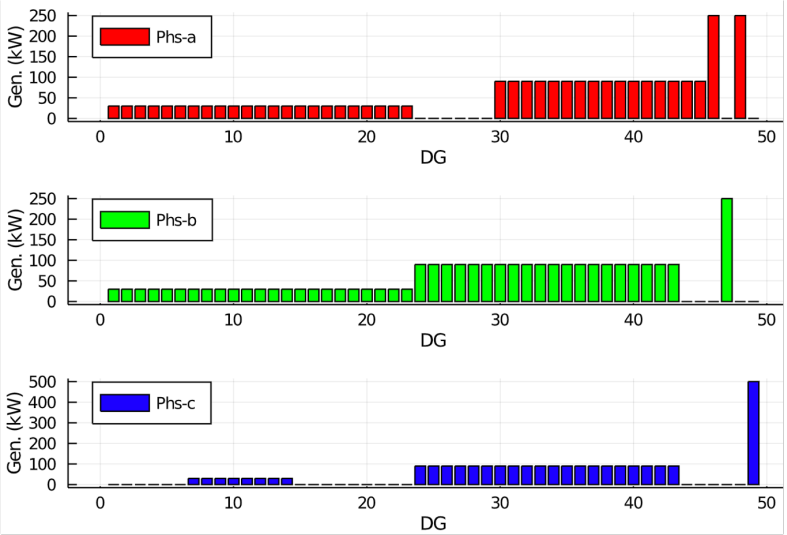

Figure 34: Optimal PV dispatch obtained from SOCP model.

Table 6: Total Gen./Demand/Losses obtained from SOCP model.

	Active Power			Reactive Power		
Phase	a	b	c	a	b	c
Tot. Gen. (MW/MVAr)	3.68	3.71	3.69	1.04	1.07	1.04
Tot. Demand (MW/MVAr)	3.65	3.65	3.65	0.98	0.98	0.98
Tot. Loss. (kW/kVAr)	28.91	55.62	38.7	60.92	94.75	67.12

6.7 Performance of OPF-Distributed Run in 2500 Node Feeder

The convergence and performance of the consensus-based ADMM distributed VVO approach is demonstrated using the 2522-bus system with 142 PV inverters. The network is partitioned into 4 areas with the regional partitioning done based on the location of the voltage regulators as illustrated in Fig. 35.

In Fig. 36, the evolution of the objective function value of the distributed VVO solution is shown in comparison to the centralized solution. The lower the tolerance value set for termination, the more likely it is to obtain an optimal objective value. This is however likely to increase the total number of iterations as a trade-off.

Fig. 37 shows the comparative voltage profiles resulting from solving the centralized and distributed VVO models. In the simulations, we were able to satisfy $< 0.1\%$ of voltage profile error.

Besides the entire voltage profile comparison, it is also valuable to check the convergence of the system variables at the terminals of tie lines connecting neighboring areas. Fig. 38 shows the iteration-wise update in voltage magnitude at branch (628,632) compared to the centralized solution. A satisfactory solution is one in which all global variables and their local copies in the areas converge to the same voltage solutions as the centralized voltage, and this is achieved as the iteration number increases. Hence, the distributed VVO algorithm converges

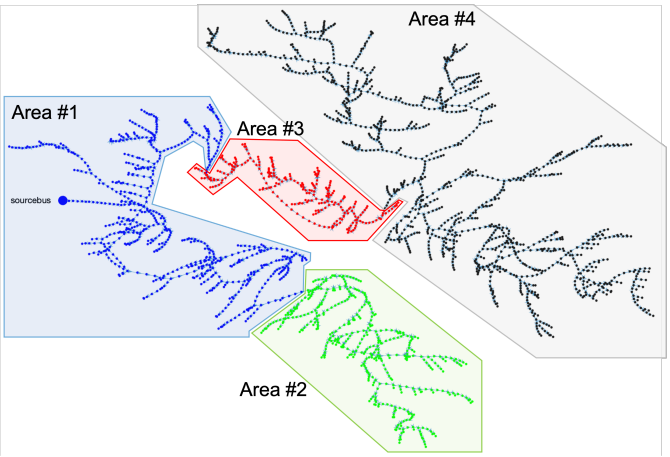

Figure 35: Partitioning of 2522-bus feeder.

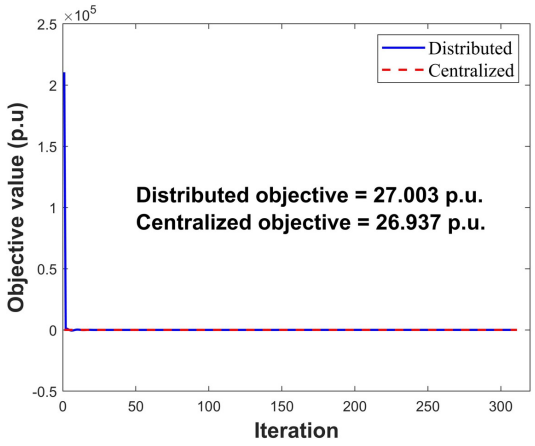

Figure 36: Convergence of objective function: centralized vs. distributed VVO.

to an optimal solution within an acceptable number of 311 iterations. In our simulation, it would take 86.7 seconds for the consensus-based ADMM distributed algorithm to converge assuming that parallel computing is considered.

6.8 Performance of OPF-R Run in 2500 Node Feeder

The computational performance of the overall Optimal Reconfiguration formulation is tested on the modified 2522-bus network as shown in 39.
. Network reconfiguration of 2522-Node feeder forms a large-scale MILP problem with multi-period solution. To reduce the solution complexity and increase the tractability property of the formulation, the 24-hour day split ted into 3 time window, consisting of 8 intervals each of 1-hour. Then, the proposed formulation was run for each time window. All time windows were successfully solved and the switch configurations, PV and BESS units are dispatched. The resulting tap change profile of the regulators are shown in Fig. 40. Since we let optimizer find the initial tap positions, there might be inconsistent tap change transition at the end and

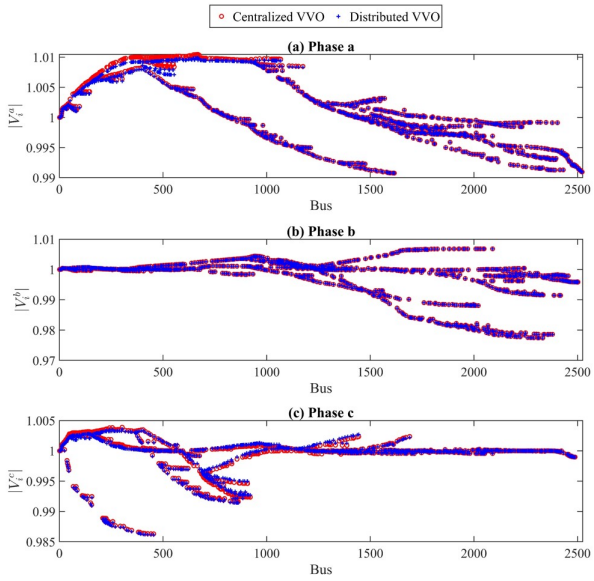

Figure 37: Centralized vs. distributed VVO voltage profile for 2522-bus system.

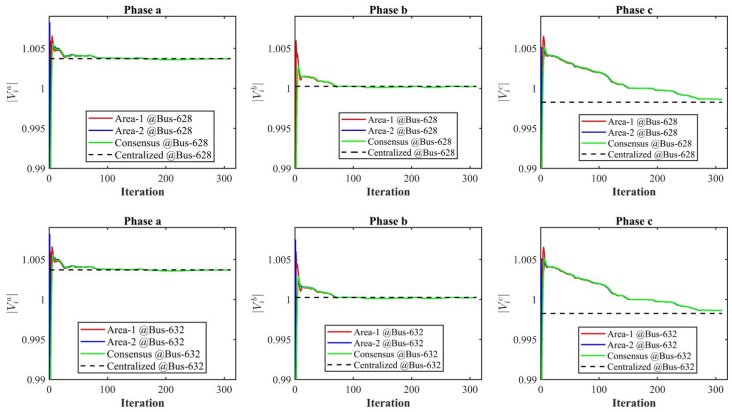

Figure 38: Convergence of voltage solution at branch (628,632).

beginning of the intermediate time windows. However, this can be eliminated by initializing the tap values of the current time window with the solution of the previous time window. It can also be observed that the reconfiguration process does not have significant negative impact on the frequency of tap change within the time window.

Fig. 41 shows per-phase temporal voltage profiles. In the optimization model, the objective function is set as minimizing the total net load. This might have the effect to push the majority of the node voltages to the 1.05 pu level. The voltage positioning can be maintained around 1.0 pu by adding another term in the objective function.

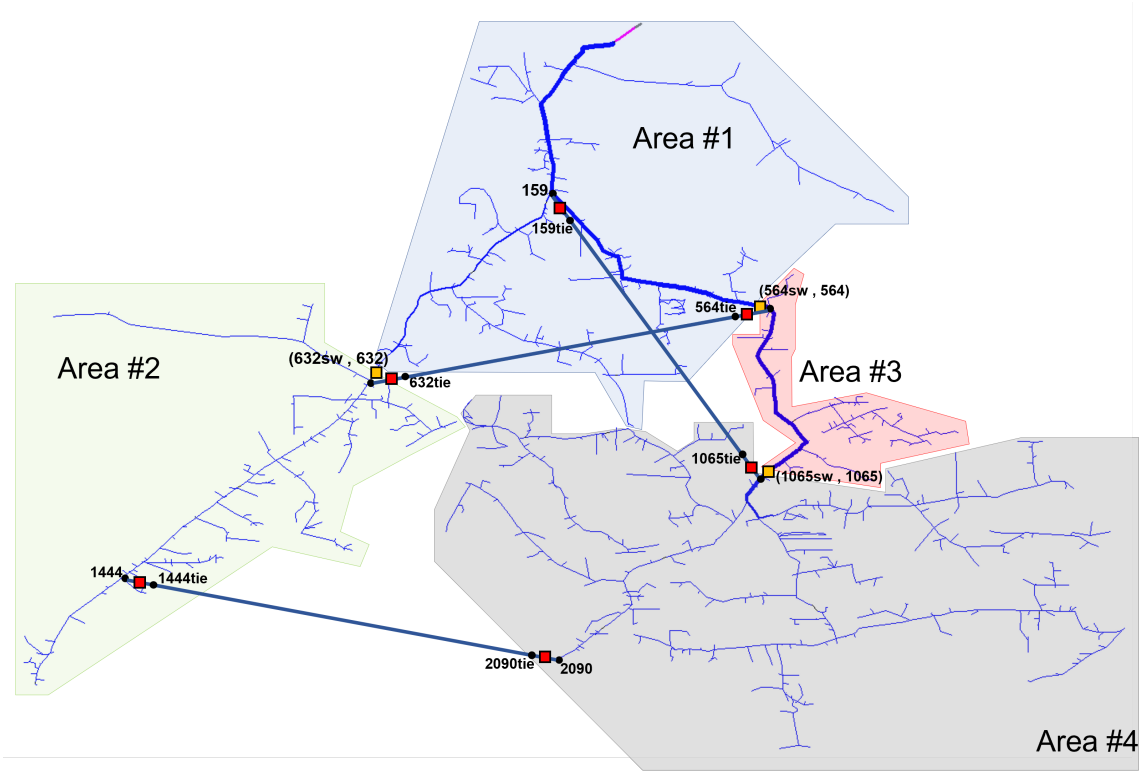

Figure 39: Modified 2522-node circuit.

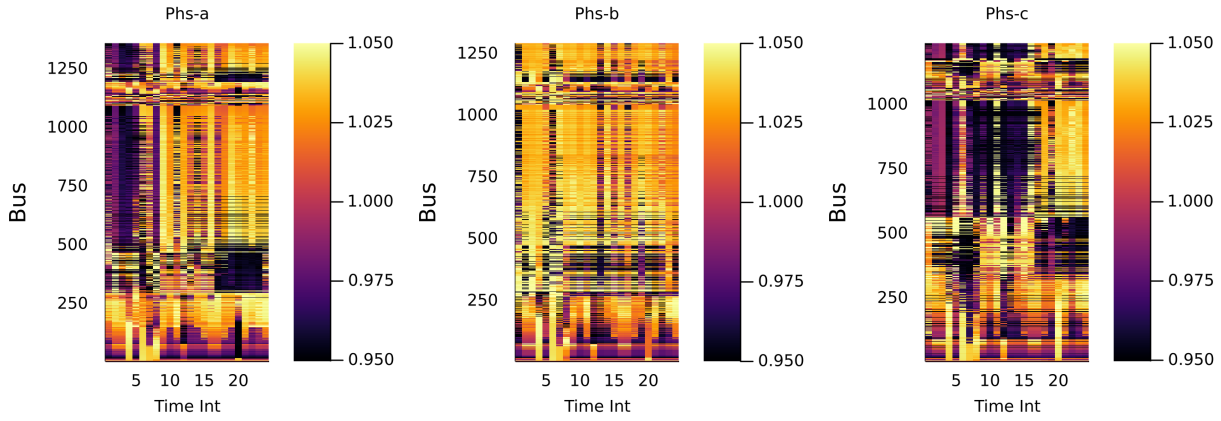

Figure 41: Case: 2522-Bus, Voltage profile over 24-hour operation period.

In the 2522-Node feeder, 148 units of PV-BSSS modules are assumed to be connected at the different nodes. Each PV-BSSS unit is rated 30 kW. The minimum level of the state-of-charge (SOC) is set to 50%. A 60% of initial SOC level is set at the second and third time window. Fig. 42-A shows the PV power generation and PV capacity profiles. It can be observed that the existing PV capacity is being utilized satisfactorily. In Fig. 42-B, SOC level profiles are shown.

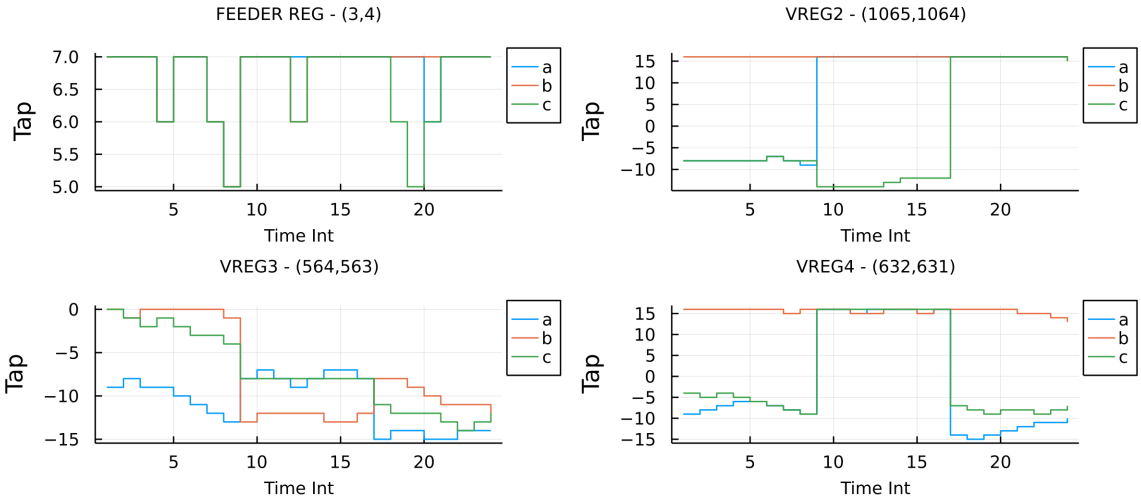

Figure 40: Case: 2522-Bus, Regulator tap position change over 24-hour operation period.

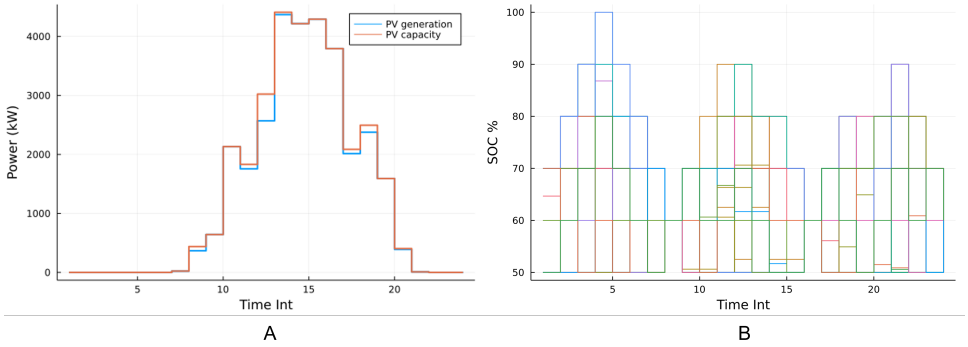

Figure 42: Case: 2522-Bus, PV generation and BESS SOC over 24-hour operation period.

The dynamic switch configuration is shown in Fig. 43. There are 42 switches considered for reconfiguring the network.

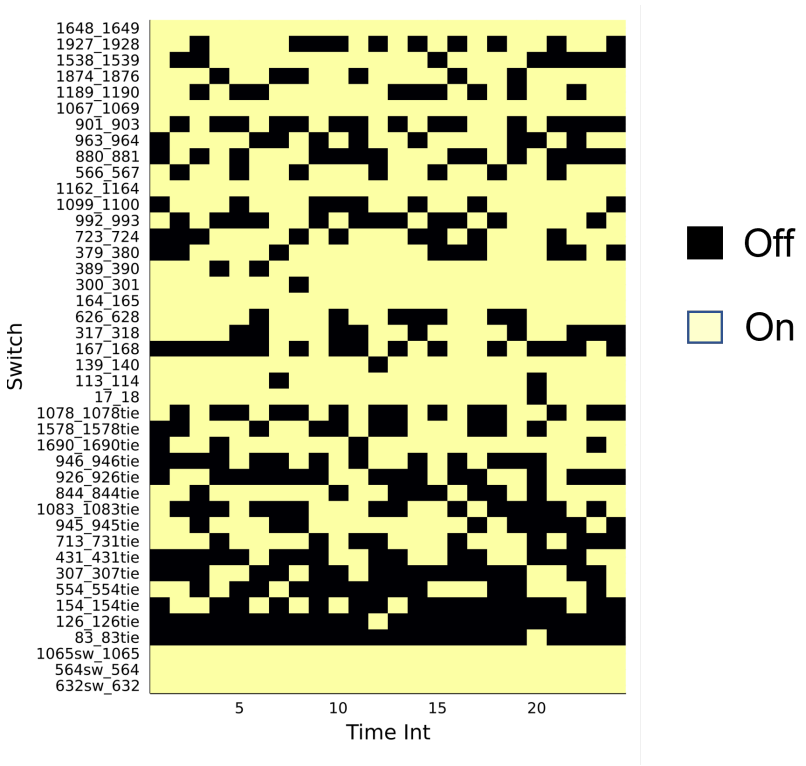

Figure 43: Case: 2522-Bus, Switching pattern 24-hour operation period.

6.9 Architecture

6.9.1 NDN Overview

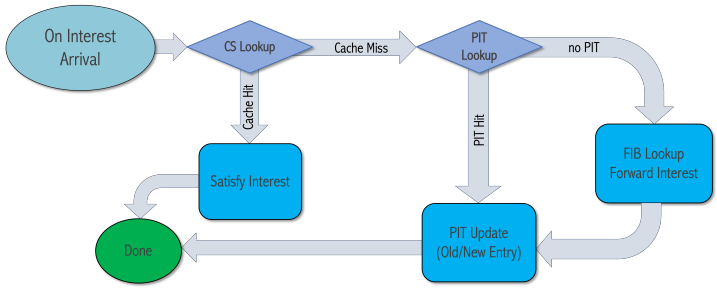

Figure 44: An overview of NDN Architecture

This work uses Named Data Networking (NDN) as it's based architecture. NDN is a pull-based communication architecture that enables a consumer to request data by name from a provider in a secure and resource-efficient manner. In NDN, each piece of data, data chunk, is assigned a unique name, which follows a hierarchical human-readable convention similar to URL addresses. Thus, enabling the consumers to request the data chunks by name and the communication network entities to cache data chunks. In NDN, the network entities forward the consumer's request to the data provider, which returns the requested chunk of data back to the consumer using the reverse path. As the data chunks travels back to the consumer, the network entities decide whether to cache the data chunk or not based on factors, such as

data popularity. NDN's built-in security mandates the data providers to sign their data upon creation, promoting source authenticity and data integrity.
In NDN, each network entity is equipped with a Pending Interest Table (PIT), Forwarding Information Base (FIB), and a Content Store (CS). The content store acts as a temporary cache to store popular data. Similar to the existing routing table, FIB helps with forwarding the request towards the provider. Figure 44 describes an overview of NDN architecture.
NDN's stateful forwarding plane uses PIT to keep track of in-flight requests and further enable request aggregation. NDN also features a strategy layer, which enables flexible and fine-grain forwarding decision-making, such as least-cost path, multi-cast, broadcast, or a customized forwarding strategy for meeting the unique requirements of a given application.

6.9.2 iCAAP: information-Centric network Architecture for Application-specific Prioritization in Smart Grid

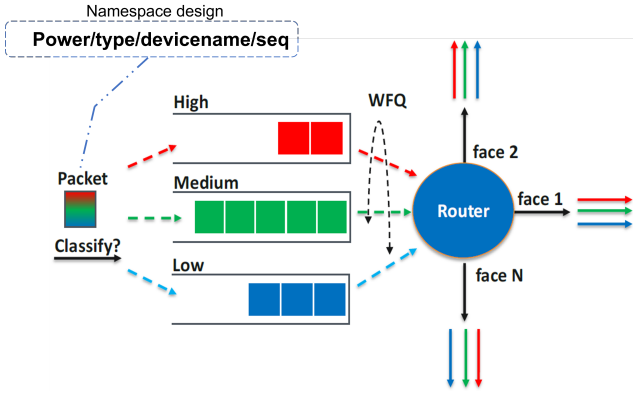

Figure 45: iCAAP Architecture

Figure 45 illustrates iCAAP architecture. iCAAP's design the data naming and forwarding strategy features unique to NDN are leveraged to promote traffic classification and preferential traffic treatment so that expected communication QoS can be achieved. The building blocks of iCAAP include a namespace design that can be generically applied to various smartgrid application, a proposed multi-queuing mechanism, and a QoS-aware strategy.
Namespace Design NDN-enabled routers use the unique names included in each request packet to forward the request to the closest replica of the corresponding data. In NDN, application developers (application providers) design the namespace of their application by including relevant and important name components into a hierarchical name format to facilitate request forwarding and cache lookup. In the iCAAP use-case, data generating entities (e.g., PMUs) send payloaded interests, which carry the generated data as payloads.

6.9.3 Traffic Prioritization

In iCAAP's design, the NDN's naming feature is used to categorize application traffic into three priority classes, as shown in Figure 45, to promote QoS-aware traffic management. The three classes include Type I as high priority, Type II as medium priority, and Type III as low priority. In particular, the Type I provides high reliability and low latency for protection and control signals, Type II provides high reliability for control and information signals, and Type III provides best

effort traffic for all other traffic flows. To encode these priority classes into network traffic, each packet includes its priority class in the “Priority Class” component of the requested data name. To meet the QoS requirements of various traffic classes, there are three distinct priority queues for each interface of every given node–one per priority class–which facilitates traffic prioritization by assigning similar priority traffic to the same queue. Upon arrival at a node, a packet will be pushed into the appropriate queues, and then dequeued when resources are available for packet transmission. The order of dequeuing packets from all queues is determined by the WFQ algorithm as shown below.

6.9.4 Token Bucket

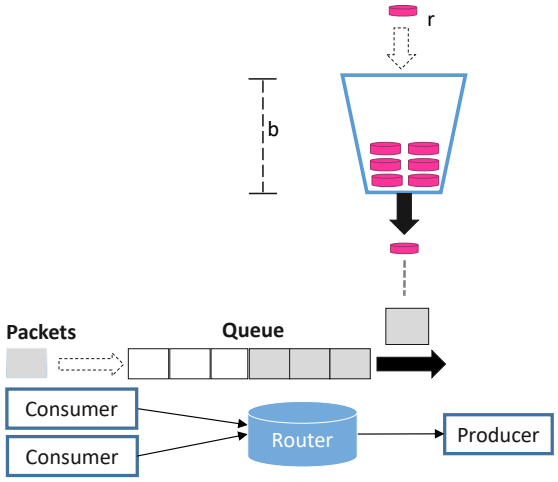

Figure 46: An illustration of token bucket architecture

To shape network traffic and control the communication rate of the traffic classes, iCAAP uses a token bucket algorithm, in which each priority queue is associated with a token bucket (a limited number of tokens). Thus, allowing a packet to be dequeued from the corresponding queue only if a sufficient number of tokens is available for the given queue; one token will be used to dequeue one packet. Each token bucket has a fixed token capacity and a token generation rate. Token generation rates for each priority class is adjusted based on the priority requirements. An illustration of toke bucket implementation and architecture is hown in figure 46. For instance, the Type I priority queue is assigned the highest token generation rate while the Type III priority queue has the lowest token generation rate.

6.9.5 Smart Forwarding strategy

To improve communication reliability, our proposed strategy uses more than one interface for packet forwarding under certain circumstances. More specifically, our strategy uses a subset of interfaces to meet the expected data delivery rates of different traffic classes based on network performance metrics, such as the network congestion and statistical information of interfaces.
Upon receiving the packet (p), the network entity node (router u) extracts the priority class (pClass) of the packet from the Type component of the packet name. Each Type has a unique success probability requirement (spr), intuitively chosen as 100%, 80%, and 0% for Types I, II,

and II respectively. Router u identifies the priority class of p and sets p's probability requirement (pr) based on the class's spr. We note that each interface has a score (Is), which is calculated based on the interface's available bandwidth, observed latency, and packet loss. Router u sorts the interfaces by score with the highest (Is) in front. It then goes down the sorted list L and enqueues p on the interfaces, adding their Is to the probability score ps, until ps is greater than or equal to the pr for p, or we reach the end of L. Router u processes the priority queues using the WFQ algorithm to dequeue the topmost packet p'. In the final step, following the token bucket algorithm, each interface forwards p' when there is a token available.

6.9.6 Co-simulation Framework

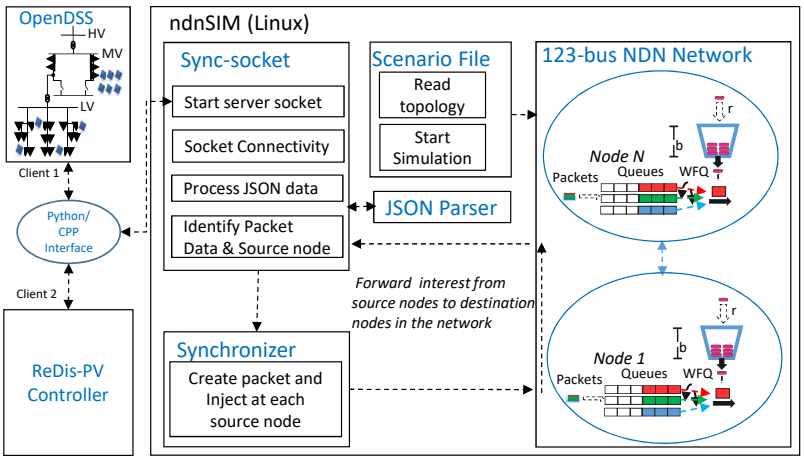

Figure 47: The proposed co-simulation framework integrates ndnSIM communication simulator with OpenDSS power simulator and the ReDis-PV controller.

We created a co-simulation framework in order to integrate the iCAAP communication architecture with the OpenDSS power system simulator and the Real-Time Photovoltaic Dispatch to Manage Critical Infrastructure (ReDis-PV) control module, a management tool meant to detect cyber & physical threats and form dynamic clusters to optimally manage energy in the system as shown in figure 47. In our co-simulation framework, we use TCP sockets to establish connections between simulators. In particular, we connected two client sockets, one from OpenDSS and the other from the control module, to the server socket in ndnSIM. We implemented the client socket interfaces in Python and ndnSIM's server interface in C++.
Our proposed co-simulation framework contains two primary communication flows: measurement data from OpenDSS to the ReDis-PV Controller and set-point information from the ReDis-PV Controller to OpenDSS. These flows are directed through ndnSIM, and by extension iCAAP++, to realistically model the communication process. We divide the co-simulation process into three phases, namely the sending phase where generated information is sent out, the simulation phase where the simulators run as normal, and the receiving phase where relevant information is received. The co-simulation framework itself has a communication component which acts as a server and a power component which acts as a client.
The co-simulation framework is responsible for facilitating communication between OpenDSS and the ReDis-PV Controller. These two entities interface with our iCAAP framework through the power interface provided by our co-simulation framework, which is implemented as a python client. They first establish socket connections to the ndnSIM server from their python

clients. OpenDSS then starts off at the simulation phase while the ReDis-PV controller starts with the receiving phase. During the simulation phase both OpenDSS and ReDis-PV will run and generate data for the current time step. During the sending phase both OpenDSS and the ReDis-PV controller will take their generated information, measurements for OpenDSS and set-points for the ReDis-PV controller, and encode it as JSON file before sending it to the Sync-socket module of ndnSIM. At this stage, the Synchronizer will simulate data transmissions from source nodes to their destination as specified in the JSON file. Finally, during the receiving phase, the ndnSIM server will send a JSON file to both simulators, which will encapsulate all the data that successfully arrived during the last time-step. This information will then be incorporated into the next instance of the simulation phase, the measurements for the ReDis-PV controller, and the setpoints for OpenDSS.
Time synchronization between simulators is a core part of any co-simulation framework. In our proposed co-simulation architecture, we adopted the time-step synchronization method. The co-simulation starts with OpenDSS, ndnSIM, and the ReDis-PV Controller all running independently. All three simulators will pause their normal operations to exchange states at predefined time steps. Note that the time step is an adjustable parameter that can be manually tuned. The larger the time step the lower the resolution of the simulation which will cause a larger communication delay to be perceived from the power simulator. As an example, for a time step of 1 second, all data sent through ndnSIM will have latencies equal to 1 second (time step value) even if their actual latencies are only a few milliseconds.
Attack Scenario An electric grid system can be subject to attacks, like DoS and DDoS. DoS and DDoS attacks are common attacks that are easy to orchestrate and hard to prevent. DoS can be used to perform network jamming, network spoofing, and data flooding that delays or completely halts communication between DERs and other devices. This disruption in communication brings the devices out of synchronization. DDoS can disrupt measurement gathering at the controller and prevent setpoints from reaching BESS devices. This can affect grid stability and in the worst case lead to differing types of grid failures. To study the extent of the impact on the system, we have modeled an attack vector against the system and DERs.
An adversary could be any node with intention of adversely affecting the network. Nodes in the electric grid can also be taken over and controlled by an adversary. An adversary can also take over multiple nodes of an electric grid, which can collude with each other to create a sophisticated distributed attack. In our experiments we spread 8 attackers through the system and had them target the Controller, sending 300 packets per second toward the target.

6.10 Mitigation Strategy

6.10.1 iCAD Architecture

While it is not possible to completely prevent DDoS attack, its effect can be reduced by blocking traffic from questionable and non-legitimate sources. We have implemented a DoS mitigation strategy that ensures packets are transferred, prioritizing Type I traffic over Type II and Type II traffic over Type III. These three types of traffic have three different queues. To forward a packet to an outgoing interface, it uses a token from the corresponding bucket. If the tokens run out, the packets will be dropped from the queue.
The solution we developed leverages iCAAP's priority levels and introduces another class of priority, referred to as Type IV. Unlike the other priority classes, there is no defined name structure for Type IV packets; Type IV priority can only be set by an individual router and

only on a local level. Type IV priority is defined as best effort. Like Type I, II, and III traffic, Type IV packets also have access to a token bucket where tokens are generated at a given rate. This allows us to remove potential DDoS flows from the base priority classes, freeing up those resources for legitimate traffic. Each router maintains a nodal loss rate, which is updated whenever an interest is completes, whether it was satisfied, timed out, etc. Once the nodal loss rate passes a predefined threshold (system parameter), the router will begin to search for problematic packet prefixes. This is done by looking through a rolling history of received interests and choosing the most popular prefix and adding it to a list of prefixes that are monitored separately. Popular prefixes can be used for determining attack packets. The nodal loss rate is then reset, and a loss rate is maintained separately for the monitored prefixes, which are now ignored by both the nodal loss rate and the rolling history. If these prefixes' loss rate surpasses a predefined loss threshold, it will henceforth be classified as a Type IV packet by the router, regardless of its previous priority class. During an attack, a router may repeat this process multiple times until the loss created by the DDoS attack flows no longer have a significant impact.
There is a chance for false positives in our detection system, in which case a legitimate prefix may be mistakenly classified as a Type IV packet. The prefix's monitored loss rate can fall under the Type IV threshold and have its original priority classification restored. Along with this, if a prefix can remain under this threshold for a predetermined amount of time the router will no longer monitor that prefix, removing its separate loss rate, and it will no longer be ignored by the nodal loss rate or rolling history. To ensure that a prefix will have a fair chance of redemption, only packets that are forwarded from the router will affect the loss rate, and any packet that is dropped locally will not get added to the loss rate.

6.11 RedisPV Visualization

Objective: This segment aims to showcase the advantages of a visualization tool for the power grid in the form of a dashboard. This dashboard will help convey the operational status of various grid elements to the operator for the reliable functioning of the grid. In this project, the visualization engine is a part of the situational awareness tool.

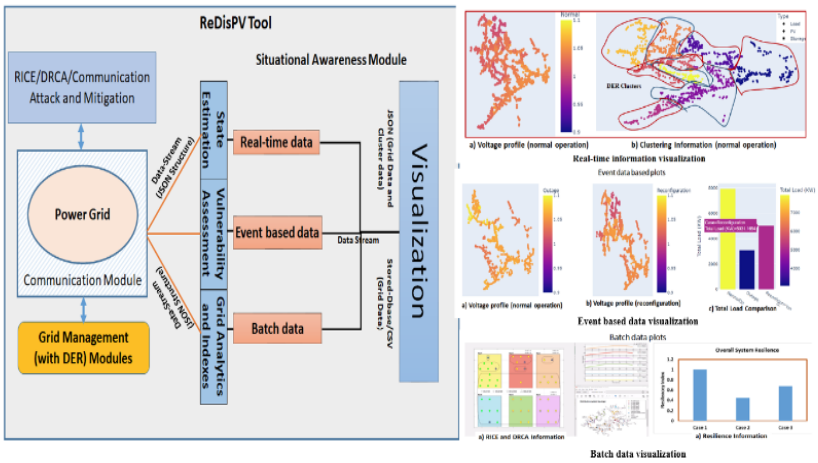

Figure 48: Flow chart of ReDisPV visualization.

6.11.1 Tools:

The system data and measurement metrics from the grid simulator will be stored in a database. This research uses a Python API to interface with the databases. The visualization platform is developed using Plotly libraries. Plotly is an interactive open-source visualization tool with over 40 chart types that can be customized using Python libraries. In addition, we use the Dash framework to create an interactive web-based interface to display the Plotly chart visualizations.

6.11.2 Methodology:

The python API receives information from the grid simulator in the form of JSON dictionaries and populates the tables in the database. The python API also extracts the necessary data from the database and passes it to the plotly dash visualization platform. Here the python API receives information from the grid simulator through CSV files generated from the RedisPV architecture and converts them to a pandas data frame. The dash application was developed as a layout component and callback component. We defined the chart types used to display the information in the layout components. Then, the dash-bootstrap components (dbc) were used to arrange the various visualization elements. The dash-bootstrap-components is a Dash library based on the Bootstrap CSS framework that helps develop consistent and responsive web page elements such as navigation panes, dropdown menus, and icons. The dbc was used to create panes of rows and columns and place each visualization element within each pane.

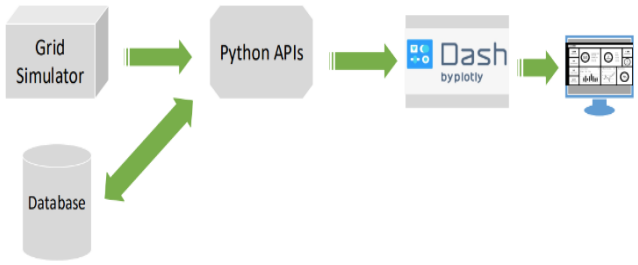

Figure 49: ReDisPV visualization framework.

6.12 Specifications

The Plotly version implemented for this project is Plotly version 5.10.0, and the Dash version is Dash version 2.6.1.

6.13 Design details:

In the main RedisPV code, vis_mod is the variable that controls the execution of the visualization module. The visualization module is executed if vis_mod is set to 1. The visualization

module is not executed if $vis - mod$ is set to zero.
The main real-time visualization file is called $networkDF\_mp\_v1.py$, located in a Viz folder. The visualization file is executed using a parallel process, as shown in the figure above. The measurements received are written into a JSON file called $measurements\_viz.json$, as shown in the code below. The $measurements\_viz.json$ file is written in the same location as the visualization module.
The $networkDFmpv1.py$ acts as a front end for visualization. The file initializes the dash bootstrap components, layout features, font size, color components, and other HTML design-related factors. The visualization files for the real-time visualization are provided in a folder called pages and are called pg1.py and pg2.py. In pg1.py, the bus and load layout information is provided in the files $businfoDF.csv$, $BusdatanophaseDF.csv$, and $DFLoadPVStorageElements.csv$ file. These are used to generate the base network visualization. The $readjsonreturndict()$ function reads the measurements visualization JSON file written by the RedisPV main python file and returns a measurements dictionary.
Like $pg1.py$, the layout section controls the layout of the various visualization elements, and the callback section controls the rate at which visualization is updated. The $Viz\_analytics$ folder contains the data analytics module for the batch visualization, which must be run after the execution of the RedisPV code. The main analytical visualization file is called $networkDF\_mp\_v2.py$, which sets up the outline and the layout of the analytic visualization file. The main analytical visualization file, called $analytics.py$ and $networkprofile.py$, is in the pages folder. In the $analytics.py$ file, the following lines provide the path to the output files of RedisPV, which are read into pandas data frames and then processed to provide visualizations.

6.13.1 Dashboard:

The dashboard shows the network visualizations for different operational parameters in the grid. For example, Figure 1 shows the voltage status in three scenarios: normal operation, outage, and reconfiguration. The color intensity shows the magnitude of the voltage. This helps to identify voltage deviations in different conditions of the grid. This dashboard also showcases the load conditions for the different scenarios. The reconfiguration algorithm helps to pick up the loads, thus exhibiting the advantages of RedisPV architecture. The cluster information for loads, PVs, and Storage elements is also displayed in the dashboard.
The callback feature is used to update the data, which is visualized. In the current version, voltages and powers of loads are updated based on predefined time intervals. The essential data are extracted from the database at predefined time intervals, which are then used to update the displayed chart types. For example, the following figure shows an updated dashboard.

6.14 IEEE 123-bus distribution system with IBRs and protections

The EMT domain IEEE 123-bus distribution system model for real-time simulation was developed from UNCC's IEEE 123-bus distribution system model. Thirty circuit breakers were added into the IEEE 123-bus system and the IEEE 123-bus system was divided into seven zones as shown in Figure 52. In each zone, the grid flowing inverter and grid forming inverter with detailed control algorithm were added. To make the model could be run in real-time without overruns, the model needs to be decoupled. The IEEE 123-bus model was first decoupled into four subsystems by using subline as shown in Figure 53. This physical decouple

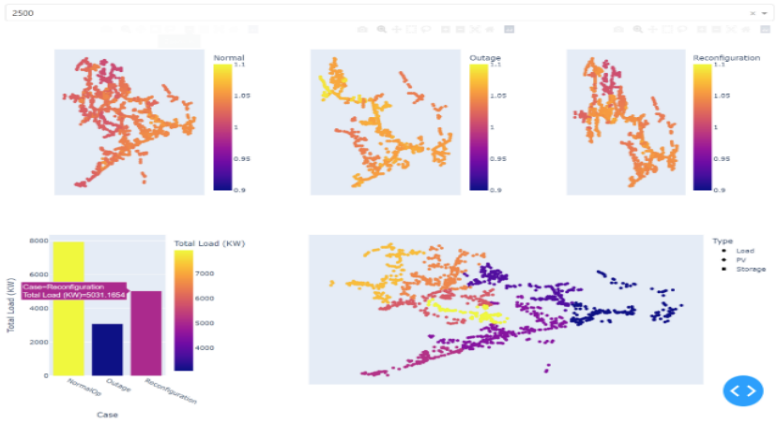

Figure 50: Network visualization.

Figure 51: Grid operational status: load voltage and power.

makes the model can be simulated by multiple cores of the real-time simulator. To achieve the optimal computation burden during the breaker event, State Space Nodal Network Interface Block (SSN NIB) and ARTEMiS SSN solver was placed to precomputes all the possible state space matrices at the time of switching event based on the location of the breakers and stores them in memory. To conduct the reconfiguration test, the zonal protection including primary protection and backup protection was integrated into the model as two additional subsystems to detect the fault and control the circuit breakers. The load shedding algorithm was put alone with the zonal protection to trip the certain mapped controllable load in the IEEE 123-bus system based on the voltage and frequency measurements. Additionally, in order to communicate with the ReDis-PV, two TCP/IP based asynchronous ethernet communication were implemented. Two communications worked independently with the same IP address, but with different ports. Both communications were set as the TCP client to instate a connection with ReDis-PV. The first communication was triggered periodically to exchange the whole measurements with ReDis-PV. The second communication was triggered by the signal coming from the protection algorithm which detected the certain event that happened in the IEEE 123-bus distribution system. After triggering by the event, the communication exchanged the

statuses and measurements of switches with ReDis-PV. The JSON template was used in both communications to map the data that is exchanged in the simulation. The GOOSE communication, as the third communication, was integrated into the IEEE 123-bus distribution system model for the hardware-in-the-loop (HiL) test. The GOOSE communication which is used to communicate with the external Schweitzer Engineering Laboratories (SEL) relay was added to the communication subsystem along with the existing two TCP/IP asynchronous ethernet communications. During the development, the data ports were created in each subsystem to exchange the data among IEEE 123-bus system, protection and communications subsystems.

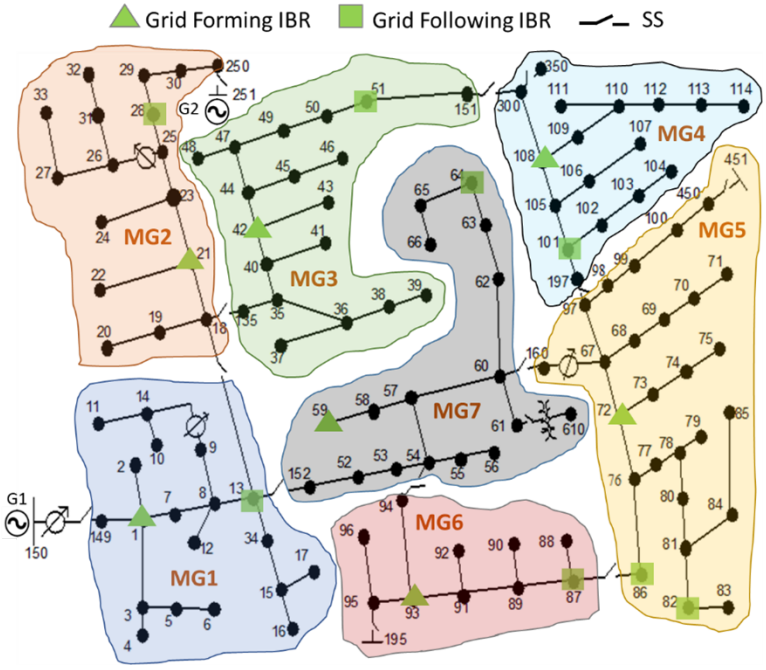

Figure 52: Diagram of modified IEEE 123-bus system with circuit breakers and IBRs

After the development, the IEEE 123 nodes distribution model was tested in real-time by using OPAL-RT's OP5707 real-time simulator and running with 62.5 µs time step. During the real-time simulation, the three-phase-to-ground faults in Zone 3, Zone 1 and Zone 7 were applied, respectively. The TCP/IP based communication worked properly to exchange the data with ReDis-PV. The real-time performance of this model was measured in this real-time simulation. Based on the computational benchmarking results as shown in Figure 54, each subsystem run within the required simulation time step. No overrun was found during the real-time simulation.

6.15 IEEE 2500-bus distribution system with IBRs and reconfiguration

The IEEE 2500-bus distribution system model for real-time simulation was developed by converting from OpenDSS model. The tool named DiTTO was used to convert the OpenDSS model to the ePHASORSIM model. This tool creates the netlist files with all the model netlists, data and proper header so that ePHASORSIM solver can read and simulate. The ePHASORSIM simulation results were validated by comparing with the OpenDSS load flow. In order to do the reconfiguration test, the additional circuit breakers were integrated into the model. Based on an OpenDSS model developed by a team member, the 2500 nodes distribution system was

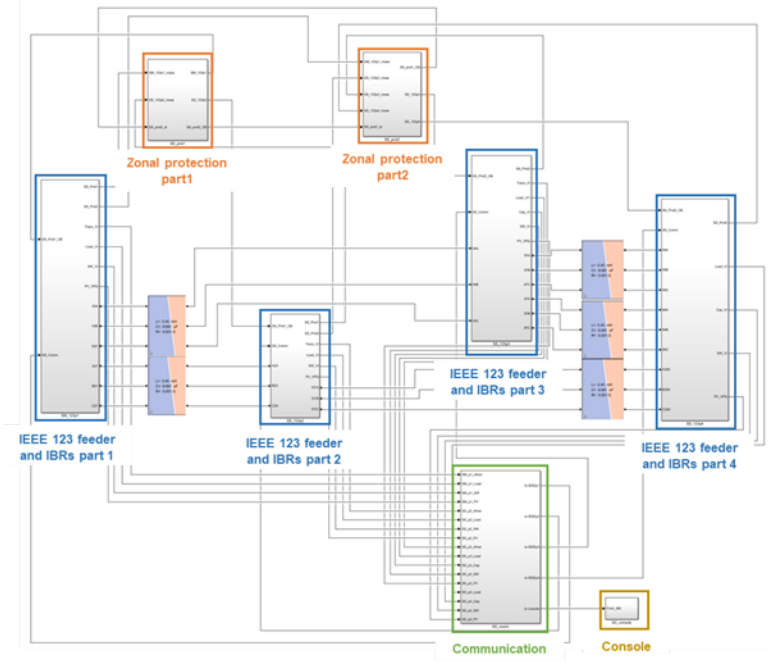

Figure 53: Structure of real-time model IEEE 123 nodes distribution feeder with zonal protection and communication

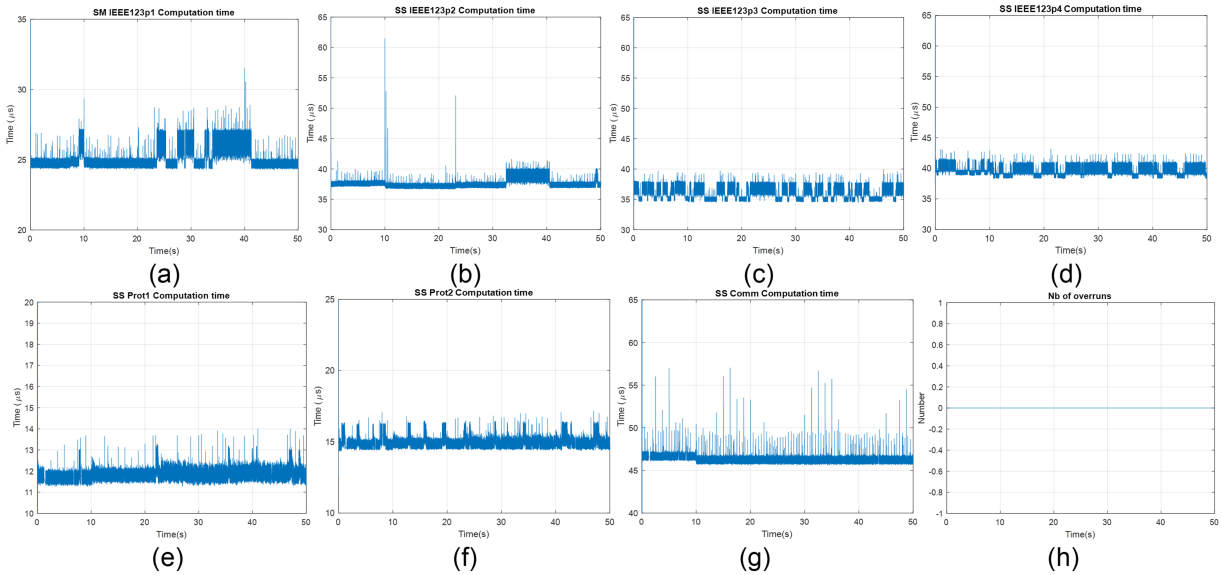

Figure 54: Computational benchmarking results of (a) – (d) IEEE123 feeder and IBRs subsystems, (e), (f) zonal protection subsystems, (f) communication subsystem, and (h) number of overruns during the simulation

partitioned into four areas as shown in Figure 55. Among each area, the inter-area normally-closed (NC) and normally-open (NO) switches were added to facilitate reconfiguration of the distribution feeder. Additionally, inside each area, some intra-area NO switches were added to create loop-type laterals. Twenty-four switches, their connection buses and lines were added to the 2500 nodes distribution model whose detailed information is shown in Figure 58. To exchange the data with ReDis-PV during the real-time simulation, a TCP/IP base asynchronous

ethernet communication was implemented into the model. The JSON format including the required measurements and setpoints was designed and used in the communication data mapping. In addition, twenty-seven grid-following (GFL) inverter and four grid-forming (GFM) inverter EMT-domain models were integrated into the grid model for the reconfiguration test. As the EMT-domain inverter model was developed with the 50 µs time step which is much faster than the time step (10 ms) in the phasor-domain 2500 nodes distribution system model. The inverter models cannot be placed in the same subsystem as the phasor-domain model. Furthermore, the integrated inverter models cannot be placed in the same subsystem when considering the computation burden of the subsystem. Because of this, the newly integrated GFL inverter models were placed into one master subsystem and four slave subsystems as shown in Figure 56. The integration method, as shown in Figure 57, was used in the GFL inverter and GFM inverter integration. The location of each inverter, and additional elements for the integration is shown in Figure 59.

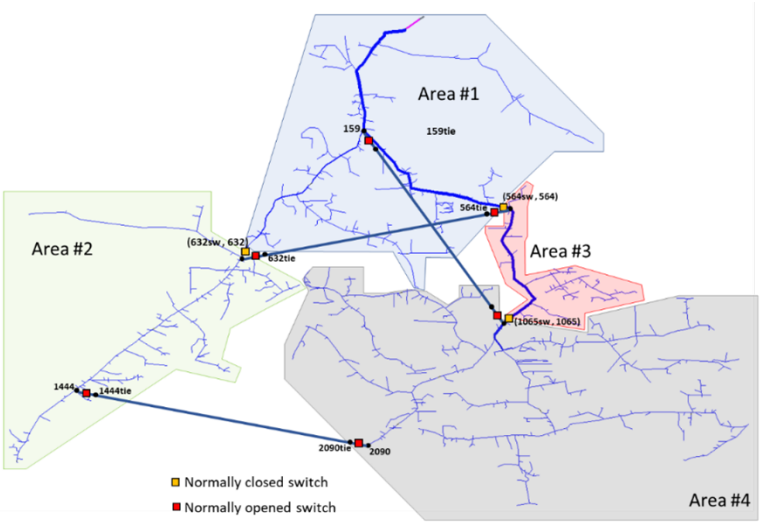

Figure 55: Diagram of 2500 nodes distribution system with inter-area switches

After the development, the model was validated and benchmarked in real-time simulation by using OPAL-RT's OP5707 real-time simulator. The islanding operation condition was applied during the simulation for all zones. The TCP/IP based communication worked properly to exchange the data with Python server. The real-time performance of the model was benchmarked in this simulation. The computation benchmarking results, as shown in Figure 60, shows that this phasor EMT co-simulation model run within the required multi-timesteps of 10 ms and 50 µs, respectively. There is no overrun was observed during the whole simulation.

6.16 Main and Backup Protection on IEEE 123-node network

6.16.1 Main and Backup Protection

The conception of the protection scheme developed for microgrids in this project is based on an extensive literature survey that shows the published approaches are highly system/topology-dependent, and/or assume infrastructure that cannot be financially justified. The proposed scheme uses the most reliable physical attributes of fault that manifest for any topology and any source types – undervoltage and current direction. For a fault on a feeder-section the

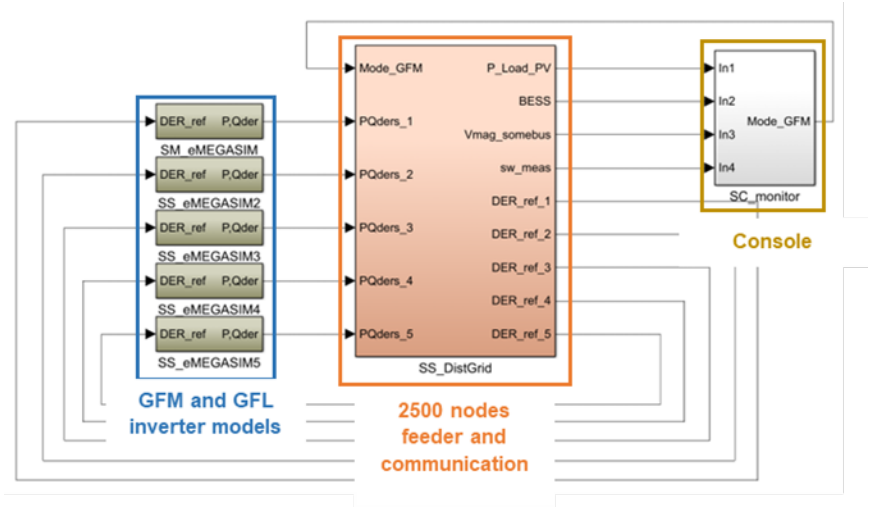

Figure 56: Structure of model of the 2500 nodes distribution system with GFL and GFM inverters and communication

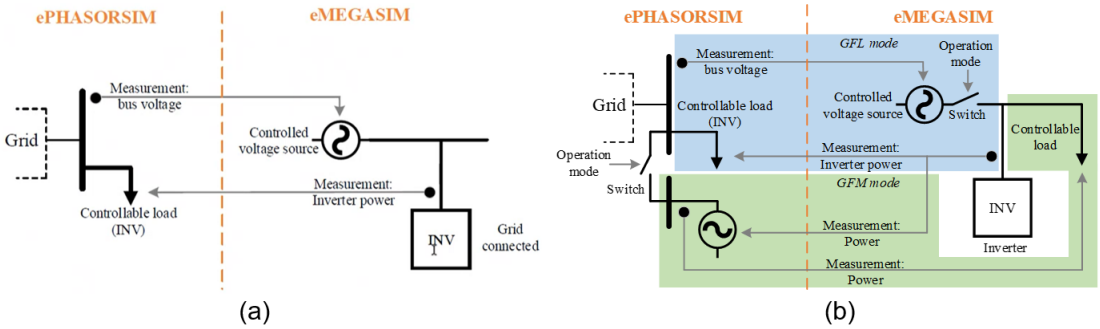

Figure 57: Diagram of integration of EMT-domain (a) GFL inverter and (b) GFM inverter into phasor-domain grid model

voltage will always be dragged down to a low value due to physics and currents from both ends of the feeder will always flow into the feeder. These attributes are utilized to form and test a source-agnostic, cost-aware protection and reconfiguration module in the project.
Primary protection zones are determined by placement of intelligent circuit breakers capable of performing undervoltage and directional functions, communicating using IEC 61850 protocol, and performing synch-check before closing. Such reclosers are available in market. The protection zones will get smaller (making protection more selective) with larger number of breakers installed, and vice versa, thus making the scheme cost-aware. Main protection relay is placed at one of the DER facilities and communicates with all boundary breakers, exchanging GOOSE messages – voltage and direction triggers going from the breakers to relays and trip signals from relay to breakers.
The backup protection is embedded with the area controller developed in this project and subscribes to GOOSE messages from the breaker IEDs about the breaker status (close/open) and a breaker failure alert in case a breaker fails to open, or from a relay if it fails to operate, or from the communication protocol if any communication link fails. It also receives the undervoltage and direction trigger from breaker, and hence also detects the fault detected by the main protection. It can send GOOSE signals to any breaker to open or close. It is set to wait for the main protection and associated breakers to trip and then operate the appropriate breakers to

	Area	From bus	To bus	New Switch	New Bus	New Line
Inter-area NC Switches	Area 1-2	632	628	area12_sw	632sw	None
	Area 1-3	564	557	area13_sw	564sw	None
	Area 3-4	1065	1062	area34_sw	1065sw	None
Inter-area NO Switches	Area 2-3	632	564	area23_sw1, area23_sw2	632tie, 564tie	area23_tieline
	Area 1-4	159	1065	area14_sw1, area14_sw2	159tie, 1065tie	area14_tieline
	Area 2-4	1444	2090	area24_sw1, area24_sw2	1444tie, 2090tie	area24_tieline
Intra-area NO Switches	Area 1	83	134	area1_sw14	83tie	area1_tie_83_134
		126	161	area1_sw15	126tie	area1_tie_126_161
		154	179	area1_sw16	154tie	area1_tie_154_179
		554	515	area1_sw17	554tie	area1_tie_554_515
		307	268	area1_sw18	307tie	area1_tie_307_268
		431	516	area1_sw19	431tie	area1_tie_431_516
	Area 2	713	759	area2_sw12	713tie	area2_tie_713_759
		945	1002	area2_sw13	945tie	area2_tie_945_1002
		1083	1172	area2_sw14	1083tie	area2_tie_1083_1172
	Area 3	844	926	area3_sw7	844tie	area3_tie_844_926
		926	888	area3_sw8	926tie	area3_tie_926_888
		946	1060	area3_sw9	946tie	area3_tie_946_1060
	Area 4	1690	2090	area4_sw12	1690tie	area4_tie_1690_2090
		1578	1917	area4_sw13	1578tie	area4_tie_1578_1917
		1078	1254	area4_sw14	1078tie	area4_tie_1078_1254

Figure 58: Details of newly added switches

clear the fault, and at the same time, perform a reconfiguration task to make sure minimum load is lost and minimum islands are formed.
This protection was designed and implemented on the IEEE 123-bus distribution feeder with 15 inverters modeled in compliance with the IEEE standard 1547, with ten breakers forming seven main-protection zones. Cases illustrating performance of main and backup protection were run to capture all types and location of faults and failures of breaker, relay and communication channels. This was illustrated first on PSCAD (controller with backup and reconfiguration module on a computer running MATLAB) with communication modeled as delays[1], and then on RTDS with relays as hardware in the loop (HIL) performing main protection, and IEEE 61850-based communication co-modeled with physical network[2]. Main and backup protection and reconfiguration functions were successfully demonstrated on both platforms.

[1]Phani Gadde, Sukumar Brahma, and Trupal Patel. Real-time hardware-in-the-loop im- plementation of protection and self-healing of microgrids. IEEE Transactions on Industry Applications, 59(1):403–411, 2023.

[2]Phani Gadde and Sukumar M. Brahma. Topology-agnostic, scalable, self-healing, and cost-aware protection of microgrids. IEEE Transactions on Power Delivery, 37(4):3391–3400, 2022. 67

	Area	Bus	New Load	New Switch	New Bus	New Vsource
GFL Inverters	Area 1	19	BESS1	None	None	None
		71	BESS2	None	None	None
		83	BESS3	None	None	None
		368	BESS4	None	None	None
		411	BESS5	None	None	None
		422	BESS6	None	None	None
		365	BESS23	None	None	None
		154	BESS26	None	None	None
		95	BESS27	None	None	None
	Area 2	686	BESS7	None	None	None
		741	BESS8	None	None	None
		904	BESS9	None	None	None
		1000	BESS10	None	None	None
		1364	BESS11	None	None	None
		1444	BESS13	None	None	None
	Area 3	966	BESS24	None	None	None
	Area 4	1386	BESS12	None	None	None
		1518	BESS14	None	None	None
		1600	BESS15	None	None	None
		1646	BESS16	None	None	None
		1658	BESS17	None	None	None
		1690	BESS18	None	None	None
		2026	BESS19	None	None	None
		2241	BESS20	None	None	None
		2397	BESS21	None	None	None
		2404	BESS22	None	None	None
		2111	BESS25	None	None	None
GFM Inverter	Area 1	282	BESS28	sw_282_282s	282s_a	V_GFM_2
	Area 2	973	BESS29	sw_973_973s	973s_a	V_GFM_3
	Area 3	966	BESS30	sw_966_966s	966s_a	V_GFM_4
	Area 4	1821	BESS31	sw_1821_1821s	1821s_a	V_GFM_5

Figure 59: Details of newly added inverters

Sample Time	5.0E-5 [s]			
Number of Overruns	0			
Probes	Usage[%]	Min Duration[µs]	Max Duration[µs]	Mean Duration[µs]
JSON_2500v12_31der_121522	64.83			
SM_eMEGASIM	69.43	33.65	37.20	34.71
SS_DistGrid	14.13	1413.24	1413.24	1413.24
SS_eMEGASIM2	72.31	36.16	36.16	36.16
SS_eMEGASIM3	72.45	36.22	36.22	36.22
SS_eMEGASIM4	75.41	37.71	37.71	37.71
SS_eMEGASIM5	85.25	42.62	42.62	42.62

Figure 60: Computational benchmarking results of 2500 nodes distribution model with inverters

6.17 RICE (Risk-Informed Condition Evaluation) Module

6.17.1 Module description:

RICE module is used operationally to assess probabilities of adverse grid events (i.e., risk of losing specific critical load(s)), given diverse real-time observed evidence across the topology of interest. RICE module bases its assessments on Bayesian inference over a Probabilistic Graphical Model (PGM), which is, in turn, built and learned during periodic (re)training with Digital Twin model data. An indicative PGM applicable to use cases of interest to ReDis-PV is illustrated in Figure 61.

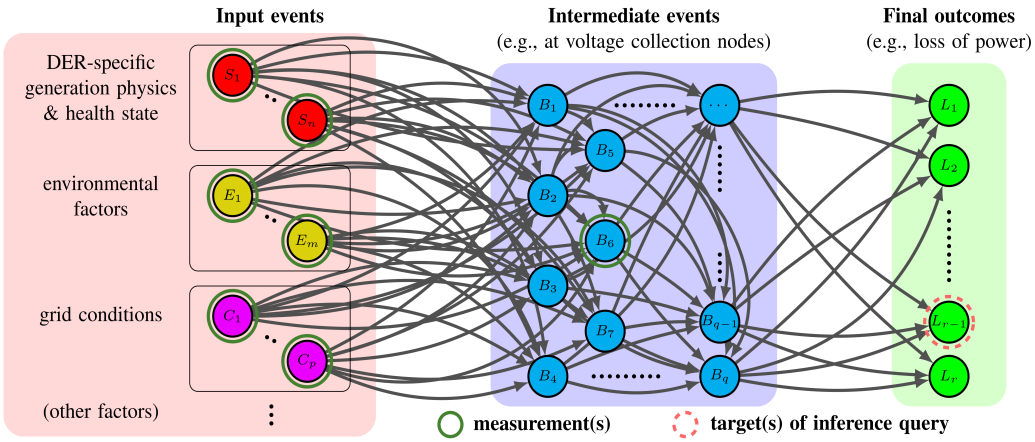

Figure 61: Conceptual illustration of a forward type of analysis for a solar-centered distributed grid, where input events of interest drive processes that ultimately lead to assessments regarding mission-critical final outcomes. RICE module is able to discover and model complex causality relationships from data.

In use cases considered in ReDis-PV, the underlying PGMs connected the physical health of specified DER fleets to distributed voltage violations and loss of power events at critical loads across the topology of interest.

6.17.2 Architectural configuration:

The RICE module consists of two distinct modules as follows:

- RICE-LRN, which uses training datasets containing operational experience from a model system to learn (and, occasionally, re-learn) the structure and parameters of the underlying PGM.
- RICE-EXC, which is used operationally to rapidly perform inference over the learned PGM and evaluate the risk of events of interest provided by the user/operator.

6.17.3 Algorithmic construction:

RICE module has been originally developed in a modality-agnostic manner to be able to cover diverse input phenomena that can cause adverse effects on the grid. In the context of ReDis-PV, such input phenomena were considered to be physical and cyber attacks on DER fleets.

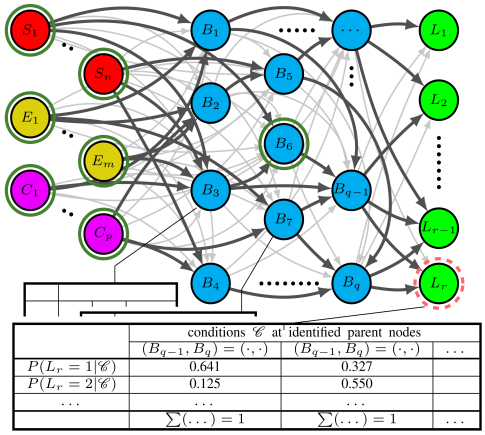

Figure 62: RICE-LRN is able to reduce the class of sought-after PGMs into models that capture observed causality relationships.

In the project nomenclature and reporting, we used identifiers (e.g., -P-, as in RICE-P-EXC for physical attack), to identify RICE modules built and configured for particular attack modalities. The learning on PGMs achieved by RICE-LRN is illustrated conceptually in Figure 62, whereas the main steps of both RICE-LRN and RICE-EXC are illustrated in Figure 63.

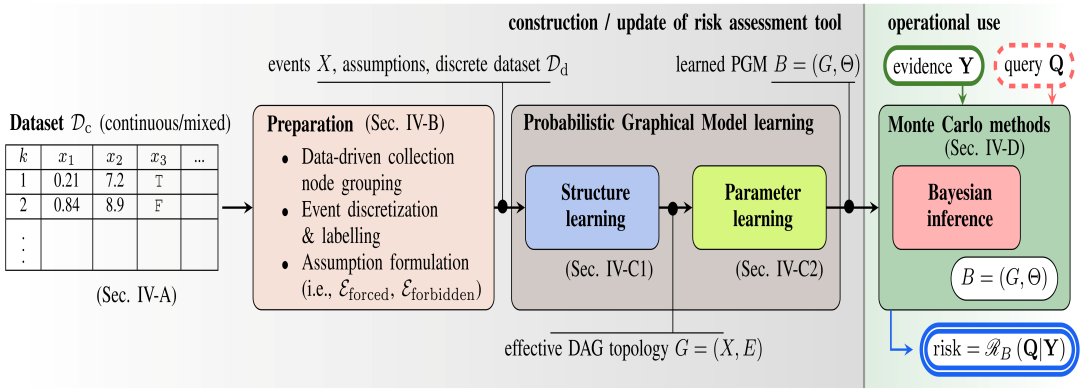

Figure 63: Main workflows of RICE-LRN (left / grey part) and RICE-EXC (right / green part).

6.17.4 Example operation:

Over the course of ReDis-PV, training datasets based on short-term, quasi-steady state simulations with randomized initial and environmental conditions were procured with Powerfactory and OpenDSS models of grid response to physical attacks on PV-DERs, with approximately 10,000 runs each. Such datasets were appropriately discretized and labeled. RICE-P-LRN was used to learn the structure and parameters of the underlying PGM, and, ultimately, construct the operational inference model used by RICE-P-EXC. In turn, RICE-P-EXC was used to address diverse inference queries, as illustrated in the table shown in Figure 65 The respective topology and the structure learned by RICE-LRN are illustrated in Figure 64.

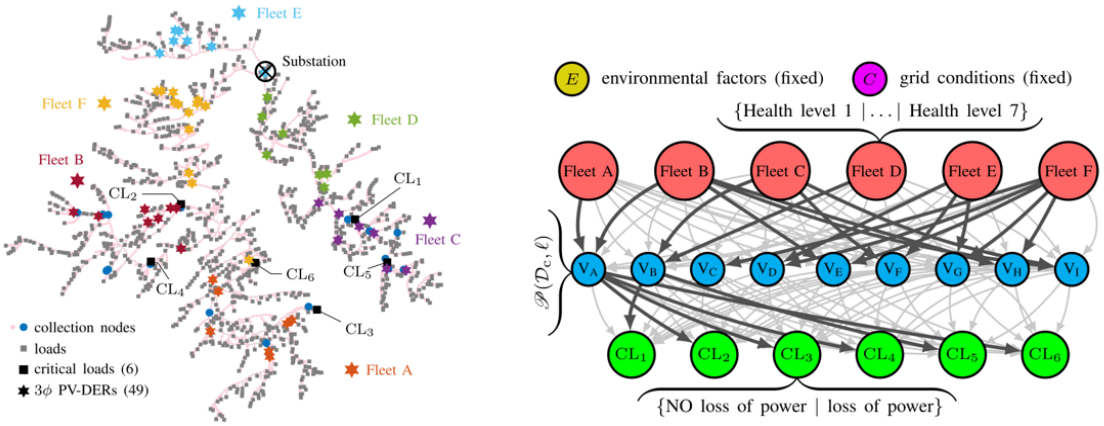

Figure 64: Topology and respective RICE-LRN-learned causality relationships between attacks on PV-DER fleets and grid events.

6.17.5 Implementation and interfacing:

RICE-P elements were implemented with a combination of MATLAB, R, and Python code and libraries. RICE-P-LRN includes MATLAB modules with no dependencies and R modules requiring **bnlearn**[1]. RICE-P-EXC is Python based, and requires **pgmpy**[2] and **genfromtxt**[3] from **numpy**. Algorithmic implementation details and related remarks are available in the respective publication[4].

- RICE-P-LRN:
  - **Input:**
    - Tabulated dataset (e.g., in *.csv or similar format), with each column corresponding to an event in the sought-after PGM (e.g., “aggregated physical health of PV-DER Fleet B”, “voltage violation in node 54, “loss of power (true/false) in critical load 5”) and each row corresponding to a different short-term, quasi-steady state simulation run.
    - Prior information regarding unallowed and/or forced causality relationships to help RICE-P-LRN understand the order of events in the network. For example, the physical health of PV-DERs does not influence critical loads directly but indirectly (by influencing, first, voltage violations). Such information can be passed to RICE-P-LRN.
  - **Output:**
    - Learned inference model in *.bif format (Bayesian Interchange Format).
- RICE-P-EXC:

[1] https://cran.r-project.org/web/packages/bnlearn/index.html
[2] https://pypi.org/project/pgmpy/
[3] https://numpy.org/doc/stable/reference/generated/numpy.genfromtxt.html
[4] D. Pylorof, H.E. Garcia and R. Bhattarai (2023). “Risk-Informed Condition Evaluation for Solar-centered Energy Generation and Distribution Networks through Bayesian Learning and Inference,” 2023 IEEE Innovative Smart Grid Technologies Conference, Washington, DC, USA. https://doi.org/10.1109/ISGT51731.2023.10066364

- Learned inference model in *.bif format (Bayesian Interchange Format).
- Sought-after inference query.
- **Output:**
  - Calculated probability (i.e., in the particular context, risk) of provided inference query. See the table below in Figure 65.

Critical load	uniform PV-DER fleet physical health levels L1 ... L7						
	L1 (poor PV-DER health)	**L2**	**L3**	**L4**	**L5**	**L6**	**L7** (excellent PV-DER health)
1	0.319	0.224	0.149	0.021	0.005	0.001	0.000
2	0.466	0.322	0.227	0.093	0.069	0.013	0.001
3	0.496	0.363	0.276	0.157	0.052	0.010	0.000
4	0.492	0.387	0.237	0.163	0.082	0.013	0.001
5	0.762	0.585	0.429	0.338	0.197	0.103	0.011
6	0.389	0.272	0.144	0.084	0.016	0.002	0.000

Figure 65: Probability to lose power at each critical load 1, . . . , 6, for PV-DER fleet health $h_i = H$ varying uniformly for fleets $i \in \{A, \ldots, F\}$ across 7 discrete levels partitioning uniformly the [0,1] interval: $\{L1 : H \in [0, 0.143), L2 : H \in [0, 0.143), \ldots, L7 : H \in [0.857, 1]\}$

Health does not have to vary uniformly in RICE queries, nor does the logic need to be so simple, as indicated in the following more complex queries:

- What is the probability of losing power at critical load 5 when Fleet C is at health level 2 and other fleets (A, B, D, E, F) are at level 4? RICE response: 0.47
- What is the probability of losing power at critical load 5 when Fleet C is at health level 1 and other fleets (A, B, D, E, F) are at level 2? RICE response: 0.71 (notice worsening risk, as expected, compared to the previous query)
- What is the probability of losing power at critical load 1 and NOT losing power at critical load 5 when Fleet C is at health level 2 and other fleets (A, B, D, E, F) are at level 4? RICE response: 0.07 (an unlikely event, as expected, given a recognized dependency between critical loads 1 and 5)

6.18 B. HE (Health Evaluation) Module

6.18.1 Module description:

HE module is used operationally to assess the health of PV-DERs by comparing, in real-time, actual observations (e.g., **actual PV-DER power output**) to physics-based estimations (e.g., **modeled PV-DER power output**), and discerning, quickly-enough, **statistically significant change** in the presence of measurement noise and other irregularities. In the particular case study of physical attacks conducted for this project, modeled PV-DER output is obtained from suitable models following the Digital Twin paradigm that cover, to some level of fidelity, the major aspects affecting PV-DER power output (e.g., locale, panel properties, size, and orientation, environmental factors, date and time), sparing integral (i.e., accumulating) effects related to physical attacks. In development efforts during ReDis-PV, suitable models were sourced and

based on pvlib[5]. Nevertheless, the choice of model is up to the HE implementer or operator. The ability of the HE module to discern a statistically significant change in monitored health levels is sourced in non-parametric, distribution-free, statistical change detection techniques for streaming data. The algorithm developed and implemented in the HE module can adapt to diverse noise patterns and understand -with quantifiable error margins- when health changes are indeed meaningful without unnecessarily alerting grid operators for no good reason. An important parameter for the operation of the HE module is related to the length of the buffer window the HE module is using to look back with regard to the present time and understand if a statistically significant change is occurring or not. Longer windows (e.g., to the order of 30-60 seconds, sampling at 1Hz) can offer more stable assessments, whereas shorter windows can offer more rapid yet potentially volatile assessments. In ReDis-PV, the possibility of using multiple HE modules with different windows of operation and attack types was also investigated. The general problem of health evaluation for PV-DERs under the motivation of ReDis-PV was investigated preliminarily (and prior to the development of the streaming data change detection approach) in an exploratory publication[6].

6.18.2 Architectural configuration:

HE module consists of two distinct submodules as follows:

- Embedded PV Models, which first uses a “solar irradiation model” to compute estimated irradiance based on estimated PV location and configuration and time. Then, it uses a “PV generation model” to estimate PV power output for current conditions and hypotheses.
- Health Computation Model, which uses PV power output measurement and estimated PV power output to compute the health index of the PV DER under observation.

6.18.3 Algorithmic construction:

As previously mentioned, the HE module utilizes algorithms based on non-parametric statistical change detection for streaming data, which are able to (i) quantify the distance of the distribution currently seen in streaming data with known distributions (e.g., with various physical/cyber health levels, or with various diverse simulated or previously seen attacks), or, more simply, inform the operator of new, never seen before situations, while preserving specified accuracy bounds on rates of false positive detections.

6.18.4 Example operation:

Figure 66 and Figure 67 illustrates the use of the developed HE module to detect two test-case attack events, where both the attack index itself increases and, later, the sensor output deteriorates.

[5]https://pvlib-python.readthedocs.io/en/stable/

[6]R. Bhattarai and H.E. Garcia (2022). “Online Health Monitoring of Photovoltaic Distributed Energy Resources,” 2022 IEEE Power Energy Society General Meeting, Denver, CO, USA. https://doi.org/10.1109/PESGM48719.2022.9916726

6.19 Implementation and interfacing:

HE module has been implemented in MATLAB functions and scripts, with no dependencies. In the broader ReDis-PV architecture, HE module is interfaced with PV-DER sensors and environment sensors (i.e., to drive modeled PV-DER output).

- **Inputs:**
  - Current PV-DER power output
  - Modeled PV-DER power output (if model implemented outside of HE boundaries)
- **Inputs:**
  - estimated PV-DER health index
  - "change" / "no change" flag
  - Other statistics on the monitored signal, as needed (e.g., recent mean, variance)

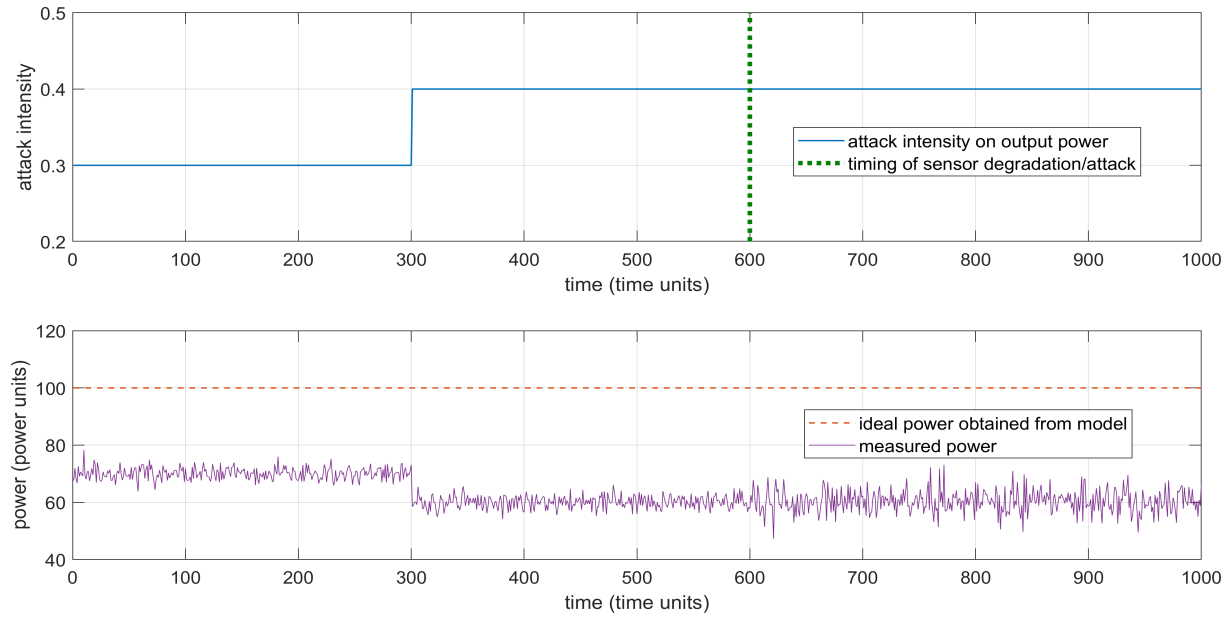

Figure 66: Example attacks happening at 300 and 600-time units. First, a physical attack is decreasing output further from 70% of what would be physically realizable to 60% (alternatively, attack intensity goes from 0.3 to 0.4). Next, an attack or malfunction at the power output sensor for the particular PV-DER is increasing the sensor output noise.

6.20 FE (Fitness Evaluation) Module

6.20.1 Module description:

FE module is used operationally to fuse risk and health information used by DRCA. The underlying motivation is that a PV-DER's "fitness" to be elected in coordinating roles by DRCA should relate to its criticality in the system, so that large and high-risk PV-DERs with regards to

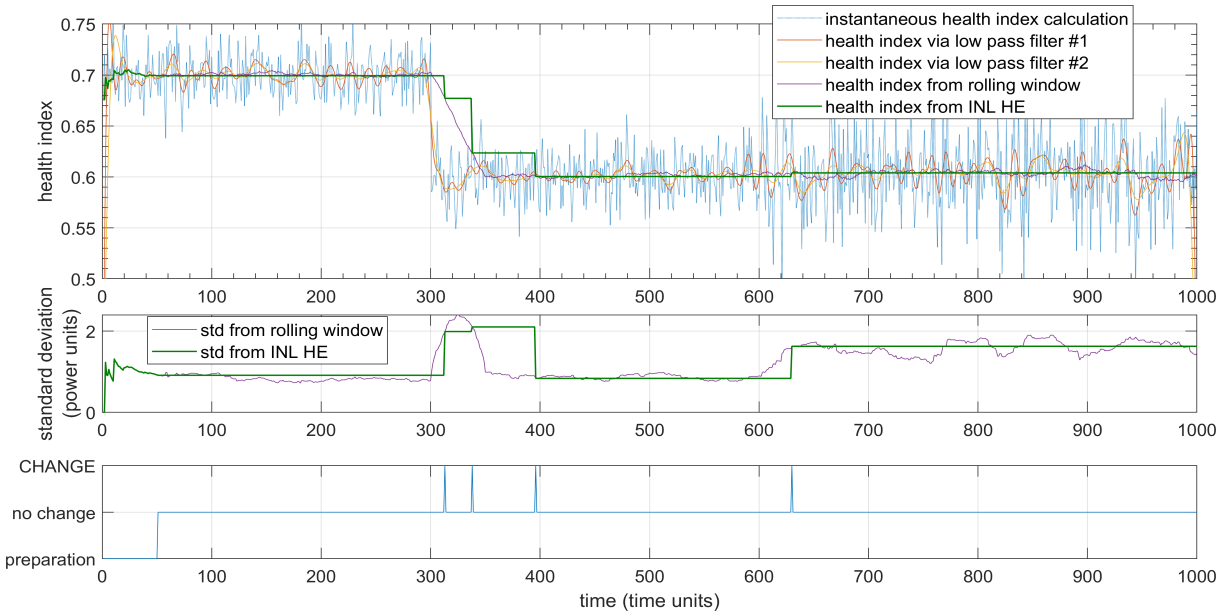

Figure 67: HE module correctly and stably identifies both attack events by noticing changes as they happen. For comparison, we also illustrate how oscillatory and perhaps misleading an instantaneous or low-pass-filtered calculation of measured vs. theoretical output would yield, further illustrating the benefits of the pursued HE approach.

critical loads are less likely to be elected (as they can attract attackers, and an attack at a PV-DER with cluster-wide functionality will harm the entire cluster), and that unhealthy PV-DERs (i.e., PV-DERs that have been attacked) should not be likely to be elected to coordinating roles either. All such considerations are captured by the so-called “fitness index”, a quantity fusing PV-DER capacity, health, risk, and user preference / sensitivities in a scalar value.

6.20.2 Architectural configuration:

HE module consists of one function as follows:
Fitness Evaluation Calculation: $FN(i) = max(0, Q(i)) \times h(i)$, where $h(i)$ is the health index for DER i, $Q(i) := 1 - \alpha \frac{c(i)}{C(f(i))} M(f(i))$, $M(f(i)) = max\ R(\mathcal{L}(f(i))|H(f(i)))$ is a RICE risk query, $\mathcal{L}(f(i))$ are critical loads influenced by DER i, $c(i)$ and $C(f(i))$ are DER and fleet capacities (i.e., in power units), respectively, and $\alpha > 0$ is a tuning parameter, making the fitness index more/less sensitive to risk.

6.20.3 Algorithmic construction:

FE is an instant, algebraic calculation (i.e., with no “memory”) that collects online health and RICE information and computes the fitness index for the given PV DER under consideration using the formulation briefly described above. FE is implemented in a MATLAB function.

6.20.4 Example operation:

Figure 68 illustrates FE calculations fusing PV-DER capacity, health, risk, and user preference / sensitivity.

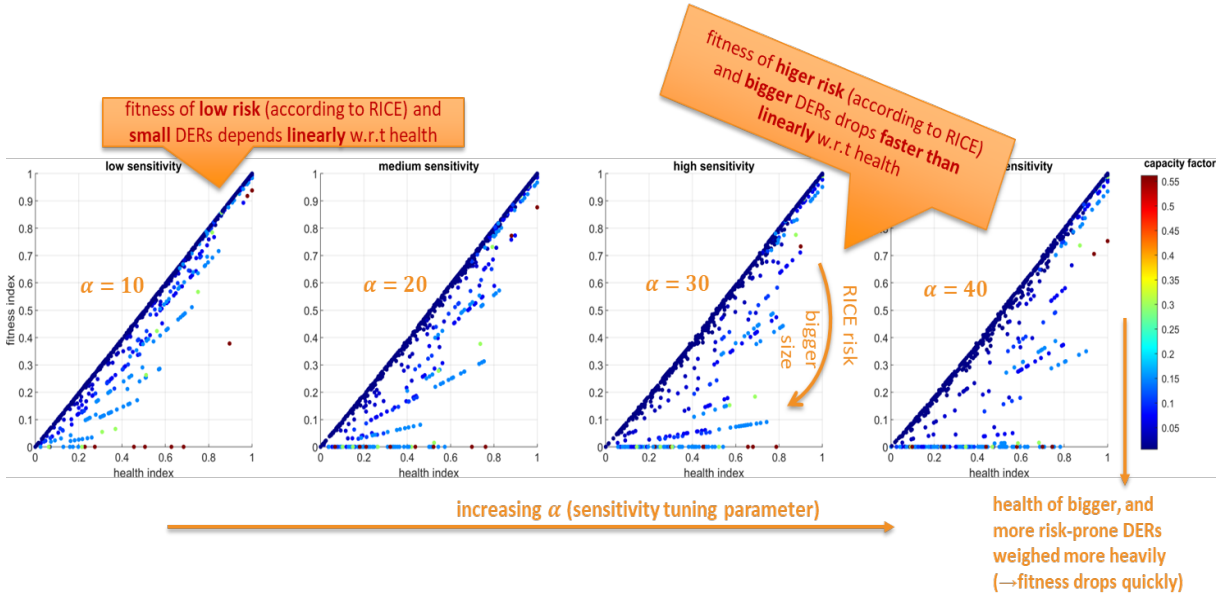

Figure 68: Application of FE calculations on ReDis-PV topology fusing PV-DER capacity, health, risk, and user preference / sensitivity. It can be seen that fitness indices drop for decreasing health. Also, higher risk PV-DERs, as identified by RICE, tend to have their fitness index decreased as the user becomes more risk-averse, by use of the tuning parameter. Finally, as evidenced by the translation downwards of the colored indices, larger DERs also tend to have decreasing fitness for coordinating roles assigned by DRCA as the user becomes more risk averse.

6.20.5 Implementation and interfacing:

FE module has been implemented in MATLAB functions and scripts, with no dependencies. In the broader ReDis-PV architecture, FE is interfaced with HE module (to obtain PV-DER health indices), RICE module (to obtain PV-DER / fleet risk with regards to each critical load), and DRCA module (to deliver the fitness evaluation result).

6.21 D. DRCA (Dynamic Reconfigurable Control Architecture) Module

6.21.1 Module description:

DRCA is integrating local- and system-wide health, risk, and mission information, to determine optimal placement of the cluster manager role within existing clusters in defense against anomalies and threats including cyber adversaries. The fundamental principle motivating the DRCA module is that threats, cyber intrusions and/or attacks are certain to happen, systems can and will be eventually compromised. However, by (a) decentralizing the communications,

command, and control roles in distributed grids by forming short-lived clusters and (b) moving these roles around logical and physical locations, following the moving target defense (MTD) principle, such threats will be less likely, in expectation, to succeed in disabling the local grid and harming its stakeholders. The concept of MTD has seen increasing use in securing diverse computer and network systems on the basis that threats have a finite power and will challenge or compromise assets sequentially or in batches, and defenders have a better chance by not remaining at the same physical /logical location permanently. The use of MTD in securing highly-distributed grids is a novelty of ReDis-PV.
DRCA performs MTD in a pseudo-random way, where the probability for each PV-DER member of the respective cluster to be elected in a coordinating role is influenced by its fitness index as calculated by the FE module. While all PV-DER locations have a probability to be selected, PV-DER locations with higher fitness will be more likely to be selected. DRCA module decides on the location and period-of-performance (POP) for each short-lived cluster manager, and repeats the pseudorandom selection process at the end of the POP. In addition to the pseudorandom selection process, a spatiotemporal game-theoretic approach based on Markov-Stackelberg game has also been preliminarily investigated.

6.21.2 Architectural configuration:

HE module consists of six distinct modules as follows and is illustrated in Figure 69:

- HE module, which is described earlier.
- RICE module, which is described earlier.
- FE module, which is described earlier.
- Candidate Nomination (CN) module, which uses the fitness index computed from integrating risk and health calculations to compute the candidate status for each PV-DER. This status assesses whether a particular PV DER can be nominated for selection to be a cluster manager. At its core, the CN module embeds a ring element in which its speed of rotation depends on the value of the given PV DER's fitness index towards accordingly reducing or increasing its likelihood of being nominated for being a cluster manager based on its fitness to be so.
- Cluster Manager Selection (CMS) module, which collects those PV DES candidates being nominated for cluster manager and applies a particular algorithm of the user's choice to select a given PV DER to be the cluster manager for the next period-of-performance (POP). Diverse algorithms for selection are available, including one that randomly selects a cluster manager among the nominated candidates.
- POP module, which computes the POP for the just-selected cluster manager. Diverse algorithms for computing POP are available, including one that sets POP to a fixed, user-selectable value.

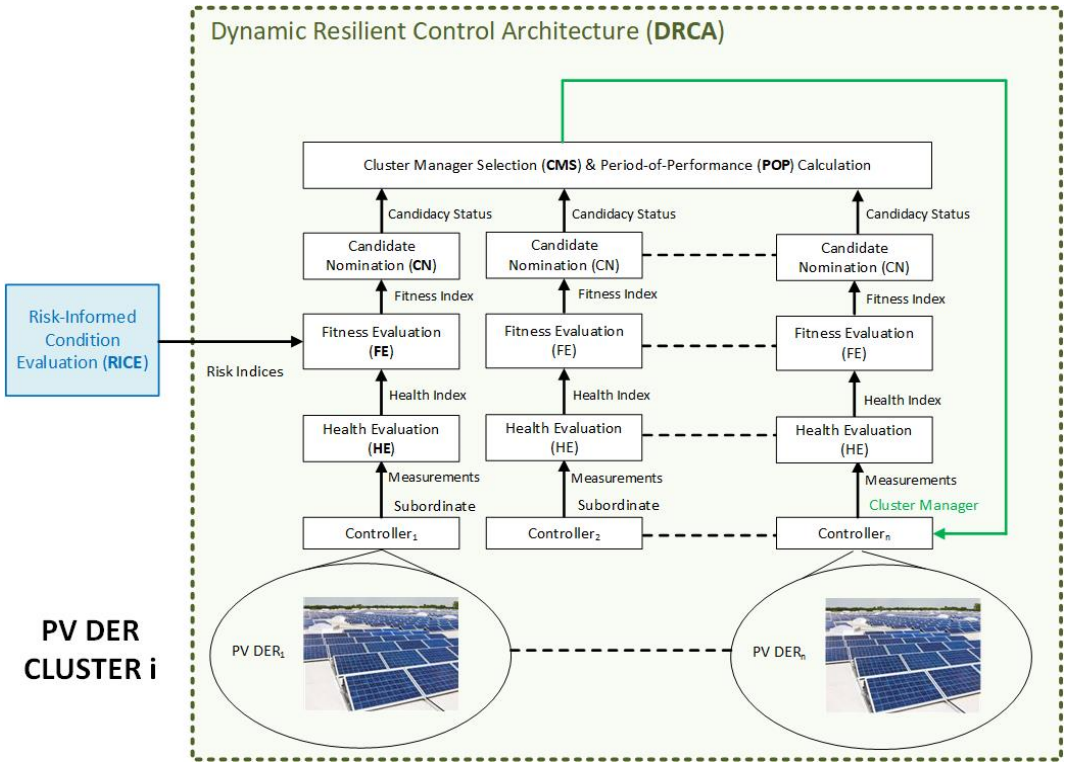

Figure 69: Computational components of the dynamic resilient control architecture.

6.21.3 Algorithmic construction:

DRCA module integrates an assortment of diverse algorithms to synthesize its six modules introduced above. Algorithms utilized for implementing HE, FE, and RICE modules have been already described in previous sections. The CN module is designed using a ring element of defined states having values within, for example, the [0, 1] interval. The rotational speed for which the ring element changes its states depends on its penalty function based on the received fitness index for the particular PV DER under consideration. The particular state in which a given ring element may be defines whether this PV DER is nominated to be a cluster manager when an election process begins. For example, if the state of the ring is within [0, 0.5), then the particular PV DER is nominated; otherwise, if its state is within [0.5, 10), the given PV DER is not nominated. On the other hand, several algorithms are available for the operation of CMS modules including as follows:

- Uniform selection amongst all eligible candidate based on a uniform random distribution where all nominees share same interval in probability distribution space [0, 1]
- Non-uniform selection with memory where the selection of the cluster manager depends on the list of nominees and their past selection history. Preference may be given, for example, to PV DERs that have not been previously selected.

Similarly, several algorithms are available for the calculation of POP including as follows:

- Fixed time period
- Time period based on fixed value plus a randomly selected period

- Time period based on fixed value plus randomly selected time period with the provision of early termination

6.21.4 Example operation:

Results reported in Figure 70 suggests that the use of DRCA may significantly reduce overall probability of lead controller/cluster manager being compromised as compared to no-resiliency case. For example, for a given random attack scenario, the lead controller/cluster manager is compromised about 17% as opposed to 3.5%of the time when operating a non-resiliency and a resiliency case (using further-right resilient algorithm), respectively. Furthermore, in order to assess the sensitivity of DRCA performance to uncertainty in HE, Figure 71 confirms that as HE uncertainty increases, the likelihood for the lead controller/cluster manager being compromised also increases. For example, the lead controller/cluster manager is compromised about 6% (an increased from the 3% when there is 0 error in estimating health index, HI) as opposed to 17% when operating a non-resiliency and a resiliency case, respectively. The increase in the likelihood the cluster manager is compromised results from the HE incorrectly assessing that the system is healthier (with estimated HI being 0.6) than what it is actually (with actual HI being 0.2). However, DRCA still performs better than the no-resiliency case. However, the uncertainty associated with HE should be analyzed to ensure that DRCA operates adequately even under the presence of attack detection inaccuracies.

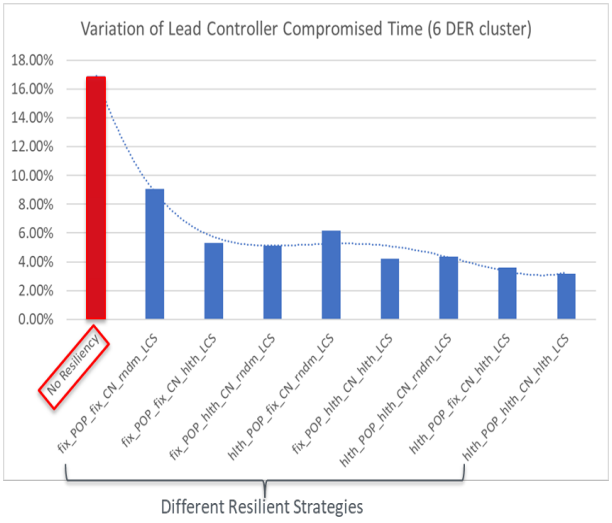

Figure 70: Variation of the time lead controller/cluster manager is compromised under different resilient strategies.

6.21.5 Implementation and interfacing:

DRCA module has been implemented in MATLAB scripts and functions, with no dependencies.

- **Inputs:**
  - cluster configuration
  - health index computed for each PV-DER in cluster

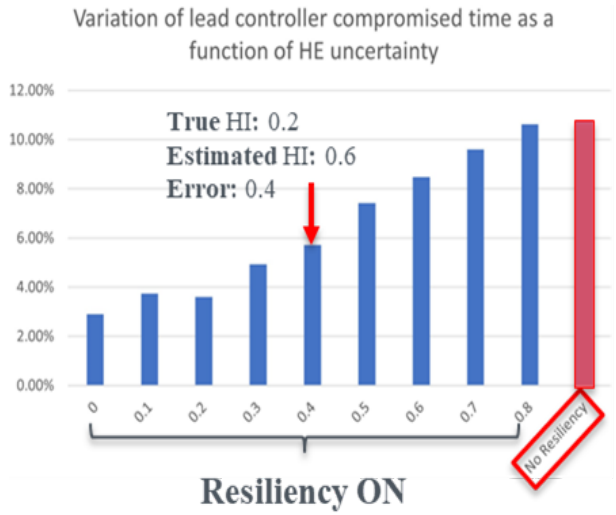

Figure 71: Variation of the time lead controller/cluster manager is compromised as a function of health index (HI) uncertainty.

- health index computed for each critical load defined for the distribution system under supervision
- selected algorithmic option for selecting cluster managers
- selected algorithmic option for computing POP for the just-selected cluster manager
- user-defined lower/upper bounds on POP

- **Inputs:**
  - PV-DER index to which managing role has been assigned to be cluster manager
  - Period-of-performance (in seconds) for current cluster manager assignment

6.22 E. Meta-Code for integrating RICE, HE, FE, and DRCA modules within ReDis-PV platform

The following material describes a Meta-code developed to guide the integration of the RICE, HE, FE, and DRCA modules previously described within the ReDis-PV platform. To this end, this Meta-code is divided into three distinct functional partitions each associated with three main computational environments existing within the ReDis-PV platform, namely, the ReDis-PV code, the Simulator Code, and DRCA code. This Meta-code was then translated into actual code during the integration phase of ReDis-PV.

Note:

- Color code: The color codes are as follows:

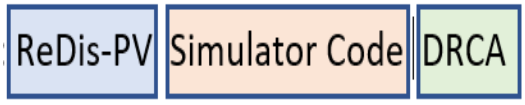

- Words "**get**" and "**pass**" indicate that the particular information at hand is collected from or injected to an outside entity without ever going through the communication layer
- Word "**load**" denotes an assignment (e.g., "load A with B" means A:= B)
- When no communication layer is included/modeled:
  - "**Port**" can simply denote a variable/record.
  - "**Send**" can simply indicate a "write", "put".

[## The following steps should be conducted whenever a new cluster organization is created ##]

If new cluster organization is created: [## Condition identified by a flag ##]

R1. **Get** from "Cluster Optimization Routine" number of clusters "ncl" and cluster organization (CO_i) and lead controller (LC_i) for each cluster "i" as well as Period-of-Performance (PoP_i) for each LC_i.

R2. For each cluster "i", i:1, ..., ncl:

a. Pack CO_i, LC_i, and PoP_i into a CLP_i package

b. Place CLP_i packages & new cluster "flag" into port (PRD) defined for ReDis-PV

R3. "**Send**" CLP_i packages & new cluster "flag" placed in PRD (defined for **ReDis-PV**) to the particular port (PLC_i) assigned to LC_i (defined for **DRCA** in **Simulator Code**) [## This line emulates DATA TRANSMISSION FROM ReDis-PV TO DRCA (VIA SIMULATOR CODE) ##]

S1. If new cluster flag in PRD specifies new cluster organization is created:

a. For each cluster "i", i:1, ..., ncl:
Load recCLP_i with the CLP_i packages received at PLC_i assigned to LC_i (defined for **DRCA** in **Simulator Code**) from PRD (defined for **ReDis-PV**) [## This line emulates DATA RECEPTION TO DRCA FROM ReDis-PV (VIA SIMULATOR CODE) ##]

S2. Pack recCLP_i into recCLPs

S3. Update DRCA with recCLPs [## DRCA does not execute internal modules ##]

a. Unpack recCLPs into CO_i, LC_i, and PoP_i

End if

[## The following steps should be conducted every time step (i.e., 1 sec) ##]

R4. Get (from NMSU) two (2) distinct sets: set (DCDER) of TRUE DoSS-compromised (1-ϕ, 3-ϕ) DERs and set (DDDER) of DoSS-detected (1-ϕ, 3-ϕ) DERs
R5. If demonstrating DoSS attacks, get critical load risks (CLRs) from RICE-DoSS module; otherwise, get CLRs from RICE-P module [## Risk estimates were computed using last known health calculations ##]
R6. Pass DCDER, DDDER, CLRs to **Simulator Code** [## WITHOUT GOING THROUGH COMM. LAYER ##]

S4. Get DER measurements (DMs) from PV DERs (in OpenDSS)
S5. Pack DM, DCDER, DDDER, and CLRs into DDDC package [## DDDC package is the INPUT set to DRCA ##]

S6. Invoke DRCA with DDDC package [## DRCA executes internal modules ##]

a. Unpack DDDC package into DM, DCDER, DDDER, and CLRs
b. Compute physical health indexes (HI-Ps) for each 3-ϕ DERs
c. Compute "physical health index for each 3-ϕ fleet DERf_i" (i.e., PHIDERf_i, i:1,…,nderf)
d. If demonstrating DoSS attacks, then:
    i. Assign DoSS health indexes (HI-DoSs) for each 3-ϕ DERs based on the set of DoSS-detected (1-ϕ, 3-ϕ) DERs
e. If demonstrating DoSS attacks, SHIs = HI-DoSs; otherwise, SHIs = HI-Ps
f. Compute fitness indexes (FIs) based on SHIs and CLRs
g. Compute candidate status (CSs) for all 3-ϕ DERs using FIs
h. Pack HI-P_i, SHI_i, and CS_i into HSC_i packages for each cluster "i"
i. For each cluster "i", i:1, …, ncl:
    i. Update PoP_i
    ii. If PoP_i <= 0,
        1. IF no 3-ϕ DER in cluster "i", randomly select a 1-ϕ DER as new LC_i and set its PoP
        2. ELSE determine new LC_i and compute its PoP_i based on SHI_i and CS_i
    iii. Pack LC_i, HI-P_i, and DM_i into an LHD_i package
    iv. If demonstrating DoSS attacks, then:
        1. Based on the set of TRUE DoSS-compromised (1-ϕ, 3-ϕ) DERs, determine whether LC_i has been DoSS-compromised
        2. If LC_i is DoSS-compromised, create a set SDDER_i listing all its subordinate (1-ϕ, 3-ϕ) DERs_i that are not DoSS-compromised (based on DCDER)
j. Pack PHIDERfs, LHDs, and SDDERs into PLS package
    i. PHIDERfs, LHDs, and SDDERs are constructed by accordingly grouping PHIDERf_i (i:1,…,nderf), LHD_i (i:1,…,ncl), SDDER_i (i:1,…,ncl), respectively.
k. Return PLS package [## PLS package is the OUTPUT set of DRCA ##]

S7. Unpack PLS package into PHIDERfs, LHDs, and SDDERs

S8. Pass shutdown commands to each (1-ϕ, 3-ϕ) DERs listed in SDDERs ([## This line should result in shutting down (1-ϕ 3-ϕ) DERs in Simulator ##]

S9. Pass PHIDERf_i, i:1,...,nderf, to **ReDis-PV** [## WITHOUT GOING THROUGH COMM. LAYER ##]

S10. For each cluster "i", i:1, ..., ncl:

a. Place LHD_i package into PLC_i

S11. For each cluster "i", i:1, ..., ncl:

a. "Send" LHD_i packages placed in PLC_i assigned to LC_i (defined for **DRCA** in **Simulator Code**) to PRD (defined for **ReDis-PV**) ([## This line emulates DATA TRANSMISSION FROM DRCA TO ReDis-PV ##]

R7. Get PHIDERf from Simulator Code

R8. Load recLHD_i with the LHD_i packages received at PRD (defined for **ReDis-PV**) from PLC_i assigned to LC_i (defined for **DRCA** in **Simulator Code**) [## This line emulates DATA RECEPTION TO ReDis-PV FROM DRCA (VIA SIMULATOR CODE) ##]

R9. Pass PHIDERf_i, i:1,...,nderf, to RICE-P module

R10. If demonstrating DoSS attacks, then:

a. get (from NMSU) "DoSS health index for each fleet DERf_i" (i.e., DHIDERf_i, i:1,...,nderf) and pass DHIDERf_i, i:1,...,nderf, to RICE-DoSS module

7 Significant Accomplishments and Conclusions

7.1 Overall Outcome

- Integrated tool that works in conjunction with the legacy and inverter-based controllers, existing communication system, meters, and DMS to monitor the 'health' of the distribution grid with high penetration of PVs and other DERs.
- A management mechanism to utilize PVs, Energy Storage, and flexible loads, to support critical infrastructure during emergencies and improve reliability during normal operation.

7.2 Main Features

- Capable of dynamically updating the grid model during normal operation and during cyber or physical threats.
- Capable of assessing cyber and physical security and developing a risk level which is then used for managing the DERs.
- Modular and can be seamlessly integrated with the existing infrastructure (a non-proprietary vendor-agnostic solution).
- Capable of dynamically re-configuring and managing DERs based on grid conditions with operator override features.

7.3 Project Relevance

- The project develops a unique management framework that allows higher penetration of DERs with increased reliability and resiliency.
- The project develops a unique situational awareness tool that can be used by the operator for organizing the DERs in terms of availability, usability and improved dispatch-ability.
- A holistic approach and a unique platform that can evaluate threats and provide a risk level.
- Fully in line with DOE program goals as mentioned in FOA.

In short, this project has a major impact on cyber and physical security, machine learning, data-driven control, distributed optimization, reconfiguration, protection, and vulnerability assessment in power distribution systems. Workforce development, training, project management, and technical knowledge base development have been done for human resources. New products and designs in power systems, renewable energy, communication systems, and data analytics and learning topics impact on teaching and educational experiences. New laboratory for micro-grid testing and DER-integrated distribution system modeling has been established.

8 Path Forward

Currently, Duke Energy does not have field visibility and control capability on the power distribution system as the DMS/DERMS platform provides only a central control option from a SCADA-enabled substation. This is not enough and a gap that needs to be addressed if they were to aggregate and integrate DERs into the grid for advances in renewable integration or supporting the power grid. ReDis-PV can bridge this gap and manage the field devices/DERs effectively. At the same time, this tool can also interact with central controllers such as DMS. This is an interesting and important capability. Duke Energy is now looking forward to using the tool at least in part on the Duke system.

8.1 User experience and benefits to the tool

This is an operational tool that manage DER clusters in the power distribution system to facilitate improving grid reliability and resiliency and at the same time supporting critical infrastructure. The main benefits of this tool are:

- The tool can analyze dynamic integrated transmission and distribution model with situational awareness.
- The tool can provide cluster organization of the distributed energy resources (DERs), provide area control and inter-cluster control of DERs,
- The tool can optimize the distribution grid and provide set point for area-control and local control module as a centralized and/or distributed optimization.
- The tool can perform dynamic cluster control and risk/threat resiliency assessment.
- The tool has developed protection and reconfiguration functions in the wake of fault and disturbances in the system.
- The tool has a dedicated communication co-simulatiom module that is threat aware and detect and mitiage threats.
- The tool has a dynamic field implementation component that can be used to evaluate the hardware.

8.2 Implementation Methodology of the Tool in the operational Environment

In the ReDisPV, ten models were run with 5 use cases. Model types with the use cases are as follows:

RedisPV

I.Model Type

```
'''
1. 123bus
2. 13bus
3. 650bus with pv
4. 2500bus with pv
5. 8500node with pv
6. 123bus+15pv
7. 123bus+15pv (Singlephase)
8. 123bus+15pv+4ss (Singlephase)
9. Duke Feeder
10. 2500bus with pv + reconfig
'''
model_id=9
```

II. Application Type

```
'''
Application Type
1. Smoothing (Minimizing netload variation)
2. Tieflow Management (Tieflow=0)
3. Cluster Netload minimization (OPF=0)
4. OPF Tracking
5. Area Error Minimization
'''
app_id=1
```

III. OPF Type

```
'''
opftype
0: No OPF
1: OPF1
2: OPF2
3: OPF1 and OPF2
'''
opftype=0
```

IV. Include Regulator

```
'''
Include Regulator setpoints (Not supported in NS-3)
1: Yes
0: No
'''
include_regulator=1
```

Figure 72: Snapshot from ReDisPV code (continue).

V. Communication Type

```
'''
Communication type or "commtype"
1: TCP based
2: NS3 based

'''
commtype=1
```

VI. Cluster type

```
'''
Clustertype
1: Active Power
2: Sensitivity based
3: Active power and Sensitivity based

'''
Clustertype=1
```

VII. Switch inclusion status

```
'''
includeswitch
1: Limit cluster boundary at switch locations
0: Do not limit cluster boundary at switch locations
'''
includeswitch=0
```

VIII. Jacobian study status

```
'''
Jacobian Study
1: Yes
'''
jacobianstudy=0
```

IX. Reconfiguration status

```
'''
Reconfiguration
1: Yes
0: No
'''
recon = 1
```

X. Visualization status

```
'''
Visualization
1: Yes
0: No
'''
vis_mod = 0
```

Figure 73: Snapshot from ReDisPV code.

Simulator Run

I. Model Type

```
'''
1. 123bus_with_10pv
2. 13bus
3. 650bus with pv
4. 2500bus with pv
5. 8500node with pv
6. 123 Bus system with15PV
8. 123bus+15pv+4ss
9. Duke Feeder
10. 2500bus with pv + reconfig
'''
modeltype=9
```

II. Regulator status

```
'''
Include Regulator setpoints (Not supported in NS-3)
1: Yes
0: No
'''
include_regulator=1
```

III. Communication type

```
'''
Communication type or "commtype"
0: No Communication(In case of solo simulation)
1: TCP based
2: NS3 based
3: TCP based lead der to follower der
'''
commtype=1
```

IV. DRC Status

```
'''
Include DRC "include_drc
0: No
1: Yes
'''
includedrc=0
```

V. Simulation type

```
'''
Simulation type "simulationtype"
1.Solo-run
2.With ReDisPV
3. OpalRT
'''
simulationtype=2
'''
Simulation Start Time and End Time
'''
starttime=43200
endtime=54000
```

Figure 74: Snapshot from Simulator Run.

For running the cases on the Duke feeder, the following steps shown in Figure 75 to **??** should be followed: After the above steps, one needs to click the 'run' icon.

Use Case 1: Netload Smoothing
Use Case 2:

1. Area Error minimization- Use the "area_setpoints_DF1.xlsx" file in the location C:\Users\Name\eclipse-workspace\CoSim_7_27_s\CoSimulator\Models\OpenDSS\123busdata
2. Change the file name in **getareasetpoints** function in Cluster_Control.py file

Use Case 3: Reconfiguration

RedisPV Settings

	Variable Name	Use Case 1	Use Case 2	Use Case 3
Model Type	model_id	9	9	9
Application Type	app_id	1	5	1
OPF Type	opftype	0	0	0
Include Regulator	include_regulator	0	0	0
Communication Type	commtype	1	1	1
Cluster type	Clustertype	1	1	1
Switch inclusion status	includeswitch	0	0	0
Jacobian study status	jacobianstudy	0	0	0
Reconfiguration status	recon	0	0	1
Visualization status	vis_mod	0	0	0

	Variable Name	Use Case 1	Use Case 2	Use Case 3
Application Type	app_id	1	5	1
Reconfiguration status	recon	0	0	1

Simulator run Settings

	Variable Name	Use Case 1	Use Case 2	Use Case 3
Model Type	modeltype	9	9	9
Regulator status	include_regulator	1	1	1
Communication type	commtype	1	1	1
DRC Status	includedrc	0	0	0
Simulation type	simulationtype	2	2	2
Simulation Start time	starttime	43200	43200	43200
Simulation end time	endtime	54000	54000	54000

	Variable Name	Use Case 1	Use Case 2	Use Case 3
Simulation Start time	starttime	43200	43200	43200
Simulation end time	endtime	54000	54000	54000

Figure 75: Duke Feeder simulation steps (continue).

How to Run the Use Cases for Duke Feeder

To run the use cases, one should follow the following steps.

Use Case 1:

a. **ReDis_PV Settings:** . first go to the "----------\CoSim_7_27\CoSimulator.ReDisPV_v03.py" and open it through the **Eclipse IDE**.

1. First set the "model_id=9" like the following picture.

```
1. 123bus
2. 13bus
3. 650bus with pv
4. 2500bus with pv
5. 8500node with pv
6. 123bus+15pv
7. 123bus+15pv (Singlephase)
8. 123bus+15pv+4ss (Singlephase)
9. Duke Feeder
10. 2500bus with pv + reconfig
'''
model_id=9
```

2. Set the "app_id=1" like the following picture.

```
Application Type
1. Smoothing (Minimizing netload variation)
2. Tieflow Management (Tieflow=0)
3. Cluster Netload minimization (OPF=0)
4. OPF Tracking
5. Area Error Minimization
'''
app_id=1
```

3. Set the "opf_type=0" , "include_regulator=0" and "commtype=2" like the following.

```
opftype
0: No OPF
1: OPF1
2: OPF2
3: OPF1 and OPF2
'''
opftype=0
```

```
Include Regulator set
1: Yes
0: No
'''
include_regulator=0
```

```
Comtype
Communication type or "comm

1: TCP based
2: NS3 based

'''
#commtype=1
commtype=2
```

4. Set the "clustertype=1", "includeswitch=0" and "jacobianstudy=0" like the following.

Figure 76: Duke Feeder simulation steps (continue).

```
89 Clustertype
90 1: Active Power
91 2: Sensitivity based
92 3: Active power and Sensitivit
93
94 '''
95 Clustertype=1
```

```
98 includeswitch
99 1: Limit cluster
100 0: Do not limit
101 '''
102 includeswitch=0
```

```
107 Jacobian Study
108 1: Yes
109 '''
```

5. Set the reconfiguration status “recon=0”.

```
120 Reconfiguration
121 1: Yes
122 '''
123 recon = 0
```

b. **Simulator Run settings:** Open the “---------- \CoSim_7_27\CoSimulator\OpenDSS\simulator_run3.py”. Then follow the following setpoints.

1. First set the “model_id=9” like the following picture.

```
36 1. 123bus
37 2. 13bus
38 3. 650bus with pv
39 4. 2500bus with pv
40 5. 8500node with pv
41 6. 123bus+15pv
42 7. 123bus+15pv (Singlephase)
43 8. 123bus+15pv+4ss (Singlephase)
44 9. Duke Feeder
45 10. 2500bus with pv + reconfig
46 '''
47 model_id=9
```

2. Set the “include_regulator=0” and “commtype=2” like the following.

```
72 Include Regulator setpoints
73 1: Yes
74 0: No
75 '''
76 include_regulator=0
```

```
78 Comtype
79 Communication type or "commtype"
80
81 1: TCP based
82 2: NS3 based
83
84 '''
85 #commtype=1
86 commtype=2
```

3. Set the “includedrc=0” and “simulationtype=2” like the following.

Figure 77: Duke Feeder simulation steps.

8.2.1 System Requirements

The current version of ReDis-PV is built on Eclipse IDE (Integrated Development Environment). Ensure to use the most recent version of the software. For Windows-based installation process follows the following steps.

- **Step-1 (Download and install Eclipse):** Eclipse can be downloaded for free from **here**

and follow the installation instructions from the same site. For ReDisPV, it is most likely that the administrator will provide you with Eclipse IDE and the folder files containing the project's source codes.

- **Step-2 (Run Eclipse):** Specify your workspace location after installation. Accept the default settings and go to the Welcome window. Then, proceed to set up the PyDev plugin using these subsequent steps.
- **Step-3 (Download and install PyDev):** With running Eclipse, activate the Eclipse Marketplace dialog box, From the installer box, type the link and click go to. This will show new features in the dialog box, as shown in Figure 78. Be sure to confirm the selection of PyDev-Python IDE for Eclipse and proceed. Then restart the application from a new pop-up **Restart Now** to apply the changes.

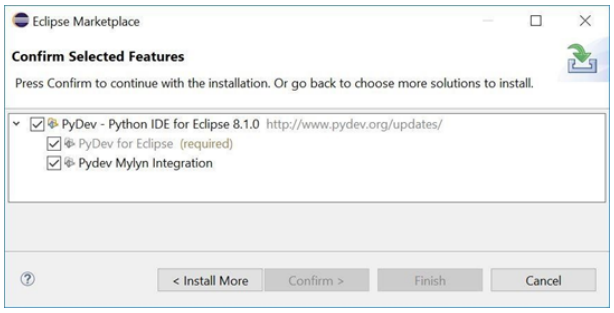

Figure 78: Installation of PyDev plugin.

- **Step-4 (Verify the PyDev installation):** Verify that PyDev installation has been completed, start a new project, and from the new project window, ensure you can see PyDev as one of the options that you can click in the window.
- **Step-5 (Configure PyDev to execute operations by using Python 3 interpreter):** To configure the PyDev environment for Python-3, You need to create a new PyDev project by navigating through this procedure on eclipse : 'File -> New ->Project -> PyDev -> PyDev Project' Then a PyDev Project window appears, as illustrated in Figure 79, and you can follow the prompt. Navigate and click on the blue line that states **"Please configure an interpreter before proceeding"**. After that, a new pop-up window shows up, navigate and click on the **"Choose from list"** (as illustrated in Figure 79). Wait on Eclipse to display all python interpreters available on your computer. When the list is presented, locate and choose the appropriate interpreter, and you should click on the OK button to proceed. A message then appears in Eclipse **"Configuring"** and then "Sync System **PYTHONPATH"**. The messages will disappear when complete. The default interpreter is displayed on the page. Suppose you would like to check the selection or change the interpreter setting at any point. In that case, You can click on the blue link that states **"Click here to configure an interpreter not listed"**, then select any desired python interpreter in a dialog box shown in Figure 80.
- **Step-6 (Validate the interpreter installation through Packages):** Most python interpreters come with default packages installed on them. Check that you are able to use some of the packages, such as numpy and pandas packages. Ensure you have them

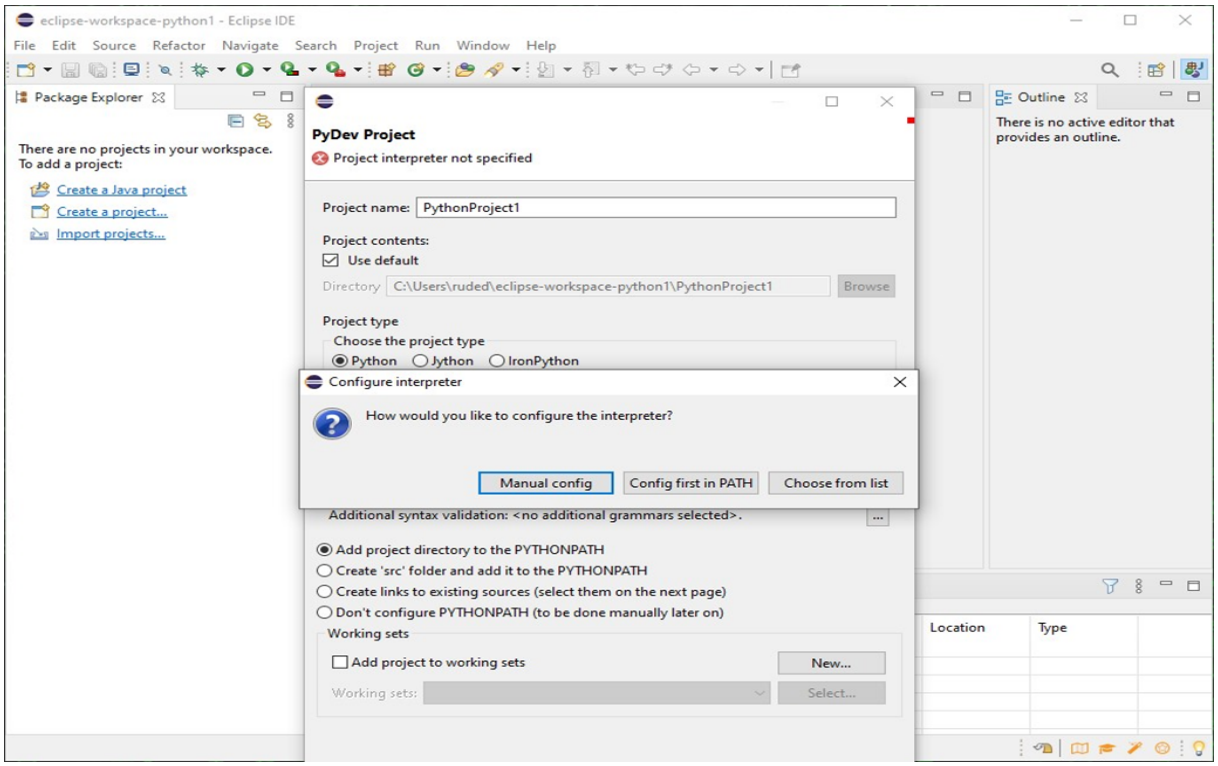

Figure 79: PyDev Project interpreter configuration.

properly set up and visible to Eclipse at this point. To verify that, you will need to access the PyDev Console:
1. Display the eclipse Console tab (illustrated in Figure 81). You can display this by navigating and selecting the following menu option 'Window -> Show View -> Console'.
2. Navigate to the Console tab and click on a yellow plus sign icon. Then select PyDev Console from the list of available consoles, as illustrated in Figure 81. You can then type the following into the console window and execute: **'import numpy'** & **'import pandas'**.

If no error is displayed in the console, the packages were installed and executed correctly. They are now ready to be used for different package applications. Otherwise, you may need to go back to **Step-5** again.

- **Step-7 (Installing Additional Python packages):** ReDisPV contains several dependencies that must be installed before some part of the simulations can be run. The following shows the installation of one of the dependencies named **'openpyxl'**. A similar procedure can be used for other dependencies. On the top bar giving the menu option of the eclipse page, navigate **'Window -> Show View -> Preferences'**.

  The Python Interpreters window is shown in Figure 81 from the list on the left-hand side. Be sure to navigate to **'PyDev-> Interpreters -> Python Interpreters'**. You can view the already installed packages. To install a new one such as **'openpyxl'**. Click on Manage with pip. Then a new pop-up window shows up as illustrated in Figure 82. On the command to execute prompt, type **'install openpyxl'** or any other package you'd like to install if available with **'pip'**. Click run and watch the progress of the installation till you see a finished or successfully installed message. The installed package will be added

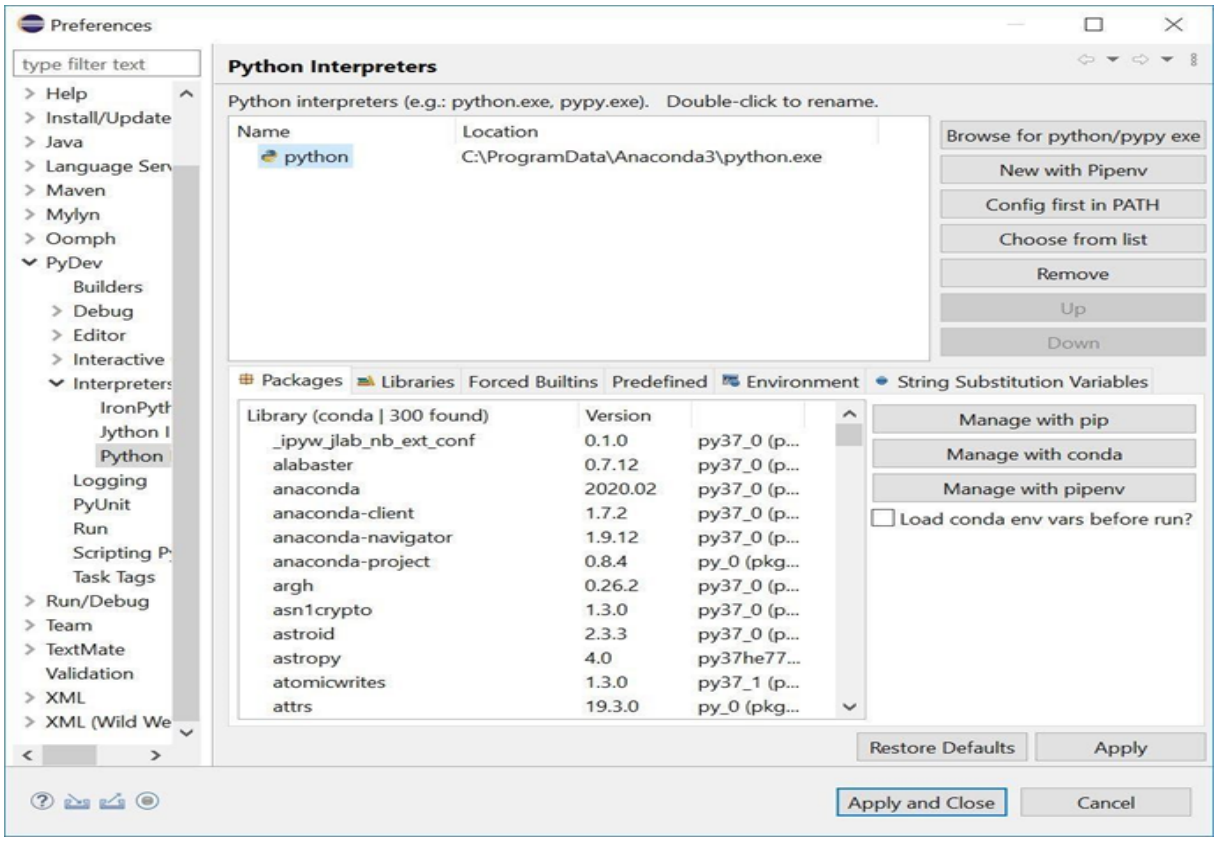

Figure 80: Configuring/Selecting Python Interpreter.

to your python libraries. Then you may go back to the console to import the package or use it in any part of our program development.

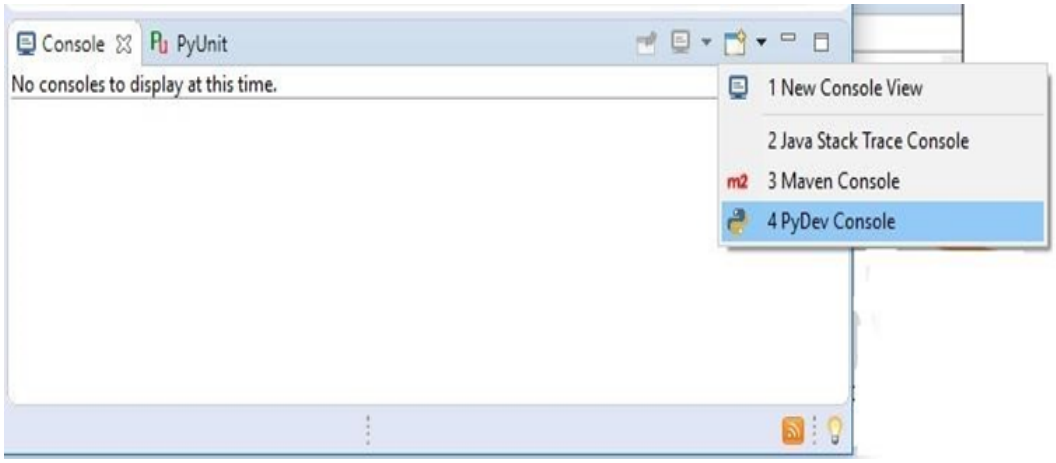

Figure 81: Navigating to PyDev Console Tab.

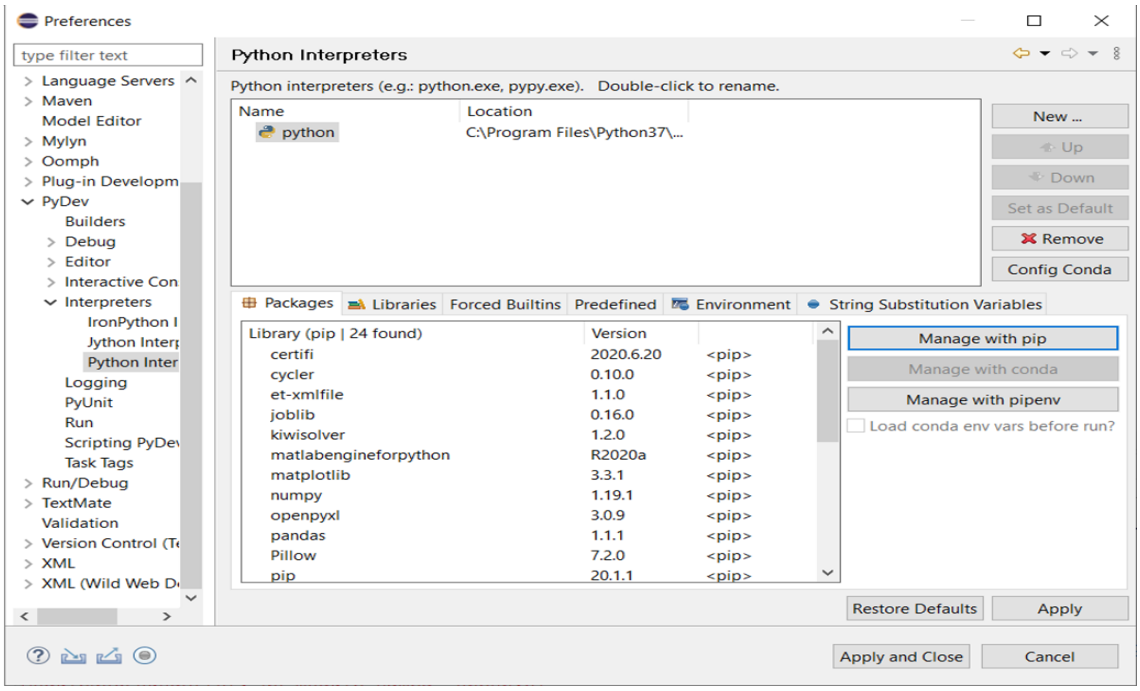

Figure 82: Adding Packages to Python Interpreter.

8.3 Next Steps beyond the DOE project

The proposed tool is currently being evaluated by the local utility (Duke Energy). Following are the path forward and next steps beyond the DOE project.

The first step is to evaluate the tool as described above. For this, the models and the entire implementation process are developed as a user guide and delivered to Duke Energy. We are expecting to have this work completed soon. The next step is to identify the part of the module and or tool that can be implemented in the field. We will have a conversation with Duke Energy in this regard after the verification. Then the next path is to identify a possible location (feeder) to test the algorithm. Then the feeder model and the communication design will be evaluated and verified using the tool. Then the field data integration and testing will be performed. Finally, a set implementation plan for a few modules will be developed and the performance will be evaluated. The goal is to accomplish these activities in stages and complete these activities in the next couple of years.

9 Products

One of the products resulting from this effort is the formulation, implementation, and evaluation of the DRC architecture mentioned and its constituting elements.

A. Publications, conference papers, and presentations

- D. Pylorof, H. E. Garcia, and R. Bhattarai, “Risk-Informed Condition Evaluation for Solar-centered Energy Generation and Distribution Networks through Bayesian Learning and Inference," 2023 IEEE Innovative Smart Grid Technologies (ISGT) Conference (to appear).
- Alper Savasci, Adedoyin Inaolaji, and Sumit Paudyal, “Optimal Coordination of On-Load Tap Changers with Local Control Rules," in Proc. IEEE IAS Annual Meeting, 2022.
- R. Bhattarai and H. E. Garcia, “Online Operational Health Monitoring of Photovoltaic Distributed Energy Resources" Proc. Power and Energy Society General Meeting (PESGM), 2022.
- Arun Suresh, Krishna Murari, and S. Kamalasadan "Injected Current Sensitivity Based Load Flow Algorithm for Multi-Phase Distribution System in the Presence of Distributed Energy Resources, accepted for publication in IEEE Transactions on Power Delivery, April 2022.
- Krishna Murari, and S. Kamalasadan "Graph Based Power Flow Algorithm for Three-Phase Distribution Network Considering Regulators and Distributed Generations, accepted for publication in IEEE Transactions on Industry Applications, May 2022.
- S.patel, Krishna Murari, and S. Kamalasadan "Distributed Control of Distributed Energy Resources in Active Power Distribution System for Local Power Balance with Optimal Spectral Clustering, accepted for publication in IEEE Transactions on Industry Applications, May 2022.
- A. Dubey, S. Paudyal, and S. Kamalasadan, "Mathematical Optimization in Active Power Distribution Systems," Tutorial in IEEE ISGT NA. 2022.
- A. Inaolaji, A. Savasci, S. Paudyal, and S. Kamalasadan, "A Consensus ADMM-Based Distributed Volt-VAr Optimization for Unbalanced Distribution Networks," in Proc. IEEE IAS Annual Meeting, 2022.
- Phani Gadde, Sukumar Brahma, "Unbalance Compensation Using Single Phase Inverters in Inverter-Dominated Microgrids" Accepted, Power System Computation Conference (PSCC) 2022.
- Phani Harsha Gadde, Sukumar Brahma, "Topology-Agnostic, Scalable, Self-Healing and Cost-Aware Protection of Microgrids, accepted for IEEE Transactions on Power Delivery, November 2021.
- Prabin Adhikari, Sukumar Brahma, Phani Harsha Gadde, Source-Agnostic Time-Domain Distance Relay, accepted for IEEE Transactions on power Delivery, November 2021.
- M. A. Mamun, S. Paudyal, and S. Kamalasadan, “Windowing based Waveform Relaxation Method for Real-Time Power System Dynamic Simulation," Proc. IEEE Power and Energy Society General Meeting (PES GM), 2021.
- A. Savasci, A. Inaolaji, S. Paudyal, and S. Kamalasadan, “Efficient Mixed-Integer Distribution Grid Optimal Power Flow with Control of Legacy Grid Devices," Proc. Power and Energy Society General Meeting (PESGM), 2021.
- A. Inaolaji, A. Savasci, S. Paudyal, and S. Kamalasadan, “Accuracy of Phase-Decoupled and Phase-Coupled Distribution Grid Power Flow Models," Proc. IEEE Innovative Smart Grid Technology (ISGT) Conference, 2021.

- G. Ravikumar, D. Ameme, S. Misra, S. Brahma and R. Tourani, "iCASM: An Information-Centric Network Architecture for Wide Area Measurement Systems," in IEEE Transactions on Smart Grid, vol. 11, no. 4, pp. 3418-3427, July 2020.
- Shyamal Patel, Krishna Murari, S. Kamalasadan, “Distributed Control of DERs in Power Distribution Grid Based on Spectral Clustering ”, IEEE PEDES 2020 , Jaipur, India.
- Aravind Ingalalli, S. Kamalasadan, “An Integrated State-Space Model For Grid Feeding and Grid Forming Inverters ”, IEEE PEDES 2020 , Jaipur, India.
- Arun Suresh, Robin Bisht, and Sukumar Kamalasadan, “ADMM Based LQR for Voltage Regulation Using Distributed Energy Resources”,IEEE PEDES 2020, Jaipur, India.
- Aravind Ingalalli, S. Kamalasadan, “A Universal Multiple Inverter Control Architecture With Droop Control For Unbalanced AC Grids ”, IEEE ISGT 2021.
- Anju James, George Torres, Sharad Shrestha, Reza Tourani, Satyajayant Misra, "iCAAP: information-Centric network Architecture for Application-specific Prioritization in Smart Grid", Innovative Smart Grid Technologies (ISGT 2021).
- Arun Suresh, Sukumar Kamalasadan, Sumit Paudyal, "Investigation of Transmission and Distribution Co-Simulation Approaches for Studying Voltage Stability Assessment and Margin", in Proc. Power Energy Society General Meeting, 2021.
- Travis Machacek, M. Biswal and Satyajayant Misra, "Proof of X: Experimental Insights on Blockchain Consensus Algorithms in Energy Markets," IEEE ISGT 2021.
- Krishna Murari and Sukumar Kamalasadan, “Graph Based Power Flow Approach for Single Phase Distribution System with Distributed Generators(DGs) Considering All Load Types”, IEEE Industry Applications Society Annual Meeting 2021, Vancouver, Canada, 2021.
- Krishna Murari, N.P. Padhy and Sukumar Kamalasadan, “Backward-Forward Sweep Based Power Flow Algorithm for Radial and Meshed AC-DC Distribution System”, IEEE Industry Applications Society Annual Meeting 2021, Vancouver, Canada, 2021.

Website(s): www.redispv.org

Technologies or techniques: NDN Network model github - https://github.com/NmsuNsol (under development)

Inventions, patent applications, and/or licenses: Nothing to Report

Other Products: Nothing to Report.

10 Project Team and Roles

The following individuals worked on this project. Their roles have also been included below.

ANL

1. Kumarsinh Jhala, Researcher, is assisting UNCC and NMSU in identifying the communication needs for the overall project objectives and leading the effort in determining the communication architecture and studying the impacts on communication systems on distribution system operation and control.

UNCC

1. Sukumar Kamalasadan, PI, is leading the overall project coordination and developing the power grid models. He also leads the overall project management. Working on Task 2, planning, reporting, and coordinating with the financial office.
2. Shyamal Patel. The researcher is leading the effort on modeling and cluster design and control.
3. Krishna Murari, Postdoctoral Fellow, is leading the effort on developing dynamic models and developing a theoretical basis on DER cluster management and control.
4. Tao Han, Co-PI, is leading the NS3 integration and coordinating with NMSU and ANL.
5. Md Shamim Hasan. The researcher is leading the effort on modeling and development of Optimization Algorithm.
6. Roopa Ramachandran. The researcher is leading the effort on modeling and design of the whole ReDisPV architecture using the Python Script.
7. Md Mahmud-ul-Tarik Chowdhury. The researcher is leading the effort on modeling of optimal power flow for the integrated transmission and distribution system.

FIU

1. Sumit Paudyal, Co-PI, is responsible for managing the project at FIU, advising two Ph.D. students to work on the Task# 3, checking the accuracy of power flow models, reporting, and participating in the bi-weekly team meeting. Dr. Paudyal was responsible for managing the project at FIU, advising two Ph.D. students to work on the Task# 3, checking the accuracy of models and simulations, reporting, and participating in bi-weekly team meetings.
2. Adedoyin Inaolaji, developed SOCP version of OPF and tested using 650-node distribution system. Adedoyin also worked on creating the case studies the part of the reports related to the Task#3.3.
3. Alper Savasci, Researcher, developed the MISOCP model for the IEEE 123-node, created the case studies, and prepared the part of the reports related to the Task#3.4.
4. Mamum M Al, Researcher, developed the ephasorsim model for electric distribution system related to the Task#10.

INL

1. Humberto Garcia, Co-PI, is responsible for managing the overall project at INL. Dr. Garcia is also leading the efforts for the formulation, development, and evaluation of the dynamic resilient control architecture and its components and supports Dr. Bhattarai and Dr. Banerjee in the implementation and testing of them.
2. Rojan Bhattarai is leading the efforts from the INL side for the development and benchmarking the distribution system as well as the integrated T&D system including DER models and supports Dr. Banerjee on the tasks related to the DRC architecture.
3. Abhishek Banerjee is working on the design, implementation, and testing of the DRC architecture and its components.
4. Dimitri L is working on the design, implementation, and testing of the RICE and DRCA Archiecture learning alrogithms.

Clemson

1. Sukumar Brahma, Co-PI, Provide guidance to the postdoctoral scholar, and project management. He also carried out initial studies on protection in the presence of inverter-based resources.
2. Hany Habib, Postdoctoral Fellow worked on enabling communication platforms to support any protection scheme that may be developed later in the year.
3. Phani Gharde, Research Associate worked on developing protection and reconfiguration algorithms.

NMSU

1. Satyajayant Misra, Co-PI, overall project coordinator on communication systems and cyber-security aspects. He guides students and engages in overall project coordination other than the technical work.
2. Dan Ameme, Researcher, has worked on the design and initial implementation of the architecture.
3. Anju James, Researcher, is working on designing the multi-priority packet treatment in the architecture and implementing it in the simulator.
4. George Torres, Researcher, New Mexico State University, is working on the designing and implementation of the token-bucket and the integration of the codebase with the simulator to get preliminary results.
5. Sharad Shreshta, Researcher, New Mexico State University, is working on the designing and implementation of the DDoSS attack and mitigation architecture.

OPAL-RT Corporation

1. Sudipta Chakraborty, Co-PI, worked on coordination activities.
2. Zerui Dong, Co-PI, worked on coordination activities.
3. Guna Bharati, Engineer, worked on modeling IEEE 8500 and 650 node system in ephasorsim.

11 References

References

[1] Sherif Abdelrazek and Sukumar Kamalasadan. A weather-based optimal storage management algorithm for pv capacity firming. *IEEE Transactions on Industry Applications*, 52(6):5175–5184, 2016.

[2] Augusto Matheus dos Santos Alonso, Luis De Oro Arenas, Danilo Brandao, Elisabetta Tedeschi, and Fernando Pinhabel Marafao. Integrated local and coordinated overvoltage control to increase energy feed-in and expand der participation in low-voltage networks. *IEEE Transactions on Sustainable Energy*, pages 1–1, 2022.

[3] Fahd Amjad, Ephraim Bonah Agyekum, Liaqat Ali Shah, and Ahsan Abbas. Site location and allocation decision for onshore wind farms, using spatial multi-criteria analysis and density-based clustering. a techno-economic-environmental assessment, ghana. *Sustainable Energy Technologies and Assessments*, 47:101503, 2021.

[4] Kyriaki E. Antoniadou-Plytaria, Iasonas N. Kouveliotis-Lysikatos, Pavlos S. Georgilakis, and Nikos D. Hatziargyriou. Distributed and decentralized voltage control of smart distribution networks: Models, methods, and future research. *IEEE Transactions on Smart Grid*, 8(6):2999–3008, 2017.

[5] George W. Arnold. Challenges and opportunities in smart grid: A position article. *Proceedings of the IEEE*, 99(6):922–927, 2011.

[6] Christian Böhm, Robert Noll, Claudia Plant, and Bianca Wackersreuther. Density-based clustering using graphics processors. New York, NY, USA, 2009. Association for Computing Machinery.

[7] Eduard Bullich-Massagué, Francisco Díaz-González, Mònica Aragüés-Peñalba, Francesc Girbau-Llistuella, Pol Olivella-Rosell, and Andreas Sumper. Microgrid clustering architectures. *Applied Energy*, 212:340–361, 2018.

[8] Ricardo JGB Campello, Peer Kröger, Jörg Sander, and Arthur Zimek. Density-based clustering. *Wiley Interdisciplinary Reviews: Data Mining and Knowledge Discovery*, 10(2):e1343, 2020.

[9] Rui Cheng, Zhaoyu Wang, Yifei Guo, and Qianzhi Zhang. Online voltage control for unbalanced distribution networks using projected newton method. *IEEE Transactions on Power Systems*, pages 1–1, 2022.

[10] Ghazal Fazelnia, Ramtin Madani, Abdulrahman Kalbat, and Javad Lavaei. Convex relaxation for optimal distributed control problems. *IEEE Transactions on Automatic Control*, 62(1):206–221, 2017.

[11] Nuwan Ganganath, Jing V Wang, Xinzhi Xu, Chi-Tsun Cheng, and K Tse Chi. Agglomerative clustering-based network partitioning for parallel power system restoration. *IEEE Transactions on Industrial Informatics*, 14(8):3325–3333, 2017.

[12] Sudipta Ghosh and Sukumar Kamalasadan. An integrated dynamic modeling and adaptive controller approach for flywheel augmented dfig based wind system. *IEEE Transactions on Power Systems*, 32(3):2161–2171, 2016.

[13] M. Girolami. Mercer kernel-based clustering in feature space. *IEEE Transactions on Neural Networks*, 13(3):780–784, 2002.

[14] Óscar Gonzales-Zurita, Jean-Michel Clairand, Elisa Peñalvo-López, and Guillermo Escrivá-Escrivá. Review on multi-objective control strategies for distributed generation on inverter-based microgrids. *Energies*, 13(13):3483, 2020.

[15] Megha Goyal and Arindam Ghosh. Microgrids interconnection to support mutually during any contingency. *Sustainable Energy, Grids and Networks*, 6:100–108, 2016.

[16] Kelsey A Horowitz, Zachary Peterson, Michael H Coddington, Fei Ding, Benjamin O Sigrin, Danish Saleem, Sara E Baldwin, Brian Lydic, Sky C Stanfield, Nadav Enbar, et al. An overview of distributed energy resource (der) interconnection: Current practices and emerging solutions. Technical report, National Renewable Energy Lab.(NREL), Golden, CO (United States), 2019.

[17] Iroshani Jayawardene, Pramod Herath, and Ganesh Kumar Venayagamoorthy. A graph theory-based clustering method for power system networks. In *2020 Clemson University Power Systems Conference (PSC)*, pages 1–8, 2020.

[18] Sukumar Kamalasadan and Adel A Ghandakly. Multiple fuzzy reference model adaptive controller design for pitch-rate tracking. *IEEE Transactions on Instrumentation and Measurement*, 56(5):1797–1808, 2007.

[19] Guannan Li and Yunpeng Hu. Improved sensor fault detection, diagnosis and estimation for screw chillers using density-based clustering and principal component analysis. *Energy and Buildings*, 173:502–515, 2018.

[20] Longlong Liao, Kenli Li, Keqin Li, Canqun Yang, and Qi Tian. A multiple kernel density clustering algorithm for incomplete datasets in bioinformatics. *BMC systems biology*, 12(6):99–116, 2018.

[21] Subir Majumder, S.A. Khaparde, Ashish Prakash Agalgaonkar, S. V. Kulkarni, and Sarath Perera. Graph theory based voltage sag mitigation cluster formation utilizing dynamic voltage restorers in radial distribution networks. *IEEE Transactions on Power Delivery*, pages 1–1, 2020.

[22] Seyedmahdi Moghadasi and Sukumar Kamalasadan. Optimal fast control and scheduling of power distribution system using integrated receding horizon control and convex conic programming. *IEEE Transactions on Industry Applications*, 52(3):2596–2606, 2016.

[23] S. Patel, M. Ahmed, and S. Kamalasadan. A novel energy storage-based net-load smoothing and shifting architecture for high amount of photovoltaics integrated power distribution system. *IEEE Transactions on Industry Applications*, 56(3):3090–3099, 2020.

[24] Shyamal Patel, Krishna Murari, and Sukumar Kamalasadan. A spectral clustering based distributed control of distributed energy resources (ders) integrated power distribution system. In *2020 IEEE International Conference on Power Electronics, Drives and Energy Systems (PEDES)*, pages 1–6. IEEE, 2020.

[25] Ali Peiravi and R Ildarabadi. A fast algorithm for intentional islanding of power systems using the multilevel kernel k-means approach. *Journal of Applied Sciences*, 9(12):2247–2255, 2009.

[26] C Piciarelli, C Micheloni, and GL Foresti. Kernel-based clustering. *Electronics letters*, 49(2):113–114, 2013.

[27] Cong Shen, Paul Kaufmann, and Martin Braun. Fast network restoration by partitioning of parallel black start zones. *The Journal of Engineering*, 2017(8):418–426, 2017.

[28] Rubén J. Sánchez-García, Max Fennelly, Seán Norris, Nick Wright, Graham Niblo, Jacek Brodzki, and Janusz W. Bialek. Hierarchical spectral clustering of power grids. *IEEE Transactions on Power Systems*, 29(5):2229–2237, 2014.

[29] Abilash Thakallapelli, Sheikh Jakir Hossain, and Sukumar Kamalasadan. Coherency based online wide area control of wind integrated power grid. In *2016 IEEE International Conference on Power Electronics, Drives and Energy Systems (PEDES)*, pages 1–6. IEEE, 2016.

[30] Abilash Thakallapelli, Hossain, Sheikh Jakir, and Sukumar Kamalasadan. Coherency and online signal selection based wide area control of wind integrated power grid. *IEEE Transactions on Industry Applications*, 54(4):3712–3722, 2018.

[31] I Tyuryukanov. *Graph Partitioning Algorithms for Control of AC Transmission Networks: Generator Slow Coherency, Intentional Controlled Islanding, and Secondary Voltage Control*. PhD thesis, Delft University of Technology, 2020.

[32] Ilya Tyuryukanov, Jairo Quirós-Tortós, Matija Naglič, Marjan Popov, M. A. M. M. van der Meijden, and Vladimir Terzija. A post-processing methodology for robust spectral embedded clustering of power networks. In *IEEE EUROCON 2017 -17th International Conference on Smart Technologies*, pages 805–809, 2017.

[33] Grigorios F. Tzortzis and Aristidis C. Likas. The global kernel means algorithm for clustering in feature space. *IEEE Transactions on Neural Networks*, 20(7):1181–1194, 2009.

[34] Muhammad Sharif Uddin, Anthony Kuh, and Marija D. Ilić. Bad data detection using kernel density estimation. 2014.

[35] Lusha Wang, Anamika Dubey, Assefaw H. Gebremedhin, Anurag Srivastava, and Noel Schulz. Mpc-based decentralized voltage control in power distribution systems with ev and pv coordination. *IEEE Transactions on Smart Grid*, pages 1–1, 2022.

[36] Xiao-Feng Wang and De-Shuang Huang. A novel density-based clustering framework by using level set method. *IEEE Transactions on knowledge and data engineering*, 21(11):1515–1531, 2009.

[37] Xingzhi Wang, Zheng Yan, Li Li, and Dong Xie. A new kernel-based clustering algorithm for the multi-machine equivalent of large power systems. In *2008 International Conference on Electrical Machines and Systems*, pages 3936–3939, 2008.

[38] Mehrdad Yazdanian and Ali Mehrizi-Sani. Distributed control techniques in microgrids. *IEEE Transactions on Smart Grid*, 5(6):2901–2909, 2014.

[39] R Yousefian and S Kamalasadan. A lyapunov function based optimal hybrid power system controller for improved transient stability. *Electric Power Systems Research*, 137:6–15, 2016.

[40] Kedi Zheng, Yi Wang, Qixin Chen, and Yuanpeng Li. Electricity theft detecting based on density-clustering method. In *2017 IEEE Innovative Smart Grid Technologies-Asia (ISGT-Asia)*, pages 1–6. IEEE, 2017.

[41] Weilin Zhong, Georgios Tzounas, and Federico Milano. Improving the power system dynamic response through a combined voltage-frequency control of distributed energy resources. *IEEE Transactions on Power Systems*, pages 1–1, 2022.

[42] Faycal Znidi, Hamzeh Davarikia, Mohammad Arani, and Masoud Barati. Coherency detection and network partitioning based on hierarchical dbscan. In *2020 IEEE Texas Power and Energy Conference (TPEC)*, pages 1–5, 2020.